CHARACTERISTICS OF TURBULENCE STRUCTURE AND UNDERTOW IN THE SURF ZONE

砕波帯内における乱れ構造と戻り流れに関する研究

Akio Okayasu

岡 安 章 夫

To Marcel
with Best Regards
A. Okayasu

CHARACTERISTICS OF TURBULENCE STRUCTURE AND UNDERTOW IN THE SURF ZONE

砕波帯内における乱れ構造と戻り流れに関する研究

by

Akio Okayasu

岡 安 章 夫

September, 1989

ABSTRACT

The characteristic motion of water under breaking waves and the turbulence structure in the surf zone were investigated through detailed two-dimensional velocity measurements in a wave flume. Significant difference was found between the breaking processes in the outer and inner regions of the surf zone. The velocity field in each region consists of steady current, periodic wave motion, organized vortex motion and turbulence. It was found that the organized vortex motion caused by wave breaking was an important fluid motion connecting the wave motion and the turbulence.

The vertical profiles of the undertow, which is the steady current below the wave trough level, were investigated from velocity histories measured by hot-film and laser-Doppler-velocimeters. The turbulence generated in the upper layer by wave breaking prevents the development of the bottom boundary layer in the inner region. The vertical distribution of the mean Reynolds stress and the mean eddy viscosity coefficient in the inner region can be approximated by linear functions of the vertical elevation. The offshore-directed mean shear stress on the bottom is so large that it can not be neglected in the modeling of the undertow.

The transition point which was the boundary between the outer and inner regions of the surf zone was defined as the offshore limit of the quasi-steady breaking region. The distance from the breaking point to the transition point was expressed in terms of the breaking water depth and the bottom slope.

In order to describe the mechanism of the energy transfer during wave breaking accurately, a model was presented in which the organized large vortexes were taken into account as a transmitter of energy in the energy transfer process from wave motion to turbulence. The distribution of the turbulence energy calculated by this model agreed with the experimental results qualitatively.

The mass and momentum fluxes by the organized large vortexes were also discussed. The mass transport by breaking waves was found to be induced by the wave motion and the organized large vortexes.

By using the models of the energy distribution and the mass transport, a model was presented for the two-dimensional distribution of the undertow. The Reynolds stress and the eddy viscosity coefficient were quantitatively evaluated from the energy dissipation rate on the basis of the dimensional analysis. The variation of the mean water level in the surf zone was also predicted with a good accuracy by considering the momentum flux by the organized vortexes. The model can evaluate the distribution of the undertow on an arbitrary beach topography from the incident wave condition.

TABLE OF CONTENTS

		page
	ABSTRACT	
	TABLE OF CONTENTS	i
	LIST OF TABLES AND FIGURES	iii
	LIST OF SYMBOLS	vi
CHAPTER 1	GENERAL INTRODUCTION	1
CHAPTER 2	TURBULENCE STRUCTURE IN THE SURF ZONE	
	2.1 Introduction	5
	2.2 Experiments on Two-Dimensional Velocity Field in the Surf Zone	9
	2.2.1 Experimental Facilities and Arrangement	
	2.2.2 Experimental Conditions	
	2.2.3 Data Processing and Analysis	
	2.3 Velocity Field and Turbulence Structure in the Surf Zone	21
	2.3.1 Difference of Turbulence Component due to the Definition	
	2.3.2 Organized Vortex Motion Caused by Wave Breaking	
	2.3.3 Vertical Distribution and Average of Undertow	
	2.3.4 Distribution of Reynolds Stress and Eddy Viscosity Coefficient	
	2.3.5 Wave Height Attenuation and Cross-Shore Distributions of the Turbulence Energy	
	2.4 Experiments on Length of Outer Region	43
	2.4.1 Experimental Facilities	
	2.4.2 Experimental Procedures	
	2.4.3 Distance from Breaking Point to Plunging and Transition Points	

CHAPTER 3 MODELING OF UNDERTOW

3.1 Introduction 53

3.2 Energy Transfer in the Surf Zone 56

3.3 Mass Balance in the Surf Zone 59

3.3.1 Mass Flux in the Surf Zone

3.3.2 Mass Flux due to Wave Motion

3.3.3 Mass Flux due to Organized Large Vortexes

3.4 Momentum Balance in the Surf Zone 68

3.5 Estimation of Energy Distribution in the Surf Zone 71

3.5.1 Governing Equations of Time-Dependent Mild Slope Equation

3.5.2 Estimation of Energy Dissipation Rate

3.5.3 Energy Transfer Factor around the Breaking Point

3.5.4 Ratio of Potential Energy to Kinetic Energy of Waves

3.5.5 Modification of the Wave Celerity

3.6 Dimensional Analysis of Turbulence Properties 86

3.7 Modeling of Vertical Distribution of Undertow 89

3.7.1 Modeling of Distribution of the Mean Reynolds Stress and the Mean Eddy Viscosity Coefficient

3.7.2 Expression of Undertow Profile by using the Eddy Viscosity Model

3.8 Computational Results 98

3.8.1 Cross-Shore Variations of Energies

3.8.2 Vertically Averaged Undertow

3.8.3 Profiles of Undertow

3.8.4 Wave Setup and Setdown

CHAPTER 4 CONCLUSIONS 113

REFERENCES 116

APPENDIXES

LIST OF TABLES AND FIGURES

TABLES

Table 2.2.1 Conditions of experiments of series A.

Table 2.2.2 Conditions of experiments of series B.

Table 2.4.1 Conditions and results of experiments of series C–1 ($\tan\beta = 1/10$).

Table 2.4.2 Conditions and results of experiments of series C–2 ($\tan\beta = 1/20$).

Table 2.4.3 Conditions and results of experiments of series C–3 ($\tan\beta = 1/30$).

Table 2.4.4 Conditions and results of experiments of series C–4 ($\tan\beta = 1/50$).

Table 3.7.1 Dimensionless parameters for the distribution of $-\rho\overline{u'w'}$ and ν_e.

Table 3.8.1 Conditions of experiments performed by Nagayama (1983).

FIGURES

Fig. 2.1.1 Wave characteristics in the surf zone.

Fig. 2.2.1 Plan and side view of the wave flume (case A–3).

Fig. 2.2.2 Arrangement of measuring points (case A–1).

Fig. 2.2.3 Arrangement of measuring points (case A–2).

Fig. 2.2.4 Arrangement of measuring points (case A–3).

Fig. 2.2.5 Arrangement of measuring points (cases B–1, B–5 and B–11).

Fig. 2.3.1 Comparison between the ensemble mean values and the moving averages of velocity.

Fig. 2.3.2 Mean Reynolds stress obtained by the ensemble mean method and the moving average method (case A–3).

Fig. 2.3.3 Velocity, vorticity and turbulent intensity immediately after wave plunging (case A–1).

Fig. 2.3.4 Ensemble mean values of velocity vectors (case A–1).

Fig. 2.3.5 Distribution of turbulent intensity (case A–1).

Fig. 2.3.6 Dropout rate of signals of the laser-Doppler-velocimeter (case A–3).

Fig. 2.3.7 Distribution of turbulent intensity (case A–2).

Fig. 2.3.8 Distribution of steady currents (case A–3).

Fig. 2.3.9 Distribution of steady currents (case A–4).

Fig. 2.3.10 Cross-shore variation of vertically averaged steady current (case A–3).

Fig. 2.3.11 Distribution of steady currents (case B–11).

Fig. 2.3.12 Distribution of turbulent intensity (case B–11).

Fig. 2.3.13 Distributions of mean Reynolds stress (cases B–2 and B–7).

Fig. 2.3.14 Distributions of mean eddy viscosity coefficient (cases B–2 and B–7).

Fig. 2.3.15 Variations of wave height and turbulence energy for plunging breakers (cases B–2 and B–6).

Fig. 2.3.16 Variations of wave height and turbulence energy for spilling breakers (cases B–3 and B–7).

Fig. 2.4.1 Relationships between H_0/L_0 and l_t/h_{0b}.

Fig. 2.4.2 Relationships between ξ_0 and $\dfrac{h_{0b}-h_{0t}}{h_{0b}}$.

Fig. 2.4.3 Relationships between $\dfrac{1}{\tan\beta}$ and l_t/h_{0b}.

Fig. 3.3.1 Comparison of the cross-shore variations of M_{SFM}, M_{LLW} and $0.8M_{LLW}$ (cases B–2, B–3 and B–5).

Fig. 3.3.2 Assumption of velocity distribution of an organized large vortex.

Fig. 3.3.3 Conceptual illustration of plural vortexes in one wave. [Nadaoka (1986)]

Fig. 3.5.1 Setting of dissipation distance l_d.

Fig. 3.5.2 Setting of coefficient α_T.

Fig. 3.7.1 Assumed distributions of mean Reynolds stress and mean eddy viscosity coefficient.

Fig. 3.8.1 Calculated and measured energy variations (case B–1).

Fig. 3.8.2 Rates of energy transfer and dissipation (case B–1).

Fig. 3.8.3 Potential energies calculated by the present model and measured by Nagayama (1983) on a uniform slope (case 1).

Fig. 3.8.4 Potential energies calculated by the present model and measured by Nagayama (1983) on a step-type beach (case 3).

Fig. 3.8.5 Potential energies calculated by the present model and measured by Nagayama (1983) on a step-type beach (case 5).

Fig. 3.8.6 Calculated and measured energy variations (case B–11).

Fig. 3.8.7 Potential energies calculated by the present model and measured by Nagayama (1983) on a bar-type beach (case 6).

Fig. 3.8.8 Potential energies calculated by the present model and measured by Nagayama (1983) on a bar-type beach (case 7).

Fig. 3.8.9 Variations of calculated and measured U_m (case B–1).

Fig. 3.8.10 Variations of calculated and measured U_m (case B–4).

Fig. 3.8.11 Variations of calculated and measured U_m (case B–8).

Fig. 3.8.12 Steady current distribution and the variation of mean water level (case B–1).

Fig. 3.8.13 Steady current distribution and the variation of mean water level (case B–4).

Fig. 3.8.14 Steady current distribution and the variation of mean water level (case B–8).

Fig. 3.8.15 Steady current distribution and the variation of mean water level (case B–11).

LIST OF SYMBOLS

A	total area of organized large vortex
A_1	section of an organized large vortex
a	amplitude of wave
a_I	amplitude of incident wave
a_τ	factor of function of sheer stress distribution
a'_τ	modified factor of function of sheer stress distribution
a_ν	factor of function of eddy viscosity distribution
B	width of wave flume
b_τ	factor of function of sheer stress distribution
b'_τ	modified factor of function of sheer stress distribution
C_τ	coefficient for evaluating τ_m from D_B
C_ν	coefficient for evaluating ν_m from D_B
c	wave celerity
c_{bore}	celerity of bore
c_g	group velocity of wave
c_{sol}	celerity of solitary wave
c_0	wave celerity in offshore region
D_B	rate of energy dissipation by wave breaking
D_{b+w}	rate of energy dissipation by bottom and wall friction
d_c	water depth at wave crest
d_t	water depth at wave trough
E_k	kinetic energy of wave motion
E_p	potential energy of wave motion
E_t	total energy of wave
E_v	energy of organized large vortex

E_w	energy of wave motion
E_1	energy of rotational component of an organized large vortex
E_2	energy of parallel component of an organized large vortex
E_3	total energy of an organized large vortex
e_v	energy of organized large vortex per unit mass
f_A	total transfer factor of energy
f_T	energy transfer factor by breaking
f_{b+w}	dissipation factor by bottom and wall friction
g	acceleration of gravity
H	wave height
H_b	wave height at breaking point
H_i	incident wave height
H_0	deep water wave height
h	mean water depth
h^*	representative water depth
h_b	mean water depth at breaking point
h_i	water depth in offshore constant depth region
h_0	still water depth
h_{0b}	still water depth at breaking point
h_{0p}	still water depth at plunging point
h_{0t}	still water depth at transition point
k	wave number ($=2\pi/L$)
L	wave length
L_b	wave length at breaking point
L_0	deep water wave length
l	representative length of turbulence
l_b	distance from crest breaking point to breaking point

l_d	length of dissipation of energy of organized large vortex
l_p	distance from breaking point to plunging point
l_t	distance from breaking point to transition point
M_{LLW}	mass flux calculated by linear long wave theory
M_{SFM}	mass flux calculated by stream function method
M_t	mass flux by wave
M_v	mass flux by organized large vortex
M_w	mass flux by wave motion
n	ratio between group velocity and wave celerity
p	pressure
p_s	static pressure
$\mathbf{Q}$	flow rate
Q_r	flow rate for wave recovering
$\hat{Q}$	amplitude of flow rate
$\hat{Q}_x$	x-component of amplitude of flow rate
$\hat{Q}_y$	y-component of amplitude of flow rate
q	representative velocity of turbulence
R_p	ratio of potential energy to kinetic energy of wave
R_τ	ratio between mean shear stress at trough and bottom
r	radial coordinate in organized large vortex
S	section of an organized large vortex
S_v	excess momentum flux by organized large vortex
S_w	excess momentum flux by wave motion
S_{xx}	radiation stress
T	wave period
T_B	transfer rate of energy from E_w to E_v
t	time

t_d	contribution to local dissipation rate by T_B at certain value of x
U	x-component of steady current
U_m	x-component of mean steady current below trough level
U_v	contribution to U_m from mass flux by organized large vortexes
U_w	contribution to U_m from mass flux by wave motion
U_{off}	steady current in offshore region
u	x-component of water particle velocity
u'	x-component of turbulent fluctuation
u'_m	square root of vertical average of mean turbulence energy
u_1	rotational component of velocity of organized large vortex
u_2	parallel component of velocity of organized large vortex
$\hat{u}$	amplitude of horizontal water particle velocity at still water level
$\tilde{u}$	x-component of moving averaged velocity
$\langle u \rangle$	x-component of ensemble mean velocity
V	y-component of steady current
v	y-component of water particle velocity
v'	y-component of turbulent fluctuation
W	z-component of steady current
w	z-component of water particle velocity
w'	z-component of turbulent fluctuation
w'_m	square root of vertical average of mean turbulence energy
$\tilde{w}$	z-component of moving averaged velocity
$\langle w \rangle$	z-component of ensemble mean velocity
x	horizontal coordinate in cross-shore direction
x_b	breaking point
x'_b	crest breaking point
x_p	plunging point

x_t	transition point
Δx	spacing between mesh points
y	horizontal coordinate in longshore direction
z	vertical coordinate
z'	vertical distance from bottom
α_T	coefficient multiplied to energy transfer factor
β	inclination of bottom
γ	ratio of water particle velocity to wave celerity
γ_b	ratio of water particle velocity to wave celerity at wave breaking
γ_H	ratio of wave height to water depth
γ_r	ratio of water particle velocity to wave celerity for wave recovering
γ_s	ratio of water particle velocity to wave celerity on constant slope
ϵ	energy of turbulence per unit mass
ε	energy dissipation rate per unit mass
ζ	water surface elevation
ζ_b	elevation of boundary between organized large vortex and wave motion
ζ_c	elevation of wave crest
ζ_r	water surface elevation of reflected wave
ζ_t	elevation of wave trough
$\hat{\zeta}$	amplitude of water surface elevation
$\overline{\zeta}$	wave setup and setdown
λ	wave length of laser light
ν	kinematic viscosity
ν_e	eddy viscosity
ν_m	mean eddy viscosity averaged vertically below trough level
ν_t	total viscosity
ν_h	eddy viscosity in horizontal plane

ξ	complex amplitude of wave
ξ_0	surf similarity parameter
ρ	density of water
σ	angular frequency ($=2\pi/T$)
τ	mean shear stress acting on horizontal plane in x-direction
τ_m	mean shear stress averaged vertically below trough level
$\hat{\phi}_0$	amplitude of velocity potential at mean water level

CHAPTER 1

General Introduction

The velocity field and the energy process in the surf zone are of great importance since they exert wide influences over the phenomena such as the wave attenuation, sediment transport and material diffusion which actively take place due to wave breaking. As the velocity field in the surf zone is rather complicated because of its variation in time and space as well as its turbulent characteristics, only qualitative descriptions of breaking waves were presented early in the last decade through observation and visualization of the flow pattern in laboratories. With the recent development of the velocity measurement techniques, many researches have been carried out thereafter to clarify the structure of the turbulent velocity field in the surf zone by measuring the velocity fluctuation. However, the understanding of the characteristics of the velocity field in the surf zone and the process of the energy transfer due to wave breaking is not yet satisfactory.

The mass transport due to breaking waves, which is larger than that due to non-breaking waves, causes the undertow which is offshore-directed steady current below the wave trough level. Since such mass movement induces a macro-scale circulation in the surf zone, it plays significant roles in the sand movement and the material diffusion in combination with micro-scale eddies, *i.e.* turbulence, generated by the wave breaking. The relatively large velocity of the undertow causes large shear stress near the trough level and on the bottom. Although some models to estimate the distribution of the undertow were presented by adopting rather crude assumptions, the application was limited to the inner region in which the wave breaking can be regarded as a quasi-steady process. Since most of these models are constructed by using the local properties of waves and turbulence, the accurate prediction of the wave field and the energy dissipation in the surf zone is required.

Numerical models for predicting the wave height or wave energy variation in the surf zone from the incident wave condition have been proposed based on simple modeling of the breaking process. In these models, the wave energy is considered to be directly transferred to the turbulence energy. However the rotational organized motion of water formed at the crests of the breaking waves cannot be neglected because the existence of the vortex motion shows an important characteristic of the energy transfer and also of the mass transport and momentum exchange in the surf zone. Most of the energy of irrotational wave motion is converted firstly to the energy of the organized large vortexes, although it finally dissipates to heat through turbulent dissipation. The previous models therefore are not able to explain the experimental results on the characteristics of the turbulent velocity field such as the spatial distribution of turbulence energy. In order to establish a practical model which is capable of dealing with various problems due to wave breaking, the comprehensive understanding of the surf zone dynamics is necessary.

The mechanisms of wave breaking in the outer and inner regions of the surf zone are much different. In the outer region, a rapid transition of wave profiles takes place with energy transfer from wave motion to the organized vortexes, especially in case of plunging breakers. On the other hand, a quasi-steady breaking occurs in the inner region and the energy transfer from the wave motion to the turbulence through the vortex is in an equilibrium state. Hence the definition and determination of the transition point which is the boundary between these two regions are important for the general description of the surf zone dynamics.

Motivated by the background mentioned above, the characteristics of the turbulent velocity field in the surf zone were investigated in the present study through detailed measurement of the two-dimensional velocity field under breaking waves. Then a model which describes the energy transfer during wave breaking is presented to evaluate the energy variation and the energy dissipation in the surf zone. In the

model, the wave energy is assumed to be transmitted to the turbulence energy through the organized large vortexes. A model for evaluating the distribution of the undertow is also proposed on the basis of the accurate description of the wave field and energy dissipation in the surf zone.

The first objective of the present study is to investigate the velocity field and the turbulence structure in the surf zone. The second objective is to describe the energy transfer in the surf zone on the basis of the understanding of the physical process and to formulate a model for estimating the vertical distribution of the steady current below the trough level which is valid throughout the surf zone.

The present dissertation is divided into two parts according to the above subjects. The former part, Chapter 2, deals with the characteristics of the velocity field through detailed and precise laboratory experiments. The organized motion of the water particle under breaking waves is investigated in terms of the velocity, vorticity and turbulent intensity. Next, the distributions of the turbulence properties such as the turbulence energy, Reynolds stress and eddy viscosity are investigated. In the last section of this chapter, the position of the transition point is discussed.

In the latter part, Chapter 3, a model which estimates the two-dimensional distribution of the undertow is presented. The transfer of energy in the surf zone is firstly described based on the results obtained in Chapter 2. Then the energy variation and energy dissipation rate in the surf zone are estimated by applying the time-dependent mild slope equation. The organized large vortexes formed at the wave crests are taken into account as transmitters of energy from the wave motion to the turbulence in order to accurately describe the energy distribution in the surf zone.

CHAPTER 2

Turbulence Structure in the Surf Zone

2.1 Introduction

The velocity field in the surf zone is much concerned with the phenomena there. Hence, it is a very important technical problem to make it clear. Since the velocity field under breaking waves is rather complicated because of its variation in time and space as well as its turbulent characteristics, only qualitative descriptions of breaking waves were presented early in the last decade through visual observation in laboratories.

Svendsen *et al.* (1978) separated the surf zone into two regions which were outer and inner regions (Fig. 2.1.1). In the outer region, rapid transitions of wave shape occurs, particularly in case of plunging breakers. Sawaragi and Iwata (1974) suggested the existence of a large scale vortex formed just below the wave plunging. It is frequently called "horizontal roller" or "plunger vortex". Miller (1976) showed the process of formation of the plunger vortex and the recirculating motion near the water surface caused by the splash of wave plunging by using photography. He also observed the same processes with a relatively smaller scale in spilling breakers. In the inner region, quasi-steady breaking waves which are similar to bores propagate shoreward with attenuation. Both such bore-like waves and plunger vortexes seem to give strong effect on the generation of turbulence in the surf zone.

With the recent development of the velocity measurement techniques, many works have been carried out to clarify the structure of the turbulent velocity field in the surf zone by measuring the velocity. Hattori and Aono (1985) measured the velocity field under breaking by using a hot-film-velocimeter. They separated the

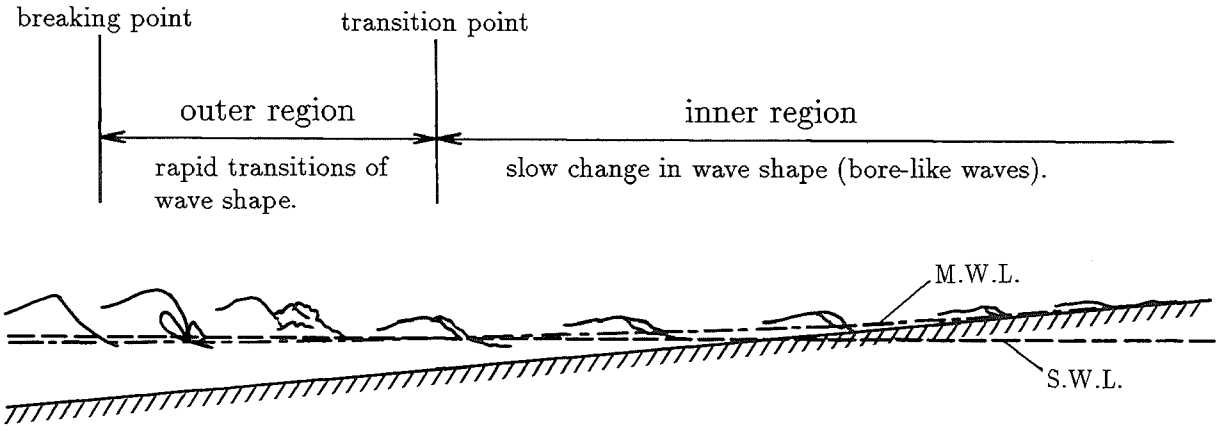

Fig. 2.1.1 Wave characteristics in the surf zone.

turbulence from measured velocity considering the coherence between the velocity and the water surface elevation and discussed the turbulence structure in the inner region, which they pointed out to be strongly three-dimensional. Nadaoka *et al.* (1989) found from flow visualization and measurement by a laser-Doppler-velocimeter that two-dimensional horizontal vortexes developed near the water surface in front of the wave crests and obliquely downward stretched eddies with strong three-dimensionality were formed behind the wave crests. Sakai *et al.* (1984) discussed the variation of the Reynolds stress in the surf zone. Okayasu *et al.* (1986) verified the initial breaking process by detailed measurements of the velocity field in the outer region and Mizuguchi (1986) also discussed the rapid transition of waves near the breaking points.

The existence of "undertow" caused by the mass transport of breaking waves was first observed by Bagnold (1940) and has been recognized for many years [see e.g. Hansen and Svendsen (1984)]. The undertow plays an important role for the circulation of material or the sediment transport in the surf zone. However our knowledge on the interaction between the turbulence and the undertow or the mass flux by the vortexes as well as on the breaking process in the surf zone is not yet satisfactory. In order to clarify the turbulence structure, the flow field and the energy dissipation process in the surf zone, it is important to investigate the motion and roles of the large vortexes which are considered to generate turbulence and characterize the velocity field in the surf zone.

In this chapter, these characteristics of the velocity field in the surf zone will be clarified through detailed and precise laboratory experiments. The distributions of the turbulent properties such as the turbulence energy, the Reynolds stress and the eddy viscosity will be investigated. The energy dissipation in the surf zone will also be discussed in relation to the variation of the wave energy.

The mechanisms of wave breaking in the outer and inner regions are much different as already mentioned. Hence, the position of the transition point which is the boundary between the two regions is also important for comprehensive descriptions of the surf zone. However, no systematic investigation to determine the position of the transition point was carried out. In this chapter, the position of the transition point and the plunging point will be discussed later.

2.2 Experiments on Two-Dimensional Velocity Field in the Surf Zone

2.2.1 Experimental Facilities and Arrangement

Laboratory experiments were carried out in a two-dimensional wave flume which was 23 m long and 0.8 m wide with a wave generator at one end. The generator was controlled by electric signals from a function oscillator which generated regular sinusoidal signals in the present experiments. The beach models which had smooth beds were set at the other side of the flume. A partition was set at the center of the beach models for the sake of keeping the phenomena to be two-dimensional, *i.e.* uniform in the longshore direction. Figure 2.2.1 shows a sketch of the flume.

The experiments were divided into series A and B. The detailed measurements of the velocity fields were performed in series A to get a basic and essential understanding of the velocity field throughout the surf zone. For case A–1, the step-type beach profile was used to elucidate the behavior of the plunger vortex. The beach model consisted of a 1/10 slope and a horizontal bed. The still water depth on the horizontal bed was 10 cm. The reasons why this type of beach topography was chosen were to fix the breaking point of each wave and to make a region deep enough for the measurement. A large amount of thin plastic strings were put on the bed at the shoreward end instead of a slope to prevent the wave reflection. The measuring area was from 0.5cm to 14.5cm above the bottom and 80 cm long in an cross-shore directed vertical plane. The measuring points were arranged to make 2 cm grids. The arrangement is shown in Fig. 2.2.2.

For cases A–2 and A–3, a constant slope of 1/20 was used to measure the whole area of the surf zone. The measuring areas were about 250 cm long in both cases, but the arrangements of measuring points were different. The 2 cm grids arrangement was adopted for case A–2 to obtain the vorticity distribution. The

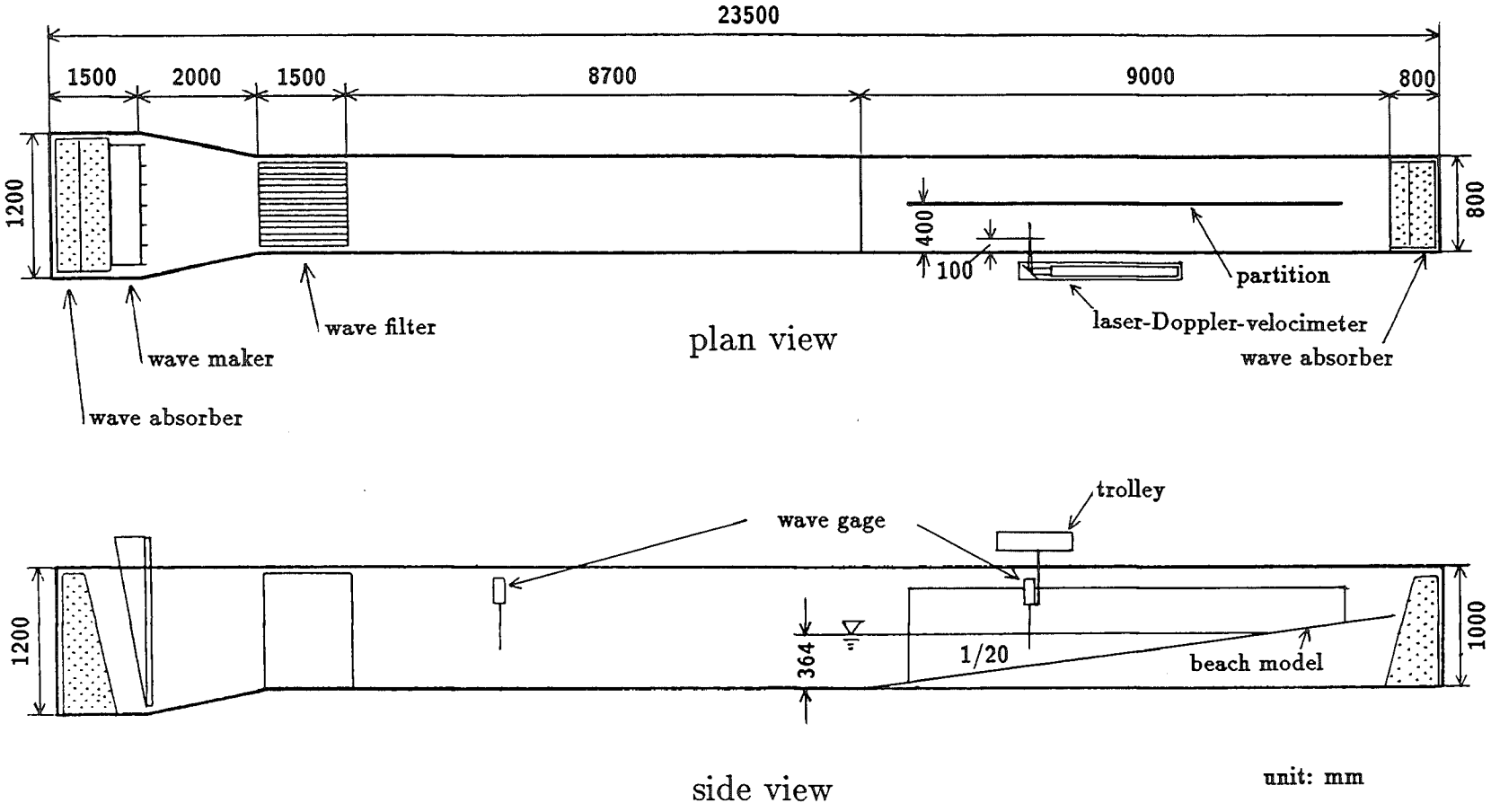

Fig. 2.2.1 Plan and side view of the wave flume (case A–3).

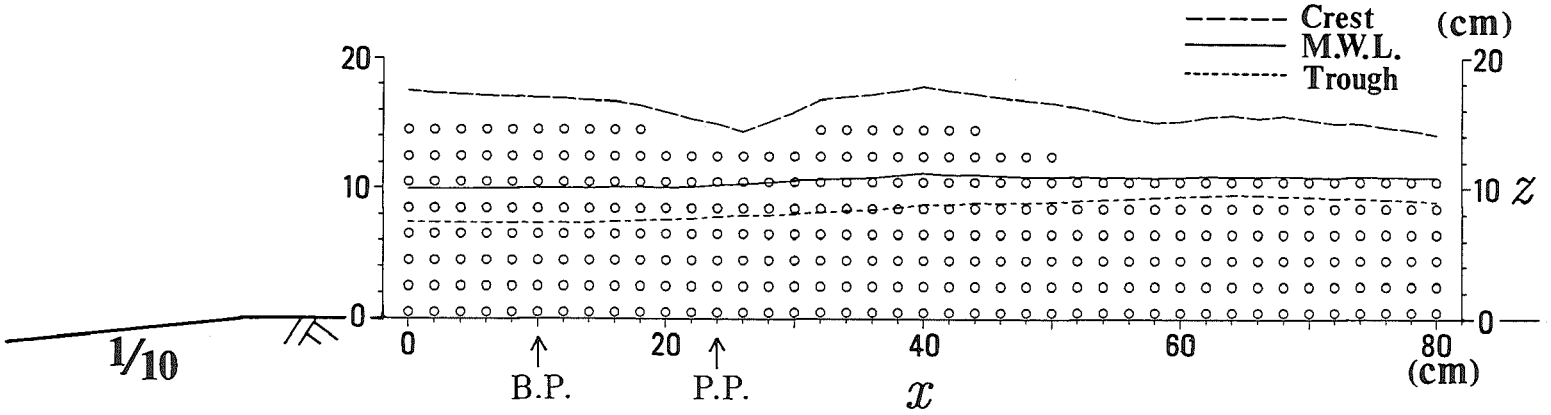

Fig. 2.2.2 Arrangement of measuring points (case A–1).

lowest points were 7mm above the bottom. The detailed arrangement is shown in Fig. 2.2.3. On the other hand, for case A–3, a grid which was sparse in the horizontal direction and dense in the vertical direction was used for the purpose of detailed measurements of the mass flux variation and the vertical profiles of the undertow. The measuring points were arranged with distance of 10 cm in the cross-shore direction and distance from 2.5 to 10 mm in the vertical direction. On every measuring line, at least seven measuring points were set below the trough level for accurate evaluation of the mass flux. The lowest points were 2 mm above the bottom. The arrangement is shown in Fig. 2.2.4 which is exaggerated in the vertical direction.

The measuring points were arranged only close to the bottom for case A–4 to investigate the details of the bottom boundary layer in the surf zone. Nine measuring lines were allocated every 40 cm from the offshore side beyond the breaking point to the still water shoreline. The measuring points were arranged 1, 2, 3, 5, 10 and 20 mm above the bottom along each line.

For series B, velocity fields were measured for various beach topographies and incident wave conditions. Three kinds of beach topographies were used. They were a 1/20 uniform slope (from case B–1 to B–4), a 1/30 uniform slope with 1 m of a 1/20 slope at its offshore end (from case B–5 to B–9) and a step-type topography which consisted of 4.11 m of a 1/10 slope, 2.85 m of a horizontal bed and a 1/10 slope at its onshore end (cases B–10 and B–11). The still water depth on the horizontal bed were 6 cm for cases B–10 and B–11. The arrangements of the measuring points were sparse in the horizontal direction and dense in the vertical direction for the purpose of detailed measurements of the undertow profiles. The measuring points were arranged along 6 or 7 vertical measuring lines in every case but case B–11. The first measuring lines were set on the wave breaking points. The second lines were located on the plunging points in case of plunging breakers, or the intermediate

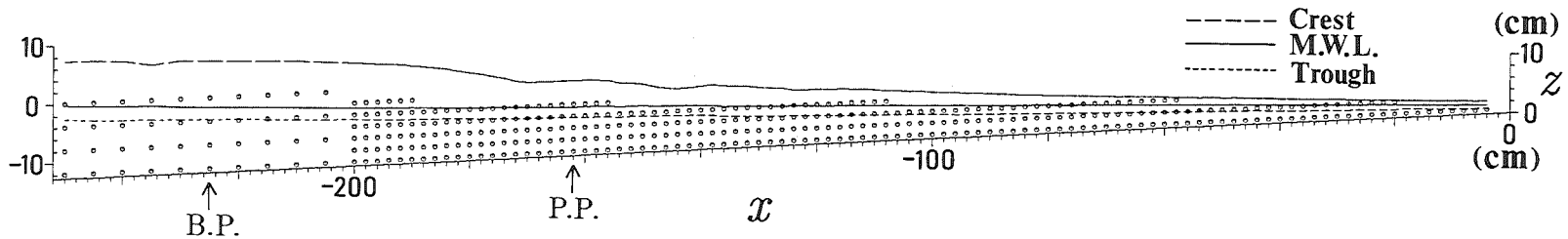

Fig. 2.2.3 Arrangement of measuring points (case A–2).

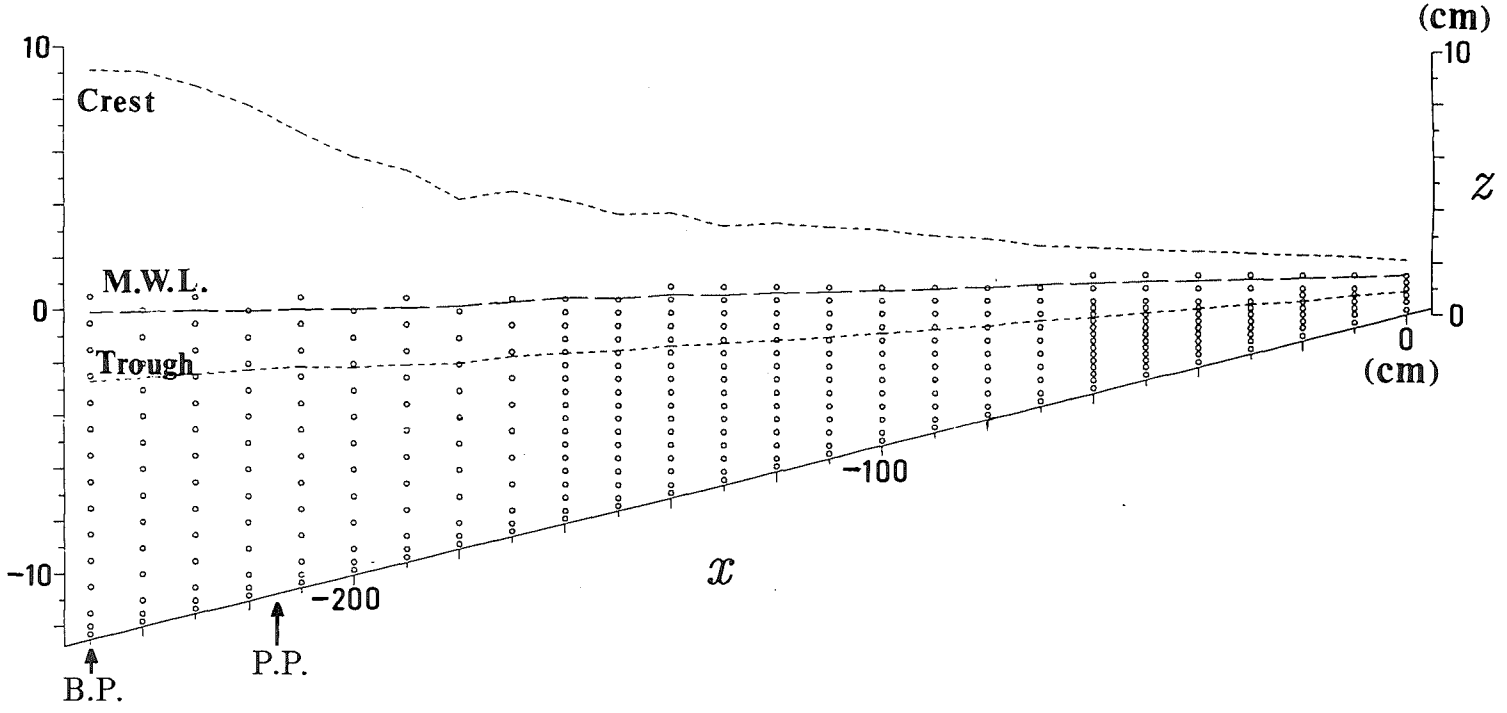

Fig. 2.2.4 Arrangement of measuring points (case A–3).

point between lines 1 and 3 for spilling breakers. From the third, the measuring lines were arranged in the inner regions where the bore-like waves developed well. In case B–11, the measuring lines were arranged to cover the wave recovery point which was at $x = -115$ cm by visual observation. The lowest measuring points in each measuring line are 1mm above the bottom in cases B–1 to B–4, and for cases B–5 to B–11, they are 2 mm above the bottom. The vertical distance of those points were from 1 to 20 mm and the highest points are near the mean water levels. As examples, the arrangement of cases B–1, B–5 and B–11 are shown in Fig. 2.2.5.

2.2.2 Experimental Conditions

The x-axis and z-axis were set to be shoreward and vertically upward, respectively. The origin of the coordinates in case A–1 was at the offshore end of the measuring area as shown in Fig. 2.2.2. In the other cases, the shoreline at the still water level was set to be the origin. The conditions of the experiments of series A and series B are listed in Table 2.2.1 and 2.2.2, respectively. In the table, T is the wave period, h_i the water depth in the offshore constant depth region, H_i the wave height there, H_0/L_0 the deep-water wave steepness, x_b the breaking point, x_p the plunging point.

Table 2.2.1 Conditions of experiments of series A.

case	slope	T (s)	h_i (cm)	H_i (cm)	H_0/L_0	x_b (cm)	x_p (cm)
A–1	1/10+flat	1.55	40.0	6.95	0.0201	10	24
A–2	1/20	1.50	40.0	7.36	0.0226	–225	–162
A–3	1/20	1.50	36.4	8.15	0.0249	–250	–215
A–4	1/20	1.50	39.5	7.48	0.0230	–250	–200

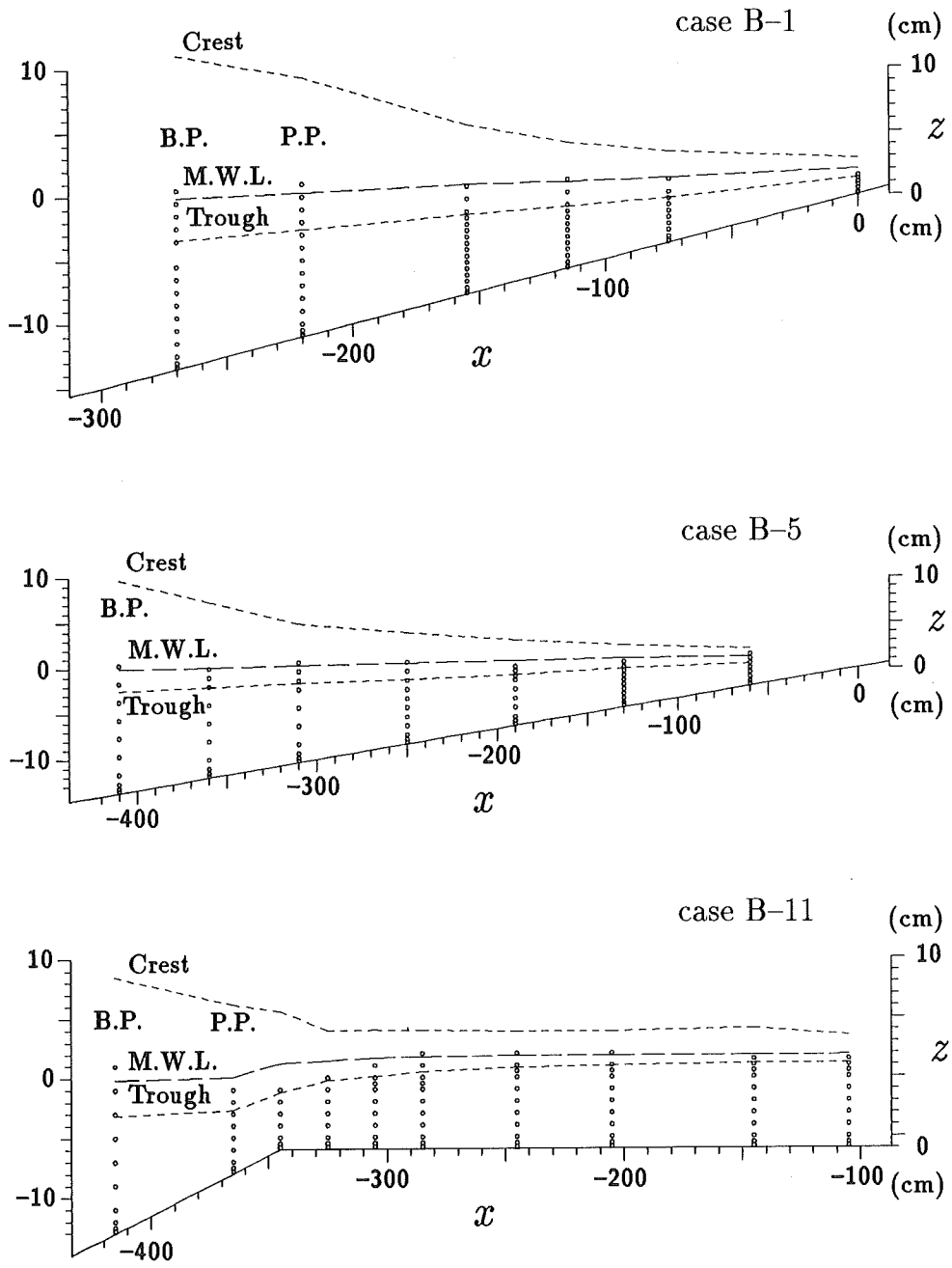

Fig. 2.2.5 Arrangement of measuring points (cases B–1, B–5 and B–11).

Table 2.2.2 Conditions of experiments of series B.

case	slope	T (s)	h_i (cm)	H_i (cm)	H_0/L_0	x_b (cm)	x_p (cm)
B–1	1/20	2.00	40.0	8.50	0.0139	–270	–220
B–2	1/20	2.00	40.0	5.63	0.0092	–200	–165
B–3	1/20	1.17	40.0	9.87	0.0502	–275	–[1)]
B–4	1/20	0.91	40.0	6.69	0.0542	–200	–[1)]
B–5	1/30	1.61	40.0	8.80	0.0232	–410	–[1)]
B–6	1/30	1.97	40.0	6.17	0.0104	–290	–230
B–7	1/30	1.96	40.0	8.22	0.0140	–410	–[1)]
B–8	1/30	1.12	40.0	8.26	0.0457	–350	–[1)]
B–9	1/30	1.23	40.0	6.05	0.0279	–290	–[1)]
B–10	1/10+flat	2.01	47.1	10.82	0.0179	–440	–385
B–11	1/10+flat	1.20	47.1	9.24	0.0447	–415	–365

[1)] spilling breaker

In addition to the table, the wave height to the water depth ratios, H_b/h_b, at the breaking points were 1.02, 0.901 and 0.954 in cases A–1, A–2 and A–3, respectively. The breaking points (abbreviated to "B.P.") and the plunging points ("P.P.") were indicated in the figures. After breaking, the wave propagates shoreward forming successive vortexes on the water surface. In case A–3, the point where these vortexes formed a rather stable bore-like waves and the point where the vortexes formed just in front of the wave crests began to attenuate were at $x = -170$ cm and $x = -80$ cm, respectively. The mean shoreline was at $x = 50$ cm in case A–3.

2.2.3 Data Processing and Analysis

A hot-film-velocimeter with a split film probe was used to measure the histories of two-dimensional velocity vectors lying on the xz plane for cases A–1 and A–2. The split-hot-film sensor consists of two platinum films on a single quartz fiber whose length is 1.2 mm and the diameter is 0.15 mm. The output from the two films provides a set of data of the magnitude of the velocity component normal to

the axis of the fiber, and of the component normal to the split plane. The magnitude of the velocity component parallel to the split plane is calculated from these two values though its sign cannot be detected. In case A–1, the sign of the cross-shore component of the velocity could not be determined. An assumption was therefore made that the surface profile and the cross-shore velocity are in phase. Hence, the sign of the velocity was reversed once in every wave period according to the surface profile. In case A–2, velocities were measured twice, once for the cross-shore and the other time for the vertical direction to avoid such an uncertainty.

Velocities for cases A–3 and A–4 and all cases of Series B were measured by a two-component laser-Doppler-velocimeter equipped with a 4 W Ar-ion laser tube. The laser beam projected from the laser tube is separated to a green light (the wave length $\lambda = 514.5$ nm) and a blue light ($\lambda = 488$ nm) by color filters. Since the two lights do not interfere each other, the two-component laser-Doppler-velocimeter works as if two completely individual velocimeters. Consequently, used with frequency shifters, full information of velocities for two component can be obtained. Moreover, the laser-Doppler-velocimeter has a great advantage for the measurements of turbulent velocity fields that it works without physical contact to the fluid. If the laser beams have transverse intensity distributions which obey the Gaussian distribution, the form of the probe of the velocimeter is considered to be ellipsoid. The longitudinal diameter of the probe was about 3.7 mm (green beam) or 3.5 mm (blue beam) and transverse diameter was 0.17mm (green beam) or 0.15mm (blue beam) in the present experiments.

The module was used as three-beam backscatter mode with frequency shifting. The laser-Doppler-velocimeter was capable of evaluating two components of velocities in the normal to the optic axis of the module by detecting the Doppler-shift frequency of the green and the blue lights scattered by particles in the focus of the laser beams. In order to obtain the scattered light with sufficient intensity, a

small amount of white paint which contained acrylic emulsion was seeded in the flume. Detailed measurements of velocity components (u, w) in a vertical plane were conducted by injecting the laser beams perpendicularly through the side wall of the flume. Though the laser beams projected with a little angle of depression for the measuring points close to the bottom, the deviation of velocities is negligible. Generally, it is difficult to measure the velocity at a point very close to the solid boundaries because of increasing noise by the diffused reflection. It became a serious problem especially for case A–4 in which the velocities near the bottom were primarily measured for investigation of the bottom boundary. Plastic mirrors were therefore placed on the bottom in case A–4 to prevent reflected laser lights from disturbing the signal. It was proved to be successful in getting velocity data with high S/N (signal to noise) ratio.

The velocity data were sampled every 10 ms for all cases except for case A–2 in which the sample timing was 12 ms and were converted into digital data over 30 (for cases A–1 and A–2) or 100 (for the other cases) wave periods. The data of the water surface elevation over the measuring point were also taken simultaneously by using a capacitance-type wave gage. The ensemble mean (equi-phase-mean) value of velocity which is expressed by $\langle u \rangle$ in x-direction or $\langle w \rangle$ in z-direction was calculated as the average of the velocity at the same phase of every wave. The steady current components (U, W) were calculated from those ensemble mean values. The turbulence components denoted by u' and w' was determined as the deviation from the ensemble mean value.

The Reynolds stress was calculated from the turbulence as $-\rho u'w'$ in case that the laser-Doppler-velocimeter was used, where ρ is the water density. The mean Reynolds stress $-\rho\overline{u'w'}$ was obtained by averaging the Reynolds stress over one wave period. From the steady current and the mean Reynolds stress, the mean eddy viscosity coefficient ν_e was evaluated by using the eddy viscosity model. It

means that the mean eddy viscosity coefficient was obtained not by averaging the instantaneous values of the eddy viscosity coefficient but from the vertical gradient of the steady current and the mean Reynolds stress.

2.3 Velocity Field and Turbulence Structure in the Surf Zone

The results of the experiments will be shown in this section. The spatial distributions and time histories of ensemble mean velocities, vorticities and turbulent intensities were obtained. The time averaged values of each quantity were also obtained. The mean Reynolds stress and the mean eddy viscosity were calculated for cases in which the laser-Doppler-velocimeter was used. From these results, the characteristics of the velocity field in the surf zone will be discussed.

2.3.1 Difference of Turbulence Component due to the Definition

Figure 2.3.1 shows a comparison between the ensemble mean values of velocity $\langle u \rangle$ and the moving averages $\tilde{u}$ of 0.11 s (time averages over 0.11 s of the instantaneous values of the velocity) at the point $x = -100$ cm and 2 cm above the bottom in case A–3. It is found in the surf zone that the variation of the velocity in one wave by the organized motion, which is caused by the fluctuation of the breaking point *etc.*, is far larger than the turbulence in higher frequency which is beyond 10 Hz. Considering the previous concept of turbulence in which the turbulence does not include the organized variation, the definition of turbulence by the ensemble-mean method may not be proper. Sakai *et al.* (1984) defined the turbulence by the moving-average method to obtain the Reynolds stress in the surf zone. However, the mean Reynolds stress calculated by using the ensemble-mean method as $-\rho\overline{(u - \langle u \rangle)(w - \langle w \rangle)}$ is far larger than that by the moving-average method calculated as $-\rho\overline{(u - \tilde{u})(w - \tilde{w})}$ as shown in Fig. 2.3.2 for case A–3. The values by the moving-average method is so small that it can hardly be distinguished in the figure. It means that the fluctuation in low frequency by the organized motion is predominant for the momentum exchange in the surf zone. It can therefore be considered that the ensemble-mean method is better for defining the turbulent component to

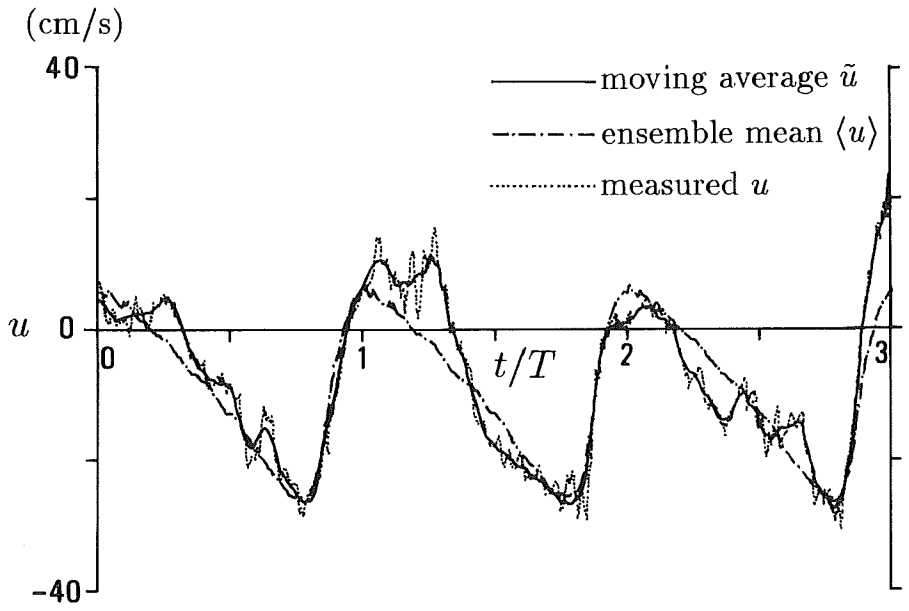

Fig. 2.3.1 Comparison between the ensemble mean values and the moving averages of velocity.

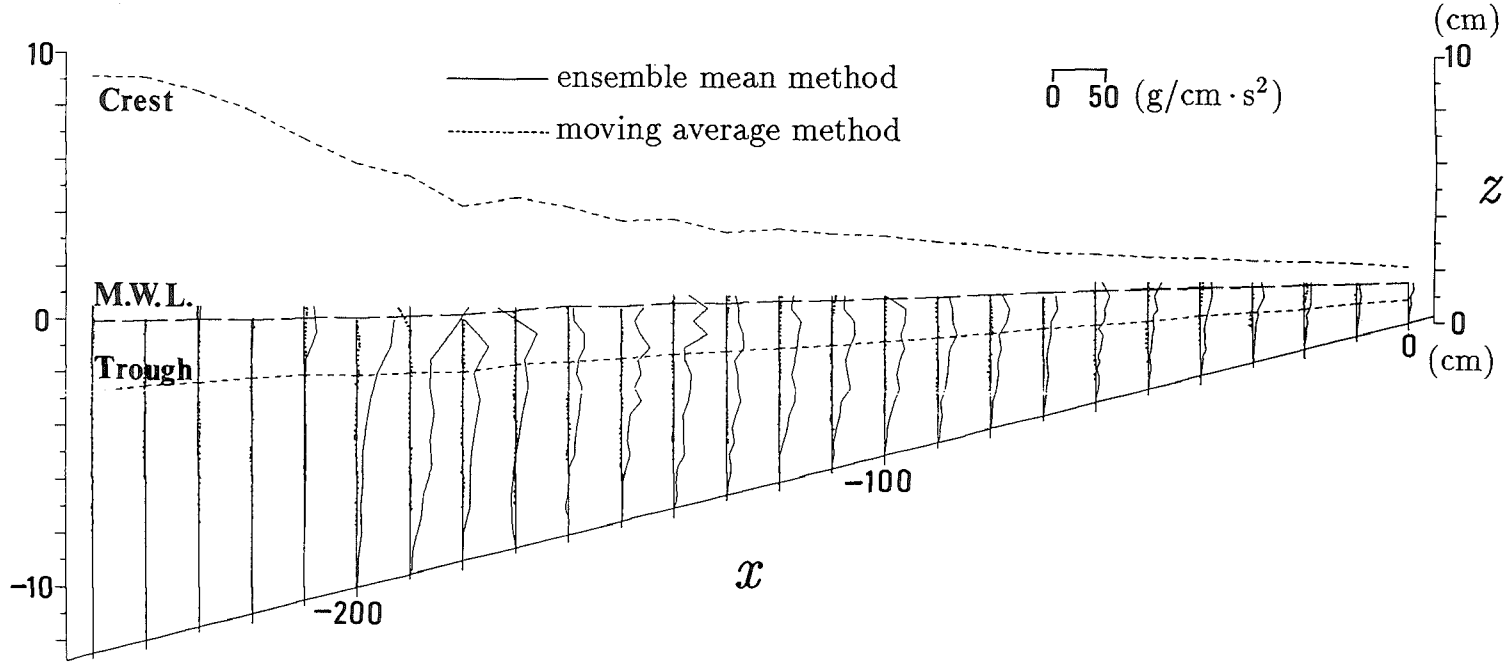

Fig. 2.3.2 Mean Reynolds stress obtained by the ensemble mean method and the moving average method (case A–3).

investigate the steady current distribution by using the eddy viscosity model which will be discussed later in the present study.

2.3.2 Organized Vortex Motion Caused by Wave Breaking

Figure 2.3.3 gives a result for case A–1. The field of the ensemble mean velocities, the vorticity field and the turbulent intensity field at the time immediately after the wave plunging are shown in the figures. A large scale vortex can be observed obviously by the velocity vectors around $x = 22$ cm and $z = 3$ cm in the figure. The high positive (clockwise in the figure) vorticity and turbulent intensity regions are in good agreement with the velocity vectors which suggest the existence of the plunger vortex.

Large magnitude of the velocity vectors can be seen at the wave crest. Another large value of the vector is seen at $x = 26$ cm. It can be considered that this small wave crest is caused by the large mass of water which penetrates into the water surface by the wave plunging pushing up the neighboring water body as Peregrine (1983) described. These crests have large magnitudes of positive vorticities, although turbulent intensities are not so large. There should be large vortexes, which rotate clockwise in this figure, also at the crests. On the other hand, negative (counterclockwise) vorticities can be seen between these vortexes. These negative vorticities should be made to cancel the positive vorticities caused by the large vortexes, although the spatially averaged vorticity is positive. The most intense turbulence exists between the regions which have positive values of vorticity and negative values of vorticity.

Figure 2.3.4 is the successive figures of the ensemble mean velocities after plunging. The process that the first plunging pushes up the neighboring water body and the second plunging occurs in a smaller scale is shown. The plunger vortex formed by the first plunging does not move according with the crest and goes downward.

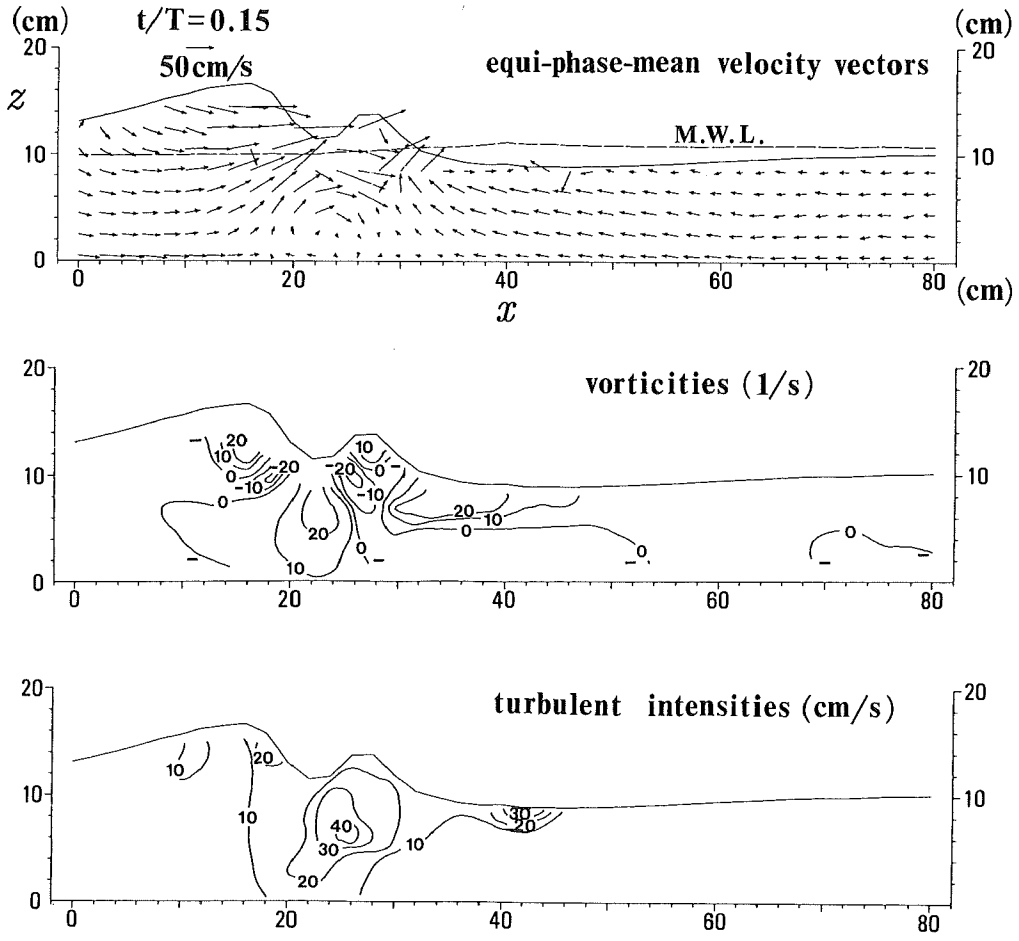

Fig. 2.3.3 Velocity, vorticity and turbulent intensity immediately after wave plunging (case A–1).

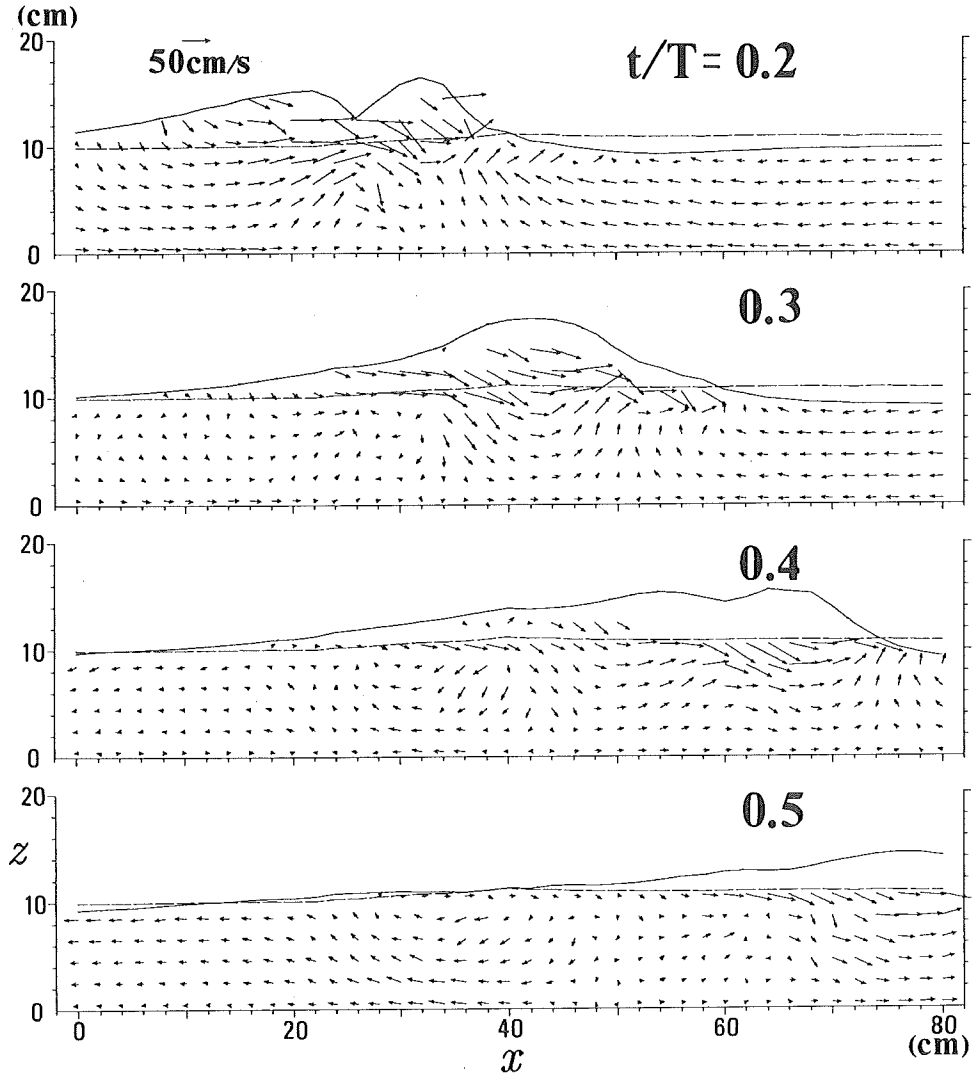

Fig. 2.3.4 Ensemble mean values of velocity vectors (case A–1).

The contour maps of the turbulent intensity at the same phases are shown in Fig. 2.3.5. The high turbulent regions caused by the first and second wave plunging go ahead slowly behind the wave crests, spread, and then dissipate. These figures show that the most part of the turbulence was produced near the surface and the turbulence generated near the bottom is little.

Figure 2.3.6 shows the distribution of the dropout rate for the measurements by the laser-Doppler-velocimeter for case A–3. The dropout rate is defined as the ratio of the time in which the intensity of the scattered light was not sufficient to resolve velocity component to the total time of the measurements. Although it is natural that the figure indicates so large values of the dropout rate above the trough level where the measuring points were beyond the water surface for a while, the values are also large in the region from $x = -120$ cm to $x = -180$ cm below the trough level. It can be considered that a large amount of air bubbles injected from the water surface obstructed the laser beams, which also confirms the existence of the plunger vortexes.

Figure 2.3.7 gives the successive contour maps of the turbulent intensity for case A–2. The figure shows a high turbulent region in front of the wave crest. It should be noticed that this turbulence is caused by the vortex motion as described by Nadaoka (1986) which is formed there. In the figure, it is also confirmed that the turbulence spreads downward, so the vortex motion in front of the wave crest should influence the turbulent flow field there and the bottom boundary layer. The figure indicates another turbulent region from $x = -40$ cm to $x = -80$ cm at the phases t/T =0.0–0.6. Since this high turbulent region stays there after the wave crest passes, it can be said that this turbulence is due to the interaction between the bore-like wave and the return flow from the swash zone. The high turbulent region caused by the wave plunging is also ascertained in this figure.

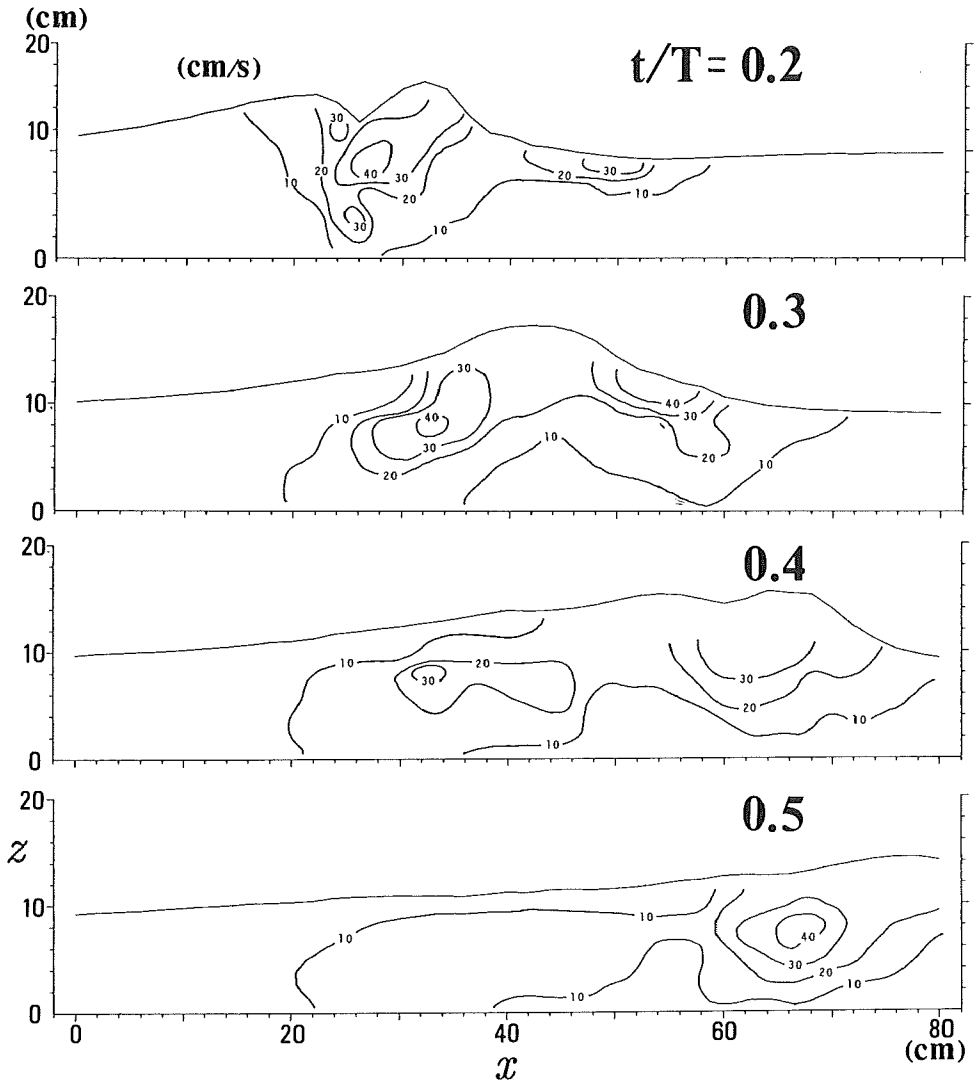

Fig. 2.3.5 Distribution of turbulent intensity (case A–1).

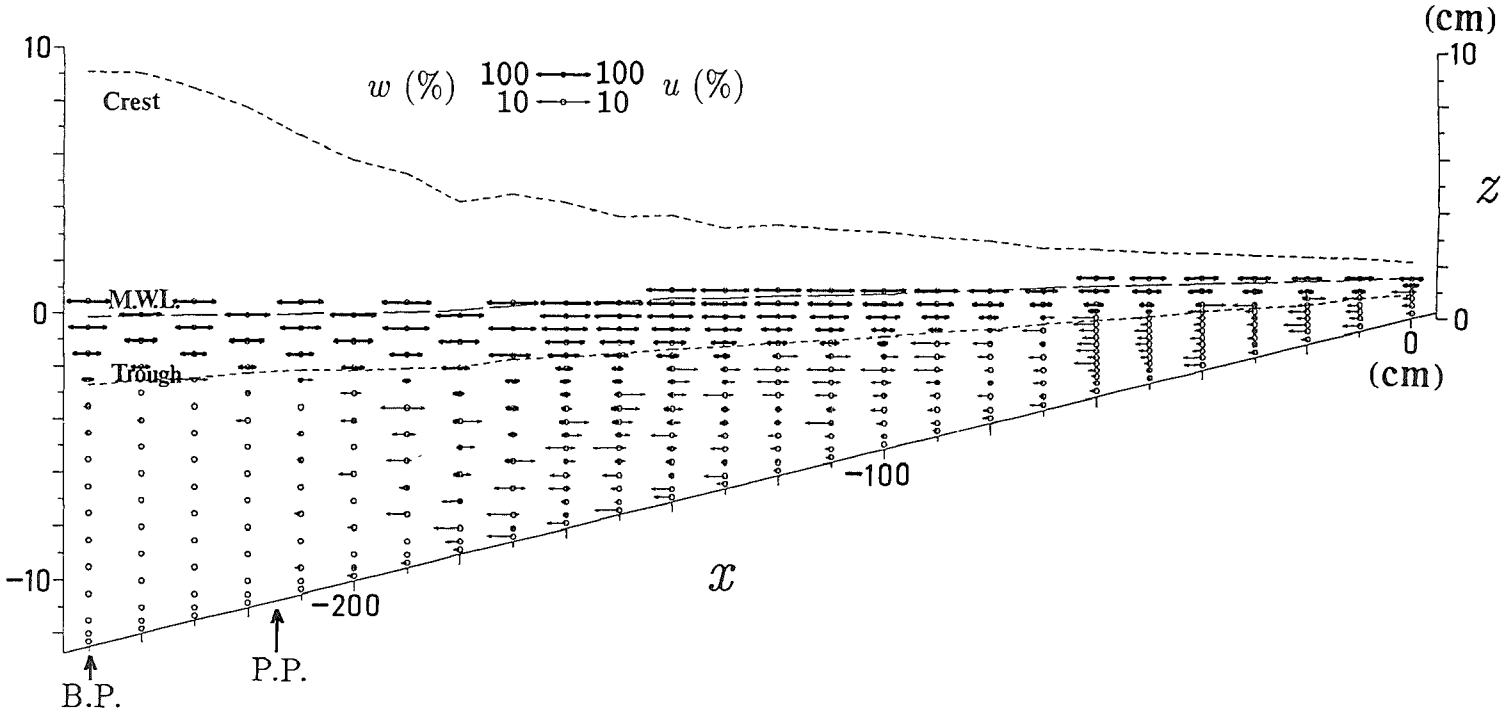

Fig. 2.3.6 Dropout rate of signals of the laser-Doppler-velocimeter (case A–3).

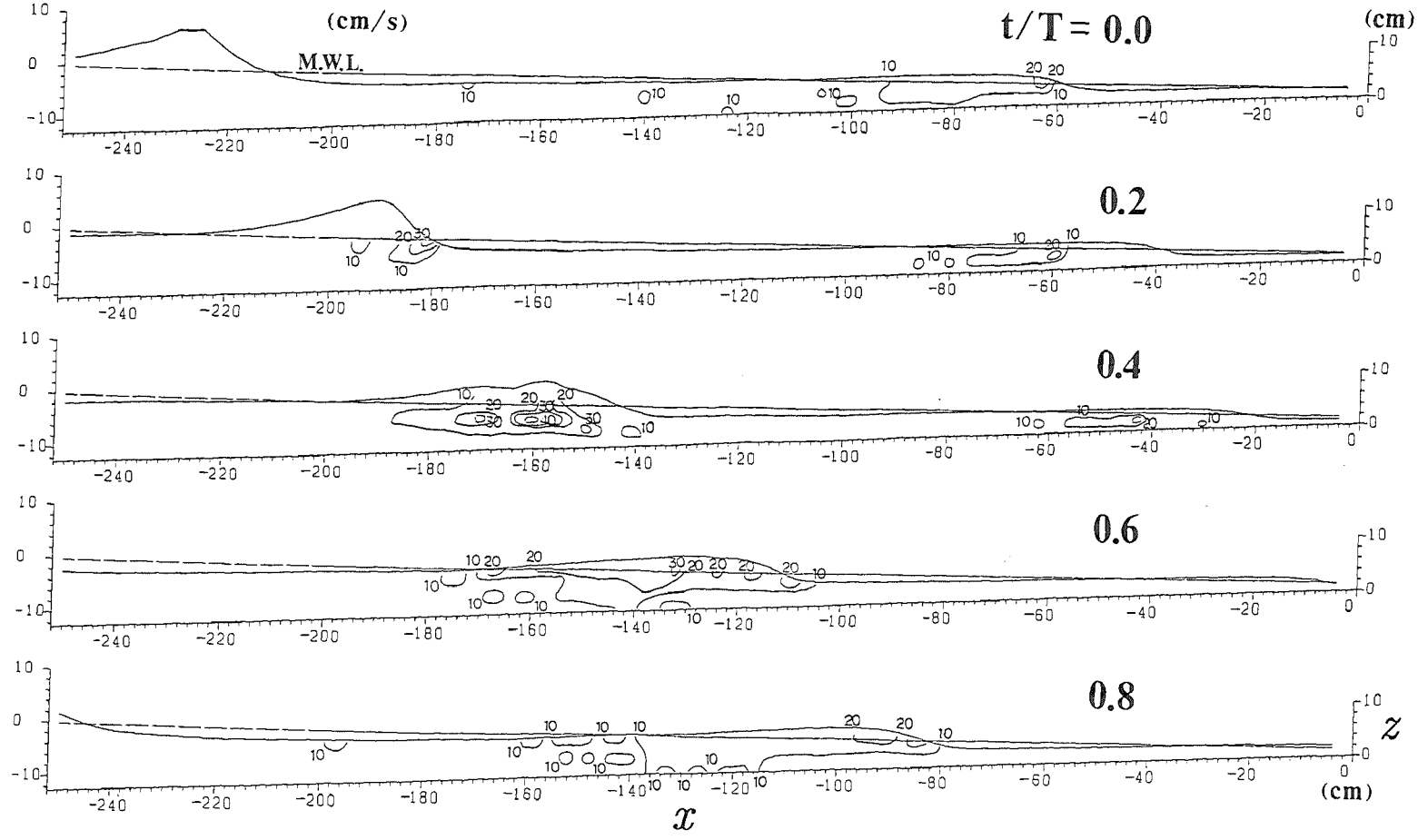

Fig. 2.3.7 Distribution of turbulent intensity (case A–2).

Based on these facts, it can be concluded that the generation of the plunger vortex has much influences on the characteristics of the velocity field and is much concerned with the energy dissipation process under plunging waves. The vortex motion formed in front of the wave crest has also important roles in the energy dissipation process. As the vortexes must have some rotational kinetic energy, it also relates to the energy transfer of breaking waves in the surf zone. Both of these vortex motions should not be included in the wave component, but they are not turbulence, either. In the present study, they are called "organized large vortexes". Since the vortex which is formed by the wave plunging is usually called "plunger vortex", the term "organized large vortexes" generally means the vortex motion formed in front of the crests of the bore-like waves hereafter.

Up to now, the velocity field in the surf zone were often described as the sum of a steady current, periodic wave motion and turbulence. This time, however, the measured results showed that the periodic component consists of the irrotational wave motion and organized rotational motion due to the wave breaking. It can be said that the organized vortexes are an important fluid motion connecting the wave motion and turbulence. Hence, it is proposed that the velocity field in the surf zone should be divided into four components as [steady current] + [irrotational wave motion] + [organized vortex motion] + [turbulence].

In the present study, the turbulence is defined as the deviation from the ensemble mean values of velocity. This definition is based on the idea that the waves are completely periodic so that the vortexes are formed at the same position and phase at every time. However, the turbulence defined here includes a part of the organized motion, which is caused by the fluctuation of the breaking point *etc.* as already shown in §2.3.1. The situation becomes much more complicated in case of irregular waves for which the ensemble mean does not make any sense. Hence, it may be

better to define the "organized vortex motion" as "a coherent structure with large-scale eddies which depends on the flow geometry concerned" as defined by Nadaoka *et al.* (1989) when the physical process of the wave breaking is considered.

2.3.3 Vertical Distribution and Average of Undertow

Figure 2.3.8 shows the steady current distribution for case A–3. It can be seen that the shape of the undertow profiles in the inner region is significantly different from that around the breaking point. The gradient of the profiles $\frac{\partial U}{\partial z}$ below the trough level is negative in the outer region, but it is positive or zero in the inner region except near the bottom. The large magnitude of the gradient shows that large shear stress works near the mean water level. The steady current distribution for case A–4 is shown in Fig. 2.3.9. In the inner region the velocity at the elevation of 1 mm above the bottom indicates large value in the offshore direction, while it still directs onshore at the plunging point. This is because the bottom boundary layer in the inner region does not develop well due to agitation of the turbulence from the upper layer. The influence by the bottom to the steady current can be seen up to 3 mm above the bottom there.

The cross-shore variation of the mean steady current U_m averaged vertically from the bottom to the trough level was shown in Fig. 2.3.10 for case A–3. The vertically averaged undertow in the bore region is larger than that at the plunging point. It keeps almost the same value from the breaking point to the plunging point, then rapidly increases from the plunging point despite the monotonous decrease of the wave height. It continues to take a large value in the region where the bore-like waves were fully developed, and then gradually decreases to the shore line. The increment of the value should be caused by the organized large vortexes formed in front of the crests of the bore-like waves.

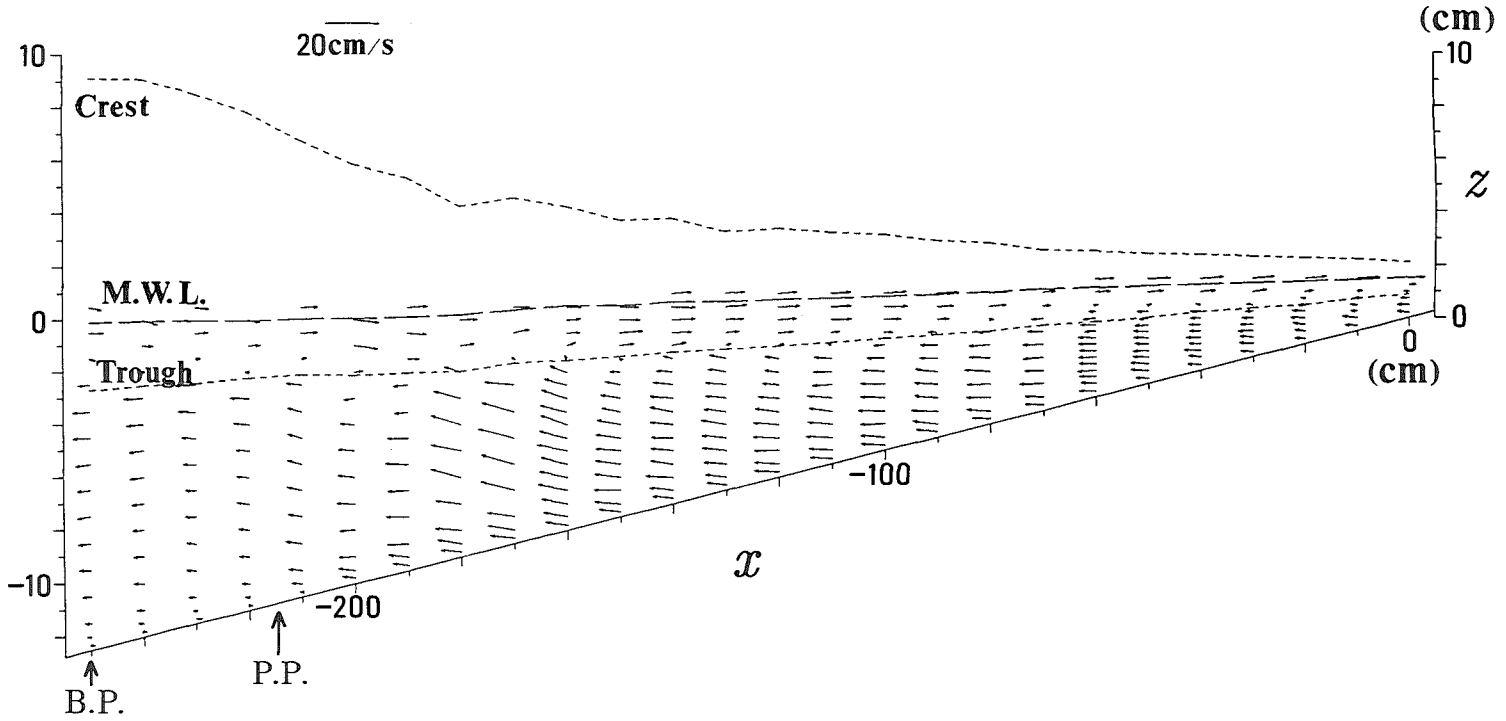

Fig. 2.3.8 Distribution of steady currents (case A–3).

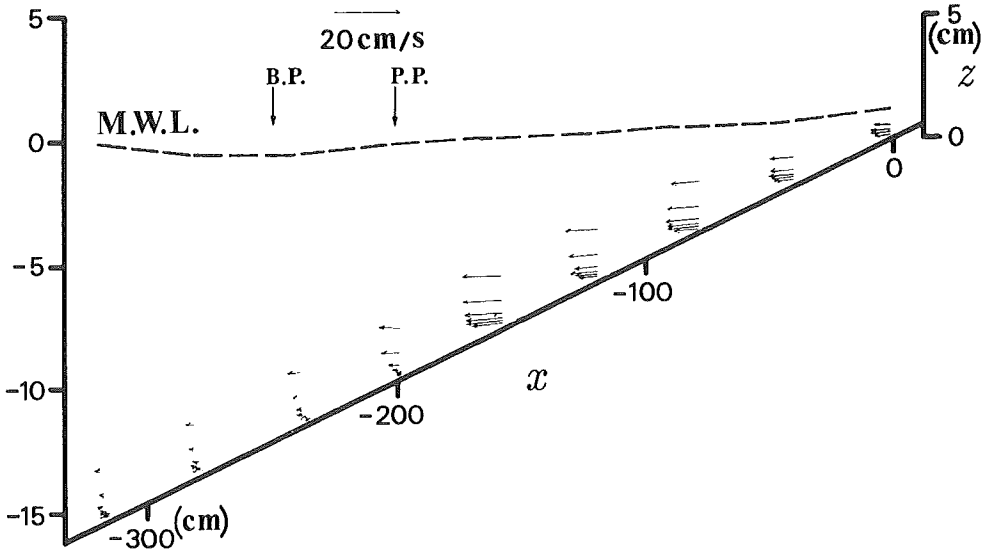

Fig. 2.3.9 Distribution of steady currents (case A–4).

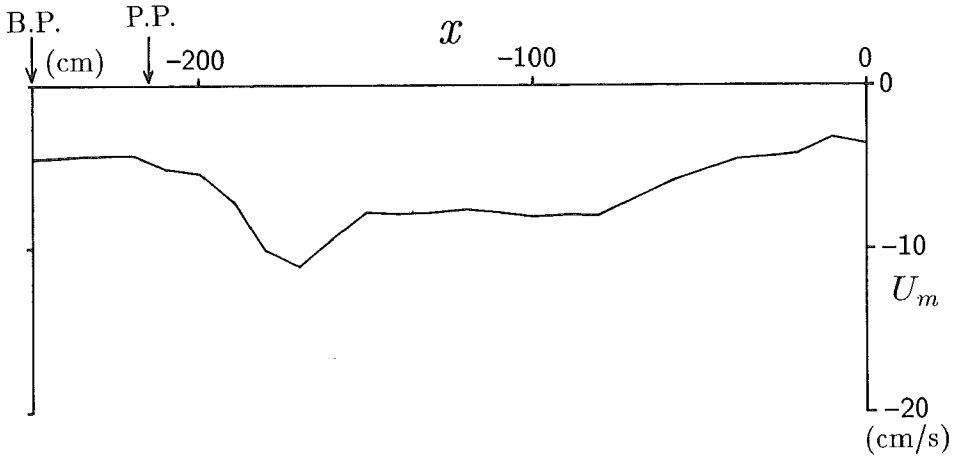

Fig. 2.3.10 Cross-shore variation of vertically averaged steady current (case A–3).

The distribution of the steady current for case B–11 in which the breaking waves recovered on the flat bed is shown in Fig. 2.3.11. The bore-like waves almost completely recovered at $x = -115$ cm. The profiles of the undertow in the recovery zone are much more similar to those at the outer region rather than those in the inner region. The wave height to the water depth ratio at the breaking point was 0.904. On the other hand, it was 0.294 in the wave recovery zone ($x = -105$ cm). The small magnitude of the steady current in $x \geq -205$ cm means that the mass transport by the bore-like waves is little.

Figure 2.3.12 gives the distribution of the turbulent intensity for case B–11. Since the turbulence is defined as the deviation from the ensemble means, the turbulence of the horizontal component near the bottom is large by fluctuation for each wave. The turbulent intensity at the trough level is still large in $x \geq -205$ cm where the steady current is small. It is consistent with the visual observation that the profile and magnitude of the distribution at $x = -105$ cm are about the same as those at the breaking point ($x = -415$ cm). It can be considered that the mass transport by the organized large vortexes are almost zero in $x \geq -205$ cm.

2.3.4 Distributions of the Reynolds Stress and the Eddy Viscosity Coefficient

Figure 2.3.13 shows the distributions of the mean Reynolds stress of cases B–2 and B–7. The distributions of the mean eddy viscosity coefficient of those cases are given in Fig. 2.3.14. In the figures, it can be seen that both of them decrease linearly from the trough level to the bottom in the inner region. And on the bottom, the value of the mean eddy viscosity coefficient is very small compared with that at the trough level. This should correspond to the fact that the turbulence produced by the large vortex on the front face of the wave crests is far larger than that generated near the bottom. But with respect to the mean Reynolds stress, it is observed that the offshoreward shear stress is too large to be neglected. The result of this study for

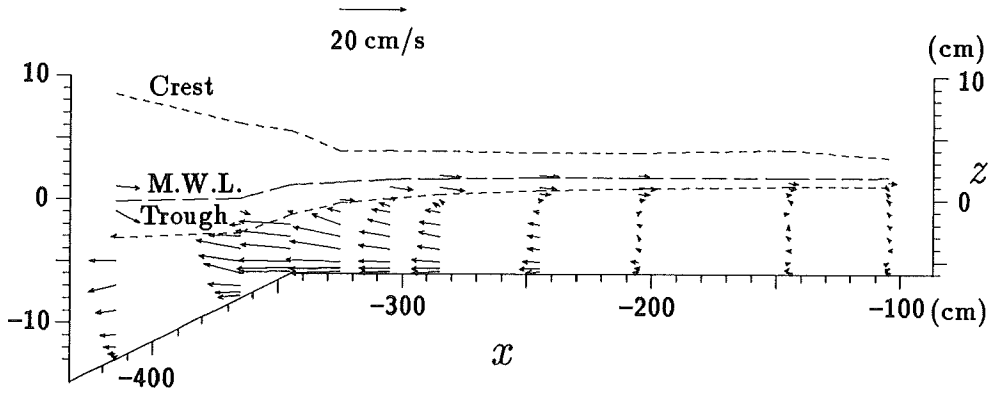

Fig. 2.3.11 Distribution of steady currents (case B–11).

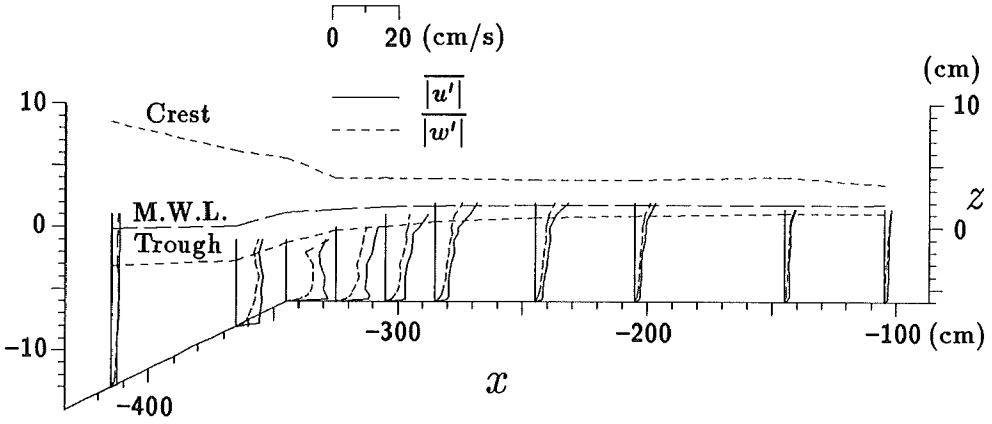

Fig. 2.3.12 Distribution of turbulent intensity (case B–11).

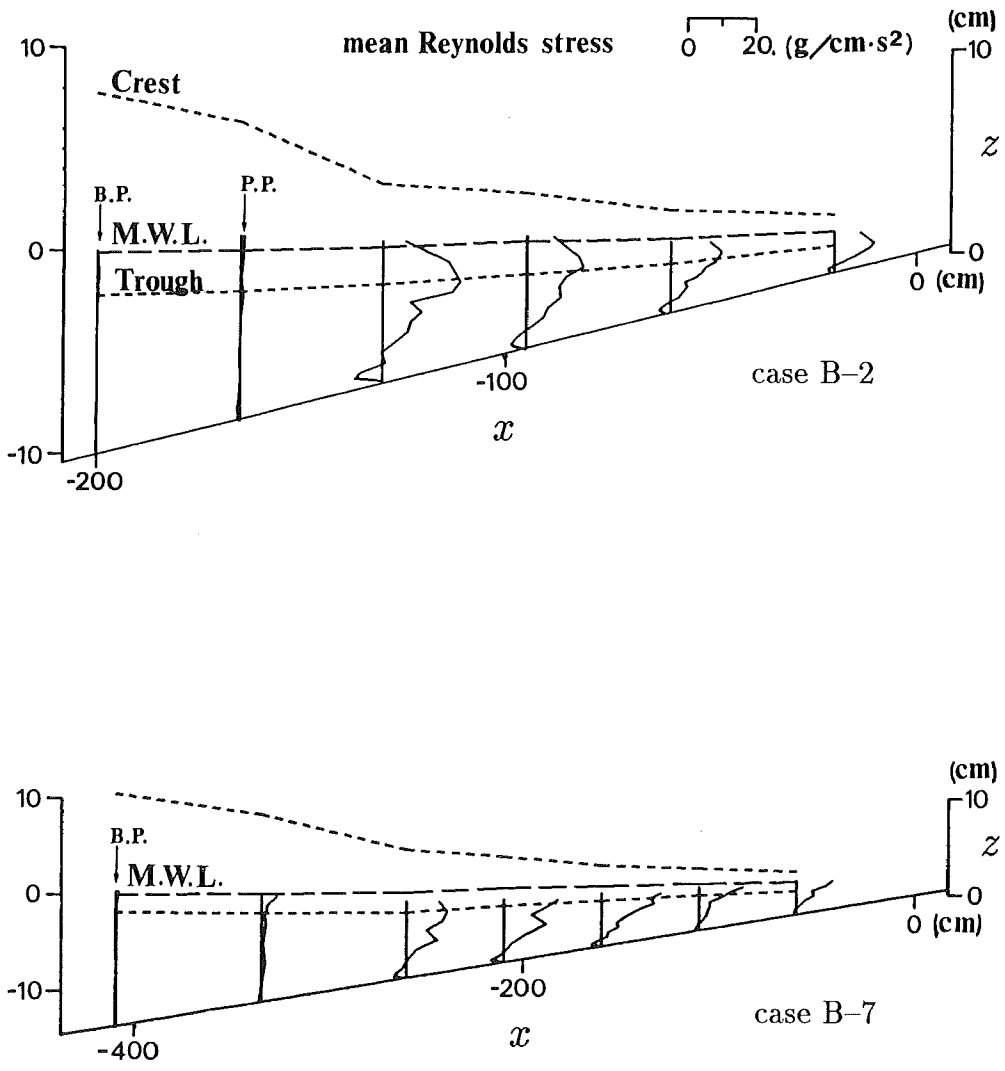

Fig. 2.3.13 Distributions of mean Reynolds stress (cases B–2 and B–7).

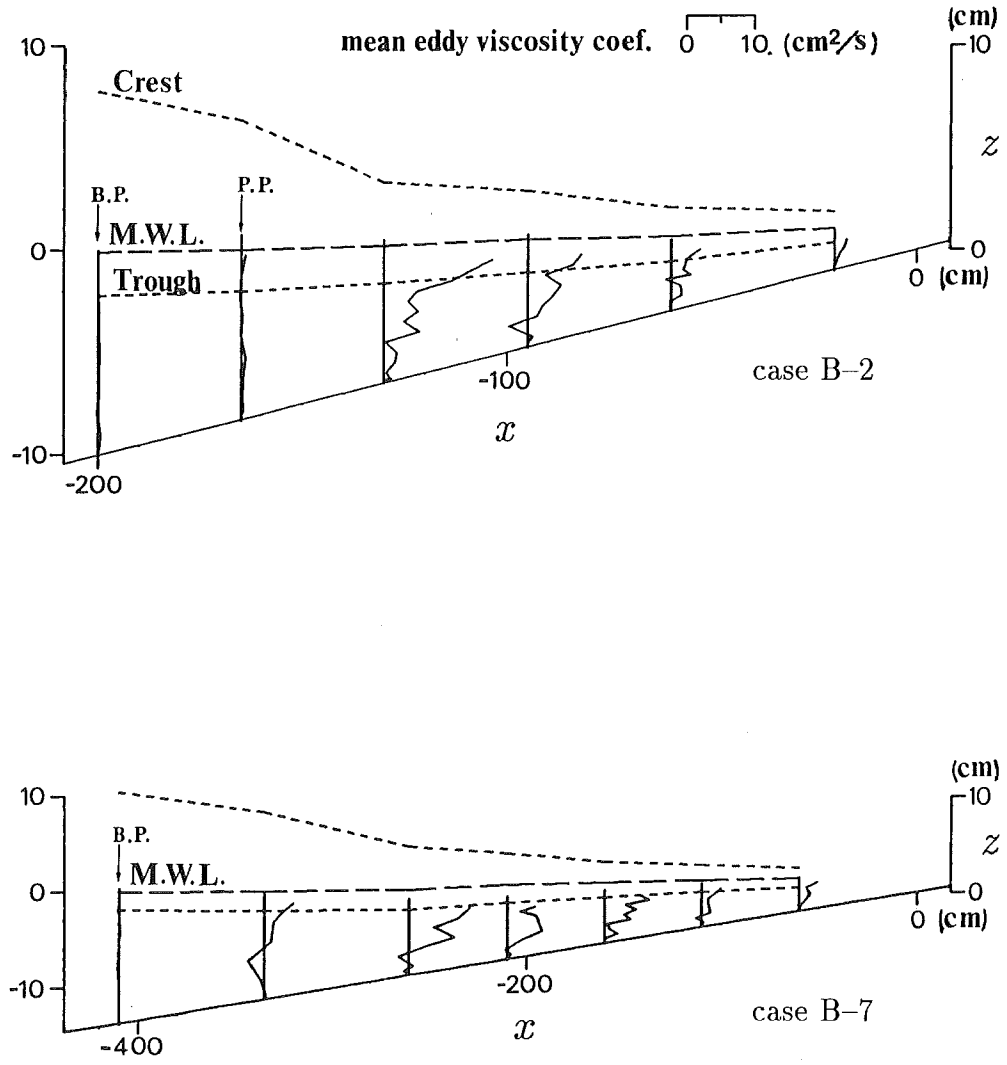

Fig. 2.3.14 Distributions of mean eddy viscosity coefficient (cases B–2 and B–7).

the vertical variation of the mean eddy viscosity coefficient is in contradiction to the analysis by Svendsen (1987) that the mean eddy viscosity coefficient is independent of the vertical coordinate.

2.3.5 Wave Height Attenuation and Cross-Shore Distributions of the Turbulence Energy

Figure 2.3.15 shows the cross-shore distribution of the vertically averaged mean turbulence energy ${u'_m}^2 \left(= \frac{1}{d_t} \int_0^{d_t} \overline{u'^2}\, dz' \right)$ and ${w'_m}^2 \left(= \frac{1}{d_t} \int_0^{d_t} \overline{w'^2}\, dz' \right)$ for cases B–2 and B–6. The wave height variations are also given in the figures. The wave height rapidly decreases after wave breaking in both cases, however the turbulence does not increase until near the plunging points. The tendency is similar in case of the spilling breakers, although the change becomes gentle as shown in Fig. 2.3.16 for cases B–3 and B–7.

Since the energy of the turbulence which is rapidly transferred to heat corresponds to the energy dissipation and the wave height attenuation implies rapid decrease of the wave energy, the figures indicate that the wave energy loss is not equal to the local energy dissipation. It is inconsistent with the previous models of the energy decay or the wave attenuation in the surf zone in which the wave energy directly dissipates to heat. One reason may be that the wave height attenuation does not mean the wave energy decay. However, the primary reason should be the existence of the organized large vortexes including both of the plunger vortexes and those formed as bore-like waves. These vortexes must have some energy which was not considered in the previous models. The little turbulence energy in the outer region means that the total energy of breaking waves which includes the vortex energy does not decrease so much. Hence, the transformation of waves in the outer region should be the process in which the energy of wave motion is transferred to the energy of the organized large vortexes. The concept in the previous models

of the energy dissipation that the wave energy decay equals the generation of the turbulence energy is not adequate. The further investigation about the magnitude of the energy of the organized large vortexes will be discussed later in Chapter 3.

2.4 Experiments on Length of Outer Region

2.4.1 Definition of Transition Point

The surf zone is divided into the "outer region (transition region)" where a rapid transformation of the wave profiles take place and the "inner region" where rather stable bore-like waves propagate according to the dynamics of wave breaking. This concept was first introduced by Svendsen *et al.* (1978) from the visual observations of wave behavior after breaking. The experimental results shown in §2.3 revealed the difference between the two regions in the distributions of the turbulence and the steady current. Since it can be considered that the mechanism of wave breaking in the outer region is essentially different from that in the inner region, it is necessary to distinguish them for modeling the energy transfer or dissipation process in the surf zone.

Svendsen (1984a) found that the mean water level is almost horizontal over some distance (5–8 times the mean water depth at the breaking point) from the breaking point, although a rather sharp increase in its slope occurs in the onshore side. He termed the point where the slope of the mean water level changes as the "transition point", and defined it as the limit between the outer and the inner region. Basco (1985) divided the surf zone into three regions which were termed Zones I, II and III according to the slope of the mean water level and the wave height variation. He mentioned that Zone I covers roughly 25–30% of the wavelength at the breaking point and it corresponds to the outer region defined by Svendsen (1984a) from the slope of the mean water level. However, he also mentioned that "the transition point will probably occur *during* the latter stages of the breaking process", which suggested that the boundary between the outer and the inner region may not be the onshore side of Zone I according to his understanding.

Yamashita *et al.* (1988) described the motion of the organized large vortexes formed by spilling breakers precisely by using a video recording system. They also separated the surf zone into three regions according to the behavior of the vortexes, which are the "rapid transformation region", "large vortex region" and "quasi-steady vortex region". They found that the size of the vortexes and the time intervals of their generations rapidly decrease in the former two regions, on the other hand, they become almost stable in the "quasi-steady vortex region".

As mentioned above, the boundary between the outer region and the inner region has not been investigated systematically yet, and its definition is not obvious, despite the importance in the energy process in the surf zone. The plunging point which is also important for the dynamics of wave breaking as the point where the turbulence increases abruptly has not been investigated systematically, either. In the present study, the transition point which is the boundary between the outer and the inner region is defined as the "point where fully developed bore-like waves are formed", and is interpreted as the offshore end of the quasi-steady energy decaying region. Since the criterion is based on the visual observation of the large vortexes formed in front of the wave crests, it is considered that the transition point defined here corresponds to the boundary between the "large vortex region" and the "quasi-steady vortex region" described by Yamashita *et al.* (1988).

The transition points and the plunging points were measured for various incident waves on different bottom slopes. The relation between the distances from the breaking point to the transition point and the bottom slope or the wave steepness will be investigated. The distance to the plunging point will also be investigated.

2.4.2 Experimental Facilities, Procedures and Conditions

Laboratory experiments were performed in a two-dimensional wave flume which was 12 m long and 20 cm wide with a glass side wall. The beach models were made

of 1/10, 1/20, 1/30 and 1/50 constant slopes which had 1/20 slope of 1 m at their feet in cases of the 1/30 and 1/50. The breaking point, plunging point (in case of the plunging breaker) and bore developing point were measured for various regular wave conditions.

The breaking point was defined as the point where the wave height took its maximum value, and the "bore developing point" which is the limit between the outer region and the inner region was determined as the point where bore-like waves which looked stable enough were formed. It may not be proper for a strict argument to decide the boundary by the visual observation because it is inevitable to imply the subjectivity. However, the determination by the visual observation is far more convenient than the way adopted by Yamashita *et al.* (1988) and it should be considered that the change in the wave attenuation, the slope of the mean water level or the distribution of the turbulent intensity is the secondary phenomenon caused by the difference of the energy transfer process of the waves.

The breaking points and others were averaged over about 10 waves because they fluctuated a little by the wave reflection or the oscillation by long period waves in the flume. The periods and the heights of the incident waves were 0.6–1.8 s and 5–8 cm for every beach slope. The still water depth in the offshore constant depth region was 18–21 cm. The detailed experimental conditions are listed in Table 2.4.1–4 together with the experimental results. In the tables, h_{0b} is the still water depth at the breaking point, l_p the distance from the breaking point to the plunging point and l_t the distance from the breaking point to the transition point.

Table 2.4.1 Conditions and results of experiments of series C–1 ($\tan\beta = 1/10$).

case	T (s)	h_i (cm)	H_i (cm)	H_0/L_0	h_{0b} (cm)	l_p/h_{0b}	l_t/h_{0b}
C–1–1	0.617	19.67	5.92	0.1040	7.34	–[1)]	4.77
C–1–2	0.705	19.68	6.38	0.0882	7.35	2.04	4.76
C–1–3	0.800	19.69	7.68	0.0840	8.25	2.31	4.85
C–1–4	0.901	19.69	7.48	0.0646	7.76	2.58	6.44
C–1–5	1.003	19.70	6.54	0.0454	7.37	2.71	6.51
C–1–6	1.105	19.72	6.79	0.0383	7.39	3.38	7.44
C–1–7	1.197	19.74	6.66	0.0316	7.22	3.33	7.35
C–1–8	1.295	19.75	5.97	0.0237	7.91	3.03	6.32
C–1–9	1.393	19.80	6.61	0.0223	6.98	3.72	7.16
C–1–10	1.501	19.81	7.67	0.0218	8.17	3.43	7.09
C–1–11	1.617	19.83	6.23	0.0149	7.50	2.53	6.40

1) spilling breaker

Table 2.4.2 Conditions and results of experiments of series C–2 ($\tan\beta = 1/20$).

case	T (s)	h_i (cm)	H_i (cm)	H_0/L_0	h_{0b} (cm)	l_p/h_{0b}	l_t/h_{0b}
C–2–1	0.631	18.12	6.46	0.1100	9.73	–[1)]	5.66
C–2–2	0.700	18.13	6.66	0.0939	9.49	–[1)]	5.80
C–2–3	0.794	18.14	6.80	0.0755	9.50	–[1)]	6.32
C–2–4	0.910	18.15	8.03	0.0679	10.75	–[1)]	6.98
C–2–5	0.998	18.16	7.57	0.0529	8.78	2.39	6.83
C–2–6	1.101	18.19	7.16	0.0404	9.55	–[1)]	7.86
C–2–7	1.182	18.19	5.11	0.0247	10.05	2.49	7.96
C–2–8	1.276	18.24	7.48	0.0304	9.35	3.85	9.63
C–2–9	1.389	18.26	6.19	0.0208	8.88	2.37	7.89
C–2–10	1.499	18.27	5.79	0.0163	8.14	2.46	7.37
C–2–11	1.613	18.28	5.80	0.0137	6.91	2.89	7.23

1) spilling breaker

Table 2.4.3 Conditions and results of experiments of series C–3 ($\tan\beta = 1/30$).

case	T (s)	h_i (cm)	H_i (cm)	H_0/L_0	h_{0b} (cm)	l_p/h_{0b}	l_t/h_{0b}
C–3–1	0.614	19.82	5.29	0.0938	7.88	–[1)]	9.52
C–3–2	0.701	19.84	5.86	0.0818	8.71	–[1)]	9.18
C–3–3	0.796	19.85	6.25	0.0690	9.21	–[1)]	9.22
C–3–4	0.895	19.87	6.36	0.0557	8.91	–[1)]	10.11
C–3–5	0.997	19.89	7.27	0.0511	10.39	–[1)]	9.63
C–3–6	1.100	19.91	7.30	0.0417	10.41	–[1)]	9.60
C–3–7	1.192	19.97	6.94	0.0332	11.78	–[1)]	9.76
C–3–8	1.300	19.99	6.07	0.0239	10.00	–[1)]	10.50
C–3–9	1.388	20.00	6.63	0.0226	10.18	–[1)]	11.30
C–3–10	1.493	20.02	6.65	0.0192	10.85	1.11	8.75
C–3–11	1.610	20.04	6.07	0.0147	9.08	2.20	8.82
C–3–12	1.697	20.06	6.22	0.0133	8.12	1.97	9.24
C–3–13	1.800	20.08	6.83	0.0127	8.14	3.32	9.21

[1)] spilling breaker

Table 2.4.4 Conditions and results of experiments of series C–4 ($\tan\beta = 1/50$).

case	T (s)	h_i (cm)	H_i (cm)	H_0/L_0	h_{0b} (cm)	l_p/h_{0b}	l_t/h_{0b}
C–4–1	0.624	20.07	6.41	0.1103	10.42	–[1)]	13.43
C–4–2	0.712	20.16	6.43	0.0872	10.21	–[1)]	13.71
C–4–3	0.810	20.21	6.73	0.0716	10.06	–[1)]	13.42
C–4–4	0.898	20.26	7.24	0.0630	11.21	–[1)]	14.27
C–4–5	0.997	20.31	7.44	0.0524	11.46	–[1)]	13.52
C–4–6	1.122	20.40	7.00	0.0383	10.75	–[1)]	14.41
C–4–7	1.196	20.44	6.66	0.0318	10.29	–[1)]	15.07
C–4–8	1.300	20.48	6.18	0.0245	8.73	–[1)]	13.74
C–4–9	1.413	20.53	6.00	0.0197	9.78	–[1)]	17.38
C–4–10	1.496	20.60	6.12	0.0176	9.85	–[1)]	15.73
C–4–11	1.605	20.67	5.82	0.0142	10.62	–[1)]	10.83
C–4–12	1.711	20.86	5.26	0.0111	7.71	3.24	11.03

[1)] spilling breaker

2.4.3 Distance from Breaking Point to Plunging and Transition Points

Figure 2.4.1 shows the dimensionless property, l_t/h_{0b}, which is obtained from the ratio of the distance between the breaking point and the transition point to the still water depth at the breaking point as a function of the deep water wave steepness H_0/L_0. As for the plunging points, the distance, l_p, from the breaking point divided by h_{0b} is shown by the dotted lines in the figure. The quantity l_t/h_{0b} is nearly independent of the wave steepness and takes an almost constant value for each slope, although it fluctuates a little. Since the incident wave height does not vary so much, it shows that the distance to the transition point does not depend on the wavelength. It can also be considered that the distance to the plunging point is slightly influenced by the wave steepness though the influence due to the bottom slope is not obvious because plunging-type breaking happened only in few cases on a mild slope such as 1/30 or 1/50.

Figure 2.4.2 shows the relation between the dimensionless value $(h_{0b}-h_{0t})/h_{0b}$ (h_{0b} and h_{0t}: the still water depths at the breaking and transition points) and the surf similarity parameter ξ_0 ($\equiv \tan\beta/\sqrt{H_0/L_0}$) in order to compare with the criterion presented by Basco and Yamashita (1986). It is obvious from the figure that it is difficult to express a general relation in terms of such parameters.

The relation between the averaged value of l_t/h_{0b} for each slope and the bottom slope is shown in Fig. 2.4.3. The marks in the figure express the averages and the vertical lines express the fluctuations. The solid line expresses

$$l_t = \left(\frac{1}{5\tan\beta}+4\right)h_{0b} \tag{2.4.1}$$

by which the transition point can roughly be estimated.

As for the plunging points, the averages are nearly constant and do not depend on the bottom slope, although the data for plunging breakers on milder slopes

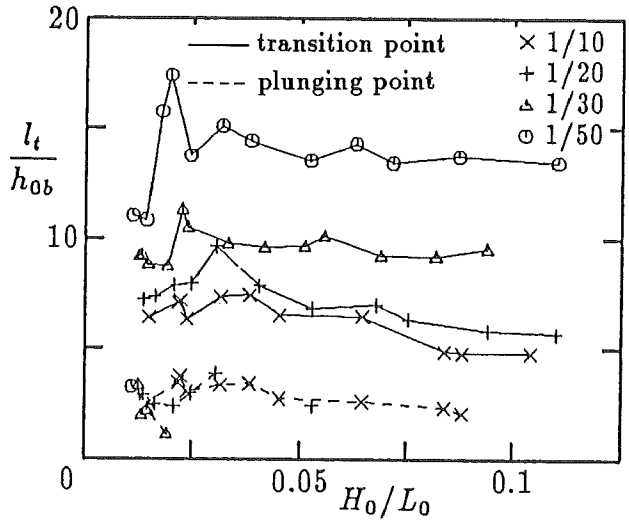

Fig. 2.4.1 Relationships between H_0/L_0 and l_t/h_{0b}.

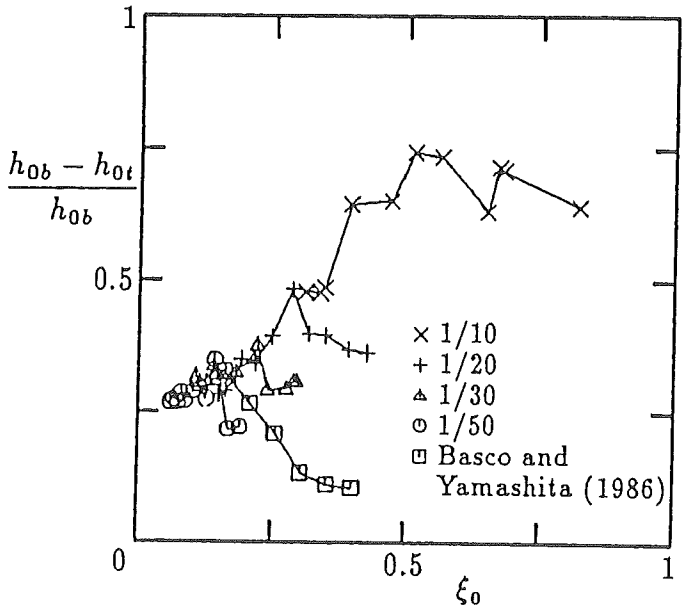

Fig. 2.4.2 Relationships between ξ_0 and $\frac{h_{0b}-h_{0t}}{h_{0b}}$.

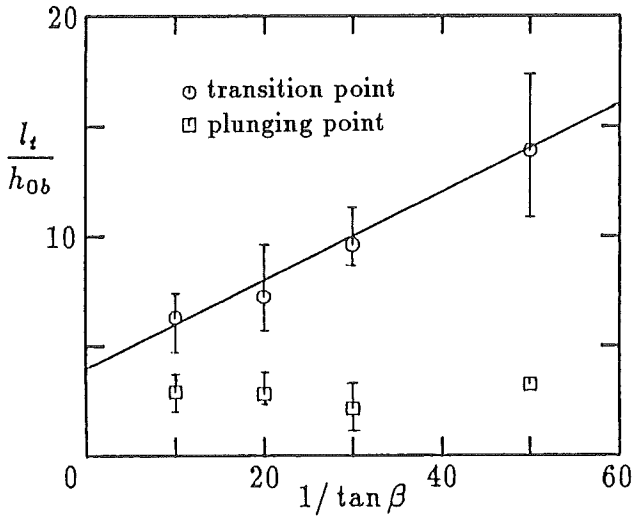

Fig. 2.4.3 Relationships between $\frac{1}{\tan\beta}$ and l_t/h_{0b}.

are few as mentioned before. Svendsen and Hansen (1986) adopted the relation expressed by $h_{0p}/h_{0b} = 0.8$, where h_{0p} is the still water depth at the plunging point, to determine the plunging point. The experimental result of the present study is contrary to it.

If the wave plunging is subject to the free fall and the water particle velocity at the top of the wave and the vertical distance for the water particle falling are assumed to be the wave celerity by the small amplitude wave theory $\sqrt{gh_{0b}}$ and the wave height $H_b \simeq h_{0b}$, respectively, the distance from the breaking point to the plunging point l_p must be $\sqrt{2}\,h_{0b}$ which depends only on the water depth. On the other hand, the distance is expressed roughly as

$$l_p = 2.5h_{0b} \tag{2.4.2}$$

in Fig. 2.4.3. It can be considered that the reasons why the factor in Eq. (2.4.2) is larger are the plunging points were determined by the onshore end of the plunging jets and the water particle velocity at the top of the wave crests should be larger than $\sqrt{gh_{0b}}$.

On the contrary, Eq. (2.4.1) can be interpreted as the sum of the distance given by the water depth and the distance depending on the bottom slope (or the surf zone width).

CHAPTER 3

Modeling of Undertow

3.1 Introduction

In order to predict the sediment transport rate, material diffusion or wave attenuation rate in the surf zone, it is necessary to estimate the velocity distribution with high accuracy. Especially for the sediment transport rate and the bottom friction, the prediction of the velocity near the bottom is necessary.

Longuet-Higgins (1953) derived a laminar solution of mass transport velocity in the fluid with assumption that non-linear acceleration term in the conduction equation is negligible compared with the viscous term. The solution obtained by Longuet-Higgins cannot be applied to the turbulent flow in the surf zone. Svendsen (1984c) presented a model of vertical distribution of cross-shore steady current in the surf zone applying the eddy viscosity model. He used a boundary condition which was the mass transport velocity on the bottom given by the Stokes wave theory. Okayasu *et al.* (1986) gave one of the boundary conditions by the slip condition on the bottom. Stive and Wind (1986) and Tsuchiya *et al.* (1988) investigated a model with a boundary condition at the trough level. Nadaoka and Hirose (1986) evaluated the diffusion coefficient in the surf zone. They also obtained the vertical distribution of the steady current from that of the mean vorticity.

However, the above mentioned studies are not adequate to evaluate the velocity distribution close to the bottom or the shear stress on the bottom. From this point of view, Okayasu *et al.* (1988) presented a model in which the distribution of the mean eddy viscosity coefficient was assumed to be a linear function of the vertical coordinate and to be zero at the bottom, while the above mentioned models were formulated with the depth-independent eddy viscosity. Svendsen *et al.* (1987) also

evolved Svendsen's model considering the bottom boundary layer and the bottom shear stress theoretically, but the application of the models is limited to the inner region.

The variation of the wave height or the cross-shore distribution of the energies in the surf zone is necessary to evaluate the undertow and to consider other various practical problems as well. Mizuguchi (1980) presented a model to estimate the wave height variation in the surf zone with formulation of the energy dissipation rate by wave breaking. Izumiya and Horikawa (1984) presented a model for evaluating the change of the wave energy in the surf zone without converting to the variation of the wave height so that the model can estimate the radiation stress accurately. These models were constructed on the concept that the loss of the wave energy is locally balanced with the energy dissipation. However the organized large vortexes whose importance was already verified in Chapter 2 should be taken into account as the transmitter of mass, momentum and energy. A comprehensive model which describes the wave and velocity field throughout the surf zone on the basis of the accurate understanding of the energy process is therefore required for practical uses.

In this chapter, based on the results obtained in Chapter 2, a model which estimates the two-dimensional distribution of the undertow will be presented. First the transfer of energy in the surf zone will be described with consideration of the physical process of the energy transfer in the surf zone. Then applying the time-dependent mild slope equation, the energy variation and energy dissipation rate in the surf zone will be estimated. The existence of the large vortexes gives a specific feature to the energy dissipation process and to the mass flux in the surf zone. Hence, the organized large vortexes formed in the wave crests will be considered for an accurate description of the wave field and velocity field in the surf zone.

An attempt to combine the previous models for the undertow and the longshore

current was made by Svendsen and Lorenz (1989) to cope with much more general conditions. The present model can easily be expanded to the comprehensive three-dimensional model by virtue of the applicability of the time-dependent mild slope equation.

3.2 Energy Transfer in the Surf Zone

The evaluation of the steady current distribution is very important for estimating the convective diffusion of materials, the sediment transport in the surf zone and others. However, the wave field in the surf zone is so different from that in offshore region that it is necessary to investigate the velocity field in all its aspects. The most different point compared with the offshore region is the wave breaking in the surf zone. The energy conveyed from the offshore region dissipates by the wave breaking. The dissipation rate of the energy is far larger than that in the offshore region. Strong turbulence is generated in the dissipation process. The turbulence gives a specific feature to the velocity field in the surf zone as shown in Chapter 2.

The bore-like waves give another specific feature to the velocity field in the surf zone. Organized large vortexes are formed in front of the crests of the bore-like waves. The large vortexes transport a large amount of mass onshoreward; therefore it is natural that the large vortexes also have considerable energy flux. Hence, it can be considered that the organized large vortexes play an important role in the generation process of the turbulence. The high turbulent intensity observed near the surface confirms the concept. The organized large vortexes are the transporter of the large mass, the transmitter of the energy and the generator of the turbulence.

First of all, an outline of the energy transfer in the surf zone will be described qualitatively in this section. It will be mentioned later, in §3.5, how each part of the energy will be estimated in the actual calculation in this model. For the proper description of the energy transfer in the surf zone, it is necessary to take the energy of the large vortexes into account as mentioned above. The total energy in the surf zone should therefore be described as

$$E_t = E_w + E_v \tag{3.2.1}$$

where E_t is the total energy, E_w the energy of wave motion and E_v the energy of organized large vortexes. Generally, the wave energy can be divided into two parts: the potential energy E_p and the kinetic energy E_k as

$$E_w = E_p + E_k \tag{3.2.2}$$

Energy exchange between the potential and kinetic energies takes place during propagation of waves. The energy E_k in Eq. (3.2.2) is therefore defined as the transferable kinetic energy. Though the energy of the organized large vortexes should be classified as the kinetic energy in the general sense, it is denoted as another variable here. The reason is that it can be considered that the energy of the large vortexes is conveyed to smaller size eddies, never transferred back to the wave motion.

In the early stage of the breaking process, the turbulent intensity is still small, although the wave height rapidly decreases as shown in §2.3.5. It can be considered that the energy transferred to the kinetic energy cannot be regarded as the wave kinetic energy E_k because the potential and kinetic energies of the wave motion is in balance in some way as mentioned just before. A little part of the lost energy should be directly transferred to the turbulence, but it is natural to consider that the most part of the energy is transferred to the energy of the organized large vortexes. Hence, in this model, it is assumed that the wave energy is first converted to that of the organized large vortexes formed in front of the wave crests. After the conversion, the energy is transferred to smaller size eddies, then dissipates.

Since the energy flux by wave motion is denoted by $E_w c_g$, the transfer rate from the wave energy to the energy of the vortexes per unit length and unit width is expressed as

$$T_B = -\frac{d(E_w c_g)}{dx} \tag{3.2.3}$$

If the energy which is directly transferred from the wave energy to the turbulence is little, the energy flux by the large vortexes can be denoted as

$$\frac{d(E_v c_g)}{dx} = T_B - D_B \tag{3.2.4}$$

where D_B is the dissipation rate per unit area by wave breaking. If it is assumed that the organized large vortexes propagate with the wave crests, the energy flux should be described by $E_v c$. But the group velocity c_g is nearly equals to the phase velocity c in the surf zone and it is not clear how fast the vortexes are. Hence the phase velocity is replaced by the group velocity for the simplicity of the model.

From Eqs. (3.2.1), (3.2.3) and (3.2.4), D_B is also expressed as

$$D_B = -\frac{d(E_t c_g)}{dx} \tag{3.2.5}$$

3.3 Mass Balance in the Surf Zone

The steady current distribution in the surf zone is much different from that of any wave theories solved in the inviscid condition. The organized large vortexes which are formed just in front of the wave crest of the bore-like wave propagating in the surf zone affects the mass flux balance and the turbulence generation as shown in Chapter 2. In this section, the general aspects of the mass balance in the surf zone will be discussed. Then it will be considered that how it can be expressed in terms of the energy.

3.3.1 Mass Flux in the Surf Zone

Since the wave field which is completely two-dimensional is considered in this study, the velocity component in the longshore direction is assumed to be zero. The continuity equation of time averaged values of the velocity components becomes

$$\frac{\partial U}{\partial x} + \frac{\partial W}{\partial z} = 0 \tag{3.3.1}$$

where U and W are the steady current components in the cross-shore and the vertical direction, respectively. Since the boundary condition is given as $U = 0$ at the shoreline, the integral property in the vertical direction of Eq. (3.3.1) is obtained as

$$\int_{-h_0}^{\zeta_c} U\,dz = 0 \tag{3.3.2}$$

where h_0 is the still water depth and ζ_c is the wave crest level. The above equation can also be expressed as

$$\begin{aligned} M_t &= \int_{\zeta_t}^{\zeta_c} U\,dz \\ &= -\int_{-h_0}^{\zeta_t} U\,dz \end{aligned} \tag{3.3.3}$$

where ζ_t is the wave trough level. The value M_t is defined as the mass flux by waves which is the mass transport above the trough level per unit time and unit width.

The second line in Eq. (3.3.3) can be considered as the compensatory flow of the mass flux by waves and is termed "undertow" in the surf zone.

Outside the surf zone, the mass flux M_t is caused only by the wave motion. But in the surf zone, the mass flux by organized large vortexes is considerably large as found in §2.3.3. In other words, the total mass flux by breaking waves should be expressed as

$$M_t = M_w + M_v \tag{3.3.4}$$

in which M_w is the mass flux by wave motion and M_v is the mass flux by organized large vortexes. Actually, it is impossible to divide the mass flux in the two parts exactly, because it is difficult to define the boundary of the organized vortexes [Peregrine and Svendsen (1978)].

3.3.2 Mass Flux due to Wave Motion

The wave component of the water particle velocity calculated by the stream function method which was presented by Dean (1965) is reliable as reported by Isobe *et al.* (1979), but the computation takes much time. Moreover, the stream function method needs full information of the time history of water surface elevation which is difficult to obtain in the surf zone. If the mass flux by wave motion can be estimated from the wave energy distribution, the problem becomes much easier. Hence in this section, application of the linear long wave theory to the estimation of the mass flux by wave motion will be considered by comparing with the stream function method.

By using the linear long wave theory, the mass flux by wave motion is described as

$$M_{\mathrm{LLW}} = \overline{\int_{\zeta_t}^{\zeta} u\, dz}$$

$$= \overline{\int_{\zeta_t}^{\zeta} \frac{c}{h}(\zeta - \overline{\zeta})\, dz}$$
$$= \frac{c}{h}\overline{(\zeta - \overline{\zeta})^2} \tag{3.3.5}$$

where M_{LLW} is the mass flux calculated by the linear wave theory, ζ the water surface elevation, c the wave celerity and h the mean water depth. Since $\overline{\ }$ expresses the time average, $\overline{\zeta}$ is the wave setup.

Figure 3.3.1 shows the comparisons between the mass flux variation calculated by the stream function method and the linear long wave theory from measured water surface profiles in the surf zone. Examples are given for cases B–2, B–3 and B–5 presented in Chapter 2. The incident wave conditions have been already shown in Table2.2.2. In Fig. 3.3.1, the solid lines show the values calculated by the stream function method and the dashed lines show those by the linear long wave theory. Though difference exists between the solid lines and the dashed lines, they agree qualitatively. From the experiments of Series B, it is found that the values calculated by the stream function method can be approximated by the linear long wave theory as

$$M_w \simeq M_{\mathrm{SFM}} \simeq 0.8 M_{\mathrm{LLW}} \tag{3.3.6}$$

where M_{SFM} is the mass flux calculated by the stream function method. The coefficient in Eq. (3.3.6) is obtained by averaging the ratio of the two values for all the cases of Series B. The values modified by multiplying 0.8 to M_{LLW} are also shown in Fig. 3.3.1 with M_{SFM} and M_{LLW}. They agree well, so that the mass flux by wave motion can be evaluated by using the linear long wave theory.

Since Eq. (3.3.5) also needs the time history of the surface elevation, it is of little advantage. The potential energy of waves is defined as

$$E_p = \frac{1}{T}\int_0^T \rho g(\zeta - \overline{\zeta})\, dt$$
$$= \frac{1}{2}\rho g\, \overline{(\zeta - \overline{\zeta})^2} \tag{3.3.7}$$

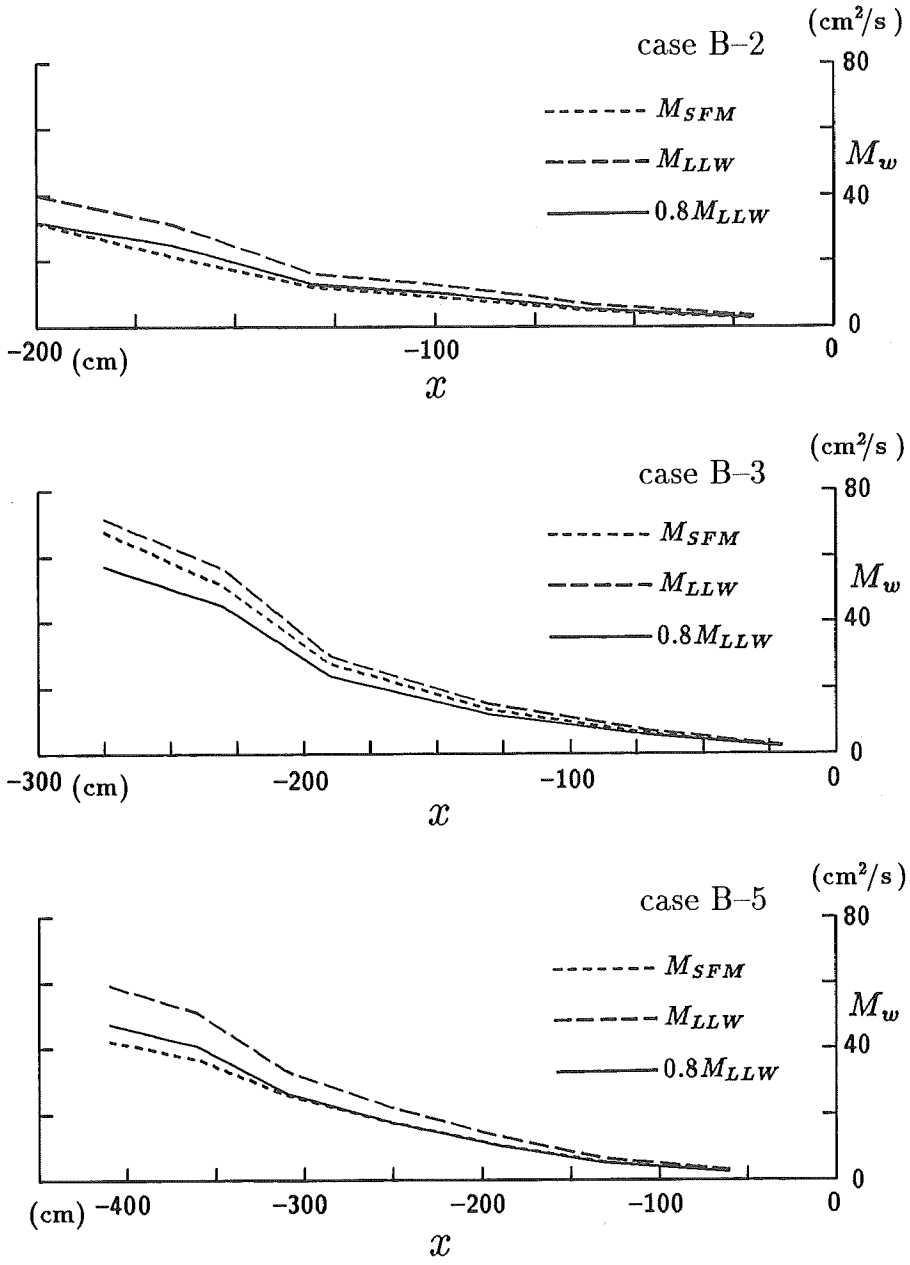

Fig. 3.3.1 Comparison of the cross-shore variations of M_{SFM}, M_{LLW} and $0.8M_{LLW}$ (cases B–2, B–3 and B–5).

where T is the wave period. Then from Eq. (3.3.7), Eq. (3.3.5) can be replaced by

$$M_{\mathrm{LLW}} = \frac{2c}{\rho g h} E_p \tag{3.3.8}$$

This means the mass flux by the wave motion can be estimated from the potential energy. Consequently, the mass flux by the wave motion can be evaluated by the following equation:

$$M_w = \frac{1.6c}{\rho g h} E_p \tag{3.3.9}$$

Equation (3.3.9) is obtained by regarding the area occupied by the organized vortexes as the area of the wave motion. However, the area of vortexes should be much smaller than that of wave motion. Svendsen (1984b) approximated the area of the vortex by $0.9H^2$ based on the experimental results on a breaker behind a towed hydrofoil obtained by Duncan (1981). Okayasu *et al.* (1986) found that it can be expressed by $0.06HL$ which was confirmed by Hansen (1989) later. In both cases, the area is small compared to the cross section of a wave.

3.3.3 Mass Flux due to Organized Large Vortexes

In this section, the velocity distribution inside the organized large vortexes formed in front of wave crests will be assumed. From the assumption, the area of the section and the mass transport by the vortexes will be estimated.

The velocity distribution inside one vortex is assumed as shown in Fig. 3.3.2 (a). Although the vortexes generated in front of the wave crests decelerate and go downward, the mean horizontal velocity can be assumed the same as the wave celerity at the first stage. The diameter of the vortex is given by the wave height H.

The velocity can be divided into the rotational component u_1 and the parallel component u_2. Figure 3.3.2 (b) shows the former part of the velocity and Fig. 3.3.2 (c) shows the latter. The total velocity u is expressed as

$$u = u_1 + u_2 \tag{3.3.10}$$

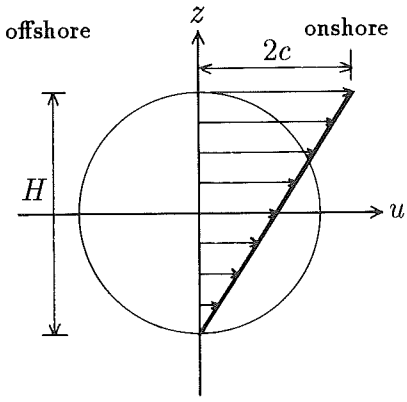

(a) total velocity

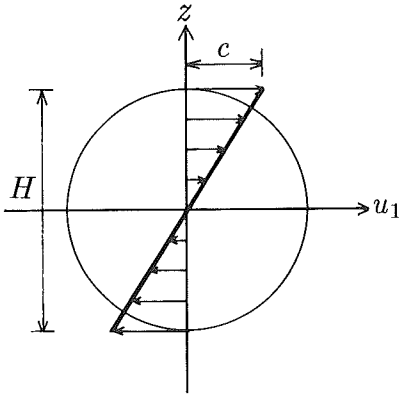

(b) rotational component

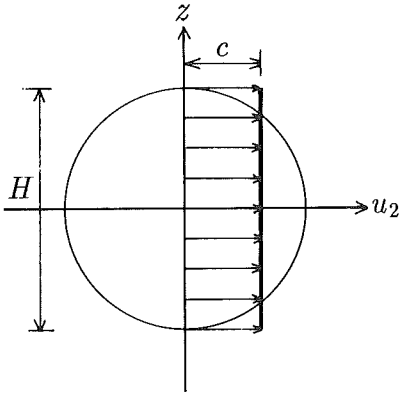

(c) parallel component

Fig. 3.3.2 Assumption of velocity distribution of an organized large vortex.

$$u_1 = \frac{2c}{H} r, \quad u_2 = c \tag{3.3.11}$$

where r is the radial coordinate. The energy, E_1, of the rotational component per unit width is given as

$$\begin{aligned} E_1 &= \int_0^{\frac{H}{2}} \frac{1}{2} \rho {u_1}^2 2\pi r \, dr \\ &= \frac{1}{16} \pi \rho c^2 H^2 \end{aligned} \tag{3.3.12}$$

The parallel component E_2 is also given as

$$E_2 = \frac{1}{8} \pi \rho c^2 H^2 \tag{3.3.13}$$

The total energy of one vortex per unit width E_3 is obtained as

$$\begin{aligned} E_3 &= E_1 + E_2 \\ &= \frac{3}{16} \pi \rho c^2 H^2 \end{aligned} \tag{3.3.14}$$

Even if the vortex is skewed or the real velocity distribution is slightly different from the assumption, it influences only the constant value in Eq. (3.3.14). The total energy should be proportional to $c^2 H^2$. Svendsen (1984b) presented the model that there is one skewed vortex, so-called "surface roller" in front of the waves. On the other hand, Nadaoka (1986) described that there should be plural vortexes (Fig. 3.3.3). The following discussion applies to both models.

The section of one vortex A_1 is given as

$$A_1 = \frac{\pi}{4} H^2 \tag{3.3.15}$$

From Eqs. (3.3.14) and (3.3.15), the energy, e_v, of the vortex per unit mass is obtained as

$$e_v \equiv \frac{1}{\rho} \frac{E_3}{A_1} = \frac{3}{4} c^2 \tag{3.3.16}$$

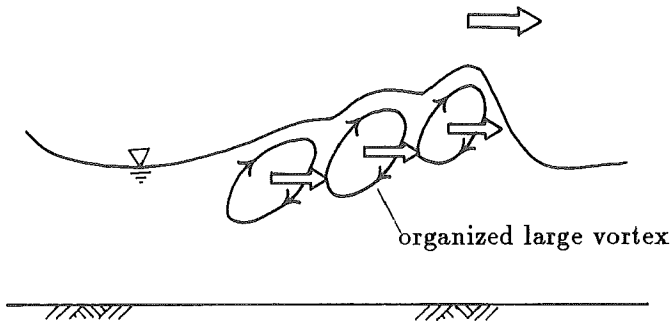

Fig. 3.3.3 Conceptual illustration of plural vortexes in one wave. [Nadaoka (1986)]

If there are some vortexes in one wave crest, for example as shown in Fig. 3.3.5, the energy, E_v, of the vortexes per unit width and unit length can be expressed as

$$E_v = \rho \frac{A e_v}{L} \tag{3.3.17}$$

where A is the total area of the vortexes per wave and L is the local wave length. Substituting Eq. (3.3.16) into Eq. (3.3.17), A is expressed as

$$A = \frac{4}{3} \frac{L}{\rho c^2} E_v \tag{3.3.18}$$

The mass flux, M_v, due to the vortexes is expressed by the following equation:

$$M_v = \frac{\rho c A}{L} = \frac{4}{3c} E_v \tag{3.3.19}$$

The above formula implies the mass flux due to organized large vortexes can be estimated from the energy of the vortexes. In actual calculation, the factor $\frac{4}{3}$ in Eq. (3.3.19) is modified to 2 so as to fit the measured values. Hence, Eq. (3.3.19) is replaced by

$$M_v = \frac{2}{c} E_v \tag{3.3.20}$$

Finally, from Eqs. (3.3.4), (3.3.9) and (3.3.20), the total mass flux due to breaking waves can be described in terms of the potential energy and the energy of organized large vortexes as

$$M_t = \frac{1.6c}{\rho g h} E_p + \frac{2}{c} E_v \tag{3.3.21}$$

3.4 Momentum Balance in the Surf Zone

In case of cross-shore vertically two-dimensional (2-VD) models such as discussed in this study, the longshore variation of the momentum flux need not be considered, but the momentum flux variation in the cross-shore direction causes the wave setup which can not be neglected to describe the wave field accurately. The radiation stress which is defined as the excess momentum flux due to waves is expressed as

$$S_{xx} = \overline{\int_{-h_0}^{\zeta} (\rho u^2 + p)\, dz} - \frac{1}{2}\rho g h^2 \tag{3.4.1}$$

where p is the pressure. The gradient of S_{xx} in the x-direction should balance the gradient of the mean water elevation, that is

$$\frac{dS_{xx}}{dx} = -\rho g h \frac{d\bar{\zeta}}{dx} \tag{3.4.2}$$

By the small amplitude wave theory, the radiation stress S_{xx} is expressed in terms of the wave energy E_w as

$$S_{xx} = \left(\frac{1}{2} + \frac{2kh}{\sinh 2kh}\right) E_w \tag{3.4.3}$$

for monochromatic waves. For the shallow water condition, the value inside the parentheses in Eq. (3.4.3) can be replaced by 3/2.

Most of the previous studies adopted a simple equation (3.4.3) for calculating the wave setup in the surf zone because of the inordinate complication of wave field. But in making an effort to describe the momentum balance correctly, at least one should consider the momentum flux by the organized large vortexes in the surf zone. If the velocity field of wave motion and the velocity field of large vortexes do not affect each other as already introduced in §3.2, the radiation stress can also be divided into two parts as

$$S_{xx} = S_w + S_v \tag{3.4.4}$$

where S_w is the excess momentum flux by wave motion and S_v is that by organized large vortexes.

Generally the small amplitude theory cannot express the wave motion adequately in shallow water condition because of the strong effect of the non-linearity of waves. The finite amplitude theories can express it much more accurately offshoreward of the breaking point; however, they cannot either be applied to the description of the wave field in the surf zone as mentioned before. The small amplitude wave theory is therefore adopted for convenience to calculate the radiation stress by wave motion in this study. The radiation stress, S_w, due to wave motion is calculated in this model according to Watanabe and Dibajnia (1988) for a complex wave field.

To calculate the total radiation stress S_{xx} by Eq. (3.4.1), it is necessary to estimate the radiation stress, S_v, due to organized large vortexes. S_v is defined as

$$S_v = \overline{\int_{\zeta_b}^{\zeta} \{\rho u^2 + (p - p_s)\}\, dz} \tag{3.4.5}$$

where ζ_b is the boundary between the velocity field of wave motion and that of vortexes and p_s the static pressure. If a vortex is flat, the quantity $\dfrac{\partial w}{\partial t}$ is so small that the the term $(p - p_s)$ is negligible except at the both ends of the vortex. At the front and rear ends, $\dfrac{\partial w}{\partial t}$ is large so that the pressure deviates a lot from the static value. It can be considered that it makes the fluctuating upper surface boundary. Since the deviation of the pressure is negligible in the most part of a vortex, the following equation can be obtained:

$$S_v = \overline{\int_{\zeta_b}^{\zeta} \rho u^2\, dz} \tag{3.4.6}$$

Here, the velocity distribution is assumed again as shown in Fig. 3.3.2 (a). The radiation stress by one vortex S_1 is denoted as

$$S_1 = \frac{1}{L} \int_{A_1} \rho u^2\, dx dz$$

$$= \frac{1}{L} \int_{A_1} \rho (u_1 + u_2)^2 \, dxdz$$
$$= \frac{1}{L} \frac{5}{3} E_3 \tag{3.4.7}$$

where A_1 is the area occupied by the vortex. From Eqs. (3.3.16) and (3.3.17), the energy of the vortexes is expressed as

$$E_v = \frac{A}{A_1} \frac{E_3}{L} \tag{3.4.8}$$

Then the total radiation stress by the organized large vortexes is obtained as

$$S_v = \frac{A}{A_1} S_1 = \frac{5}{3} \frac{A}{A_1} \frac{E_3}{L}$$
$$= \frac{5}{3} E_v \tag{3.4.9}$$

As well as for the wave induced momentum flux, the momentum flux due to organized large vortexes is expressed as a function of the energy of the vortexes.

3.5 Estimation of Energy Distribution in the Surf Zone

In this section, the wave energy distribution will be estimated by using the time-dependent mild slope equation. The time-dependent mild slope equation can deal with wave transformation under combined reflection, refraction, diffraction and breaking in horizontal two-dimensional (2-HD) models. The present model which is developed by considering the phenomena in the surf zone more precisely has also an advantage that it can easily be combined with the 2-HD nearshore wave field models such as Watanabe and Maruyama (1986) and extended to three-dimensional (3-D) nearshore current models.

Since the mild slope equation was originally derived by using the linear wave theory, the energy calculated by the time-dependent mild slope equation should be considered as the energy of wave motion which is denoted as E_w in Eq. (3.2.1). Consequently, the energy of the organized large vortexes is not included in the calculation because it can be considered that the energy of the large vortexes is never transferred to the wave motion as already mentioned in §3.2. The estimation of the energy of the organized large vortexes needs another equation based on Eq. (3.2.4). The method will also be discussed in this section.

3.5.1 Governing Equations of Time-Dependent Mild Slope Equation

The mild slope equation was first obtained by Berkhoff (1972) for a stationary wave field as

$$\nabla \cdot (cc_g \nabla \hat{\phi}_0) + \sigma^2 \frac{c_g}{c} \hat{\phi}_0 = 0 \tag{3.5.1}$$

where $\nabla = \left(\frac{\partial}{\partial x}, \frac{\partial}{\partial y} \right)$, y is the horizontal coordinate in the longshore direction, c the phase velocity, c_g the group velocity, σ the angular frequency and $\hat{\phi}_0$ the amplitude of the velocity potential at the mean water level given by the small-amplitude wave theory. Watanabe and Maruyama (1986) derived a set of equations

equivalent to Eq. (3.5.1) in terms of the water surface elevation ζ and the flow rate $\mathbf{Q}$ as follows:

$$\frac{\partial \mathbf{Q}}{\partial t} + \frac{c^2}{n}\nabla(n\zeta) = 0 \tag{3.5.2}$$

$$\frac{\partial \zeta}{\partial t} + \nabla \cdot \mathbf{Q} = 0 \tag{3.5.3}$$

where

$$n = \frac{1}{2}\left(1 + \frac{2kh}{\sinh 2kh}\right) \tag{3.5.4}$$

$$\mathbf{Q} = (Q_x, Q_y) \tag{3.5.5}$$

$$Q_x = \int_{-h}^{0} u\, dz\,, \quad Q_y = \int_{-h}^{0} v\, dz \tag{3.5.6}$$

and u and v are horizontal velocity components in x and y direction, respectively. A set of equations completely equivalent to Eq. (3.5.1) was also presented by Nishimura *et al.* (1983) as

$$\frac{\partial \mathbf{Q}'}{\partial t} + c^2 \nabla \zeta = 0 \tag{3.5.7}$$

$$\frac{\partial \zeta}{\partial t} + \frac{1}{n}\nabla \cdot (n\mathbf{Q}) = 0 \tag{3.5.8}$$

The variable $\mathbf{Q}'$ has a difference of order of ∇n from the flow rate $\mathbf{Q}$ in Eq. (3.5.5).

Watanabe and Maruyama (1986) added a term to Eq. (3.5.2) so that the equations could express the energy attenuation due to the breaking. The equation is as follows:

$$\frac{\partial \mathbf{Q}}{\partial t} + \frac{c^2}{n}\nabla(n\zeta) + f_T \mathbf{Q} = 0 \tag{3.5.9}$$

The third term of Eq. (3.5.9) is generally called "the energy dissipation term", but it is termed "the energy transfer term" in this study because the lost energy does not dissipate directly but is once transferred to the energy of the organized large vortexes in the present model. The value f_T which is also termed "the transfer factor" by the breaking is determined as

$$f_T = \alpha_T \tan\beta \sqrt{\frac{g}{h}\left(\frac{\hat{Q}}{Q_r} - 1\right)} \tag{3.5.10}$$

$$\hat{Q} = \sqrt{\hat{Q}_x^2 + \hat{Q}_y^2}, \quad Q_r = \gamma' \sqrt{gh^3} \tag{3.5.11}$$

where $\tan\beta$ is the averaged bottom slope, $\hat{Q}_x$ and $\hat{Q}_y$ are the amplitude of the flow rate components. α_T and γ' were set to 2.5 and 0.25, respectively. By setting $f_T = 0$ after breaking (if $\hat{Q} < Q_r$), wave recovery can be described as well as wave decay in the surf zone. In case of progressive waves, Eqs. (3.5.3) and (3.5.9) reduce to the wave energy equation, that is expressed as

$$\frac{\partial(E_w c_g)}{\partial x} = -f_T n E_w \tag{3.5.12}$$

where E_w is the wave energy per unit area. Considering the physical meaning and the experimental results, Isobe (1987) presented the following equation

$$f_T' = n f_T = -\frac{5}{2} \tan\beta \sqrt{\frac{g}{h}\left(\frac{\gamma - \gamma_r}{\gamma_s - \gamma_r}\right)} f_d(kh) \tag{3.5.13}$$

where $\gamma\,(= k\sqrt{2E_w/\tanh kh}\,)$ is the ratio of water particle velocity to wave celerity. The quantity f_d comes from the formulation in terms of the ratio of water particle velocity to wave celerity instead of wave height to water depth ratio. The value f_d is unity for small kh. The values of γ_s and γ_r were given as

$$\gamma_s = 0.4(0.57 + 5.3\tan\beta) \tag{3.5.14}$$

$$\gamma_r = 0.135 \tag{3.5.15}$$

Watanabe and Dibajnia (1989) added the energy transfer term to Eq. (3.5.7) in the same manner as Watanabe and Maruyama and obtained an one-dimensional model as follows:

$$\frac{\partial Q}{\partial t} + c^2 \frac{\partial \zeta}{\partial x} + f_T Q = 0 \tag{3.5.16}$$

$$\frac{\partial \zeta}{\partial t} + \frac{1}{n}\frac{\partial(nQ)}{\partial x} = 0 \tag{3.5.17}$$

The energy transfer factor f_T was given as

$$f_T = \alpha_T \tan\beta \sqrt{\frac{g}{h}\left(\frac{\gamma - \gamma_r}{\gamma_s - \gamma_r}\right)} \tag{3.5.18}$$

with the shallow water approximation of Eq. (3.5.13). The value α_T is a coefficient which varies from 0 to 2.5 around the braking point for preventing numerical reflections. In Eq. (3.5.18), γ_s was given by Eq. (3.5.14). According to Maruyama and Shimizu (1986), γ_r was replaced by

$$\gamma_r = 0.4 \left(\frac{a}{h}\right)_b \tag{3.5.19}$$

where $\left(\frac{a}{h}\right)_b$ is the ratio of the wave amplitude to the mean water depth at the breaking point.

The time-dependent mild slope equation was obtained by using the small amplitude wave theory. However, waves in the surf zone are no more small amplitude waves. In that sense, the time-dependent mild slope equation may not be appropriate for waves in the surf zone, but it is also a fact that there is no wave theory which can express the waves in the surf zone adequately. It was reported by the above mentioned researchers that the wave energy calculated by the time-dependent mild slope equation fits well with the measured wave energy. Hence, in the present study, Eqs. (3.5.16) and (3.5.17) are essentially adopted as the governing equations to estimate the wave energy variation in the surf zone. The wave height distribution is not discussed in this study.

The wave energy dissipation due to bottom friction should be taken into account for accurate estimation of the wave energy variation. The dissipation by wall friction should also be considered in case of laboratory experiments. Since the computational results will be compared with laboratory experiments in the present study, the dissipation factor by the bottom and wall friction f_{b+w} is added to the attenuation factor by breaking.

The bottom and wall boundary layers in the surf zone may not be laminar flow, but the dissipation by wave breaking is so large that the damping due to the

bottom and wall friction is negligible. In the present study, the energy dissipation by the friction is calculated from the theory for laminar flow.

Iwagaki and Tsuchiya (1966) dealt with laminar damping due to bottom and wall friction for finite amplitude waves. When deducing in the linearized theory, the dissipation factor by friction f_{b+w} is expressed as

$$f_{b+w} = \frac{1}{n}\sqrt{2\nu\sigma}\left(\frac{1}{B} + \frac{k}{\sinh 2kh}\right) \tag{3.5.20}$$

where ν is the kinematic viscosity and B is the width of the wave flume. The dissipation rate by the bottom and wall friction is obtained as

$$D_{b+w} = f_{b+w} n E_w \tag{3.5.21}$$

if no reflected wave exists in the field.

The lost energy by the wave breaking is transferred from the wave energy E_w to the energy, E_v, of large vortexes, but on the contrary, it can be considered that the lost energy by the bottom and wall friction directly dissipates to heat. A series of equations from Eq. (3.2.3) to Eq. (3.2.5) is therefore replaced by following equations:

$$\frac{d(E_w c_g)}{dx} = -T_B - D_{b+w} \tag{3.5.22}$$

$$\frac{d(E_v c_g)}{dx} = T_B - D_B \tag{3.5.23}$$

$$\frac{d(E_t c_g)}{dx} = -D_B - D_{b+w} \tag{3.5.24}$$

On the slope milder than $\tan\beta = 1/10$, the reflection by wave breaking is so small that D_{b+w} is evaluated by Eq. (3.5.21). The variation of E_w is calculated by the scheme expressed as

$$\frac{\partial Q}{\partial t} + c^2\frac{\partial \zeta}{\partial x} + f_A Q = 0 \tag{3.5.25}$$

$$\frac{\partial \zeta}{\partial t} + \frac{1}{n}\frac{\partial (nQ)}{\partial x} = 0 \tag{3.5.26}$$

which are obtained by replacing the energy transfer factor f_T in Eq. (3.5.16) by the total attenuation factor f_A determined as

$$f_A = f_T + f_{b+w} \tag{3.5.27}$$

The energy transfer factor, f_T, of breaking waves expressed by Eq. (3.5.18) is used after Watanabe and Dibajnia. The detailed description of the coefficients γ_s and γ_r in Eq. (3.5.18) will be mentioned in §3.5.4. Since the wave energy is calculated by Eqs. (3.5.25) and (3.5.26), the energy transfer rate can be obtained by using Eq. (3.5.22).

The shoreline and offshore boundary conditions are given according to Watanabe and Dibajnia (1989). They imposed the shoreline boundary condition as $Q = 0$. As for the offshore boundary condition, a non-reflective boundary and sinusoidal incident waves are considered. The incident wave condition is given in terms of the water surface elevation ζ as

$$\zeta(x_0) = \zeta(x_0 + \Delta x) + a_I[\sin(kx_0 - \sigma t) - \sin\{k(x_0 + \Delta x) - \sigma(t - \tau_0)\}] \tag{3.5.28}$$

where $\tau_0 = \dfrac{\Delta x}{c_0}$, Δx is the spacing between mesh points, and σ and a_I are the frequency and the amplitude of the incident waves, respectively. The subscript $_0$ denotes quantities at the offshore boundary.

The method of the numerical computation and the adopted mesh scheme are the same as those employed by Watanabe and Dibajnia. But the convergence of solution is assumed when the absolute errors between the values obtained from two successive cycles of the calculation at every point are less than a tolerance error throughout the field. The required absolute error is equal to $0.02a_I$ for both the wave amplitudes and the setup calculation in the present study.

The functional form of α_T which is different from that proposed by Watanabe and Dibajnia will be mentioned later in §3.5.3. The wave celerity is modified to

prevent the variation of f_T from increasing the numerical reflection. It will be discussed in §3.5.5.

3.5.2 Estimation of Energy Dissipation Rate

Since the time-dependent mild slope equation was obtained by the small amplitude wave theory, the energy calculated by the equation is the energy due to the wave motion. From the discussion in §3.2 it is assumed that the wave energy is first transferred to that of the organized large vortexes formed in front of the wave crests. The transferred energy which is obtained from T_B should dissipate anyhow, because the total amount of the transferred energy throughout the surf zone should be equal to the total amount of the dissipation.

Here it is considered that after the transfer, the energy is converted to smaller size eddies, and then dissipates. This idea is the same as so called "the energy cascade model". Hence, there should be retardation of dissipation. It also means that the energy transferred to the large vortexes takes some distance during the dissipation because the vortexes propagate onshore with the waves.

The problem is how long the transferred energy takes to dissipate. Yamashita *et al.* (1988) performed detailed measurements of behavior of the organized large vortexes in the surf zone and obtained a result that the time interval of the generations of vortexes in front of one propagating wave are almost constant in the inner region and are much larger around the breaking point. The interval should have a relation to the life of a vortex.

In the present model, the energy transferred at one point constantly dissipates within the distance given as

$$l_d = \begin{cases} (4\,\dfrac{x_t - x}{x_t - x_b'} + 4)\,h & (x \le x_t) \\ 4h & (x > x_t) \end{cases} \tag{3.5.29}$$

where x_b' is the crest breaking point which will be discussed in the next section, and x_t the transition point which is given by Eq. (2.4.1). A schematic illustration of Eq. (3.5.29) is shown in Fig. 3.5.1. The values of the constants in Eq. (3.5.29) need further verifications.

A contribution from the energy transferred at $x = x'$ (*i.e.* $T_B(x')$) to the local dissipation rate is expressed as

$$t_d(x,x') = \begin{cases} 0 & (x \le x') \\ \dfrac{T_B(x')}{l_d(x')} & (x' \le x < x' + l_d(x')) \\ 0 & (x' + l_d(x') \le x) \end{cases} \tag{3.5.30}$$

Finally, the total dissipation rate, D_B, by wave breaking is obtained as

$$D_B(x) = \int_{-\infty}^{x} t_d(x,x')\,dx' \tag{3.5.31}$$

3.5.3 Energy Transfer Factor around the Breaking Point

In relation to the breaking of composite waves, Watanabe *et al.* (1984) proposed a breaker index in terms of the ratio of water particle velocity to the wave celerity so as to agree with the breaking criterion proposed by Goda (1970). This criterion was determined to give an accurate prediction of the breaking point when the water particle velocity and the wave celerity by the linear wave theory were used. For convenience for the numerical calculations, Isobe (1987) approximated it by the following formula:

$$\begin{aligned} \gamma_b &\equiv (\hat{u}/c)_b \\ &= 0.53 - 0.3\exp\{-3\sqrt{h_b/L_0}\} + 5\tan^{3/2}\beta\exp\{-45(\sqrt{h_b/L_0} - 0.1)^2\} \end{aligned} \tag{3.5.32}$$

where $\hat{u}$ is the amplitude of horizontal water particle velocity at the still water level, L_0 the deep-water wavelength, and subscript b denotes the quantity at the breaking point. The above equation is adopted in the present study to predict the breaking point.

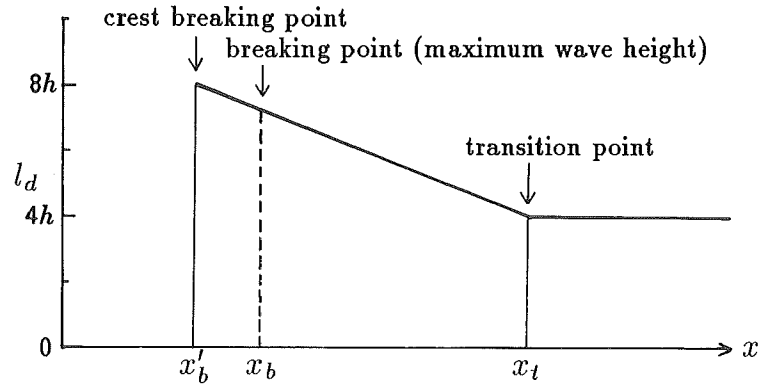

Fig. 3.5.1 Setting of dissipation distance l_d.

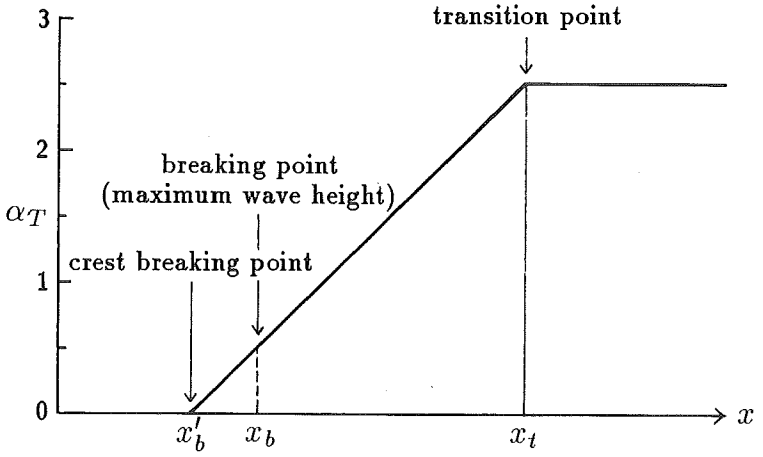

Fig. 3.5.2 Setting of coefficient α_T.

Watanabe and Maruyama (1986) linearly changed the coefficient α_T in Eq. (3.5.18) around the breaking point to avoid numerical reflection caused by the sudden increase of the transfer factor f_T. They set $\alpha_T = 0$ at the point $L_b/4$ before the breaking point and linearly increased to 2.5 at the point $L_b/4$ after the breaking point. The distance L_b is the local wave length at the breaking point. However, the distance $L_b/4$ has no physical reason. The dissipation and the transfer of the energy should occur from the breaking point.

The breaking points slightly differ in accordance with its definition. Seyama and Kimura (1988) measured cross-shore variations of the wave height on constant slopes in the surf zone for irregular wave condition. They defined the breaking point as the point where the crests of propagating waves begin to break and gave a formula presenting the wave height variation of irregular waves for various bottom slopes. From their formula, the distance l_b from the breaking point according to their definition to the point where the wave height takes its maximum value was given as

$$\begin{aligned} l_b &\equiv x_b - x_b' \\ &= \frac{h_b}{\tan\beta}\left\{\frac{1.65\exp(-2.3\tan\beta) + 0.01\tan\beta + 0.37}{1.54\exp(-11.5\tan\beta) - 0.0458\tan\beta(-8.41\tan\beta)}\right. \\ &\qquad \left.\frac{}{-0.67\exp(-3.1\tan\beta) + 0.01\tan\beta + 1.37} - 1\right\} \end{aligned} \tag{3.5.33}$$

in which x_b' is the point where the crest of propagating waves begin to break and x_b is the point where the wave height takes its maximum value.

The energy transfer from the wave motion to the organized large vortexes and also the energy dissipation should occur from the point where the wave crests begin to break. On the other hand, though the breaker index proposed by Watanabe *et al.* deals with the ratio of the water particle velocity to the wave celerity, it can be considered that their index presents the point where the wave height takes its

maximum value for an analogy from the criterion by Goda. The formula proposed by Isobe is also for the same point.

Also in this model, the breaking point is defined as the point where the wave height takes its maximum value, but the energy transfer and dissipation are made to take place from offshoreward of the breaking point determined by using Isobe's formula for the exact description of the energy transfer around the breaking point. The distance between the two points can be calculated by Eq. (3.5.33), and found to be

$$l_b = \begin{cases} 2.55h_b & (\tan\beta = 1/20) \\ 1.96h_b & (\tan\beta = 1/30) \end{cases} \tag{3.5.34}$$

The distance is given by $2h_b$ for the simplicity of the calculation in the present study. Then the crest breaking point x_b' is given as

$$x_b' = x_b - 2h_b \tag{3.5.35}$$

The coefficient α_T in Eq. (3.5.18) is set to be 0 at the crest breaking point x_b' and to be the maximum value 2.5 at the transition point x_t. In other words, α_T is increased in the transition region and fixed in the inner region in the model.

$$\alpha_T = \begin{cases} 0 & (x \le x_b') \\ 2.5\,\dfrac{x - x_b'}{x_t - x_b'} & (x_b' < x \le x_t) \\ 2.5 & (x_t < x) \end{cases} \tag{3.5.36}$$

The variation of α_T is illustrated in Fig. 3.5.2.

3.5.4 Ratio of Potential Energy to Kinetic Energy of Waves

The value of the potential energy is equal to that of the kinetic energy according to the small amplitude wave theory, but the actual ratio of the kinetic energy to the potential energy is not unity in general. Dibajnia *et al.* (1988) calculated the ratio by using finite amplitude wave theories. They obtained the result that the

maximum ratio of the kinetic energy to the potential energy calculated by the finite amplitude wave theory is 1.2 as far as the calculation converged.

Watanabe and Maruyama (1986) imposed the energy dissipation factor from $L_b/4$ before the breaking point to cope with the rapid decreasing of the potential energy after breaking. In this model, although the energy transfer from wave energy takes place from the crest breaking point x_b', the ratio $R_p \equiv \dfrac{E_p}{E_k}$ is made to change linearly from 1 to its minimum at the wave plunging point. Because it can be considered that the breaking waves keep the minimum value as for the ratio R_p. The relationship is expressed as

$$R_p = \begin{cases} 1 & (x \leq x_b') \\ 1 - \left(1 - \dfrac{1}{1.2}\right) \dfrac{x - x_b'}{x_p - x_b'} & (x_b' < x \leq x_p) \\ \dfrac{1}{1.2} & (x_p < x) \end{cases} \tag{3.5.37}$$

where x_p is the wave plunging point. Though the distance from the breaking point to the plunging point is not clear yet, the plunging point x_p $(= x_b + l_p)$ is estimated by Eq. (2.4.2) for convenience.

Adopting Eq. (3.5.37), the calculated potential energy is reduced to about 90% of $\dfrac{1}{2} E_w$. The constant coefficient 0.4 in Eq. (3.5.14) for the value γ_s in Eq. (3.5.18) which can be considered to express the strength of the wave decay was determined so that the potential energy which was given by $\dfrac{1}{2} E_w$ agreed well with the measured value. It should be reduced in proportion to the decrease of the potential energy calculated by means of Eq. (3.5.37), because the variation of R_p accelerates the decrease of the potential energy apparently. Hence, Eq. (3.5.14) is replaced by

$$\gamma_s = 0.35\,(0.57 + 5.3 \tan\beta) \tag{3.5.38}$$

For the same reason, the constant coefficient 0.4 in Eq. (3.5.19) should be increased to keep the potential energy in the recovery zone. γ_r in this model is determined

as

$$\gamma_r = 0.45 \left(\frac{a}{h}\right)_b \tag{3.5.39}$$

3.5.5 Modification of the Wave Celerity

The energy dissipation by wave breaking occurs with little wave reflection, but the calculation by using the time-dependent mild slope equation generates numerical reflection. It is necessary to keep it small for the accurate description of the wave field. Since a rapid change of the energy transfer factor generates considerable wave reflection, one of the reasons why the coefficient α_T in Eq. (3.5.18) is made to change linearly around the breaking point is to diminish the numerical reflection. In this section, another way to diminish the numerical reflection will be discussed.

The governing equations of the time-dependent mild slope equation applied to this model are given by Eqs. (3.5.25) and (3.5.26). If considering a wave field bounded into two regions in which only the transfer factors f_T are different, namely f_T is zero in the incident wave side region and takes non-zero value f_2 in the other region, the reflected wave ζ_r generated by the sudden change of f_T is expressed as

$$\zeta_r = \left[\left\{\left(\frac{1}{2} - a_k\right) p_2 + b_k q_2\right\} + i\left\{-b_k p_2 + \left(\frac{1}{2} - a_k\right) q_2\right\}\right] e^{-i(kx+\sigma t)} \tag{3.5.40}$$

where p_2 and q_2 are the real part and the imaginary part of the complex amplitude of the transmitted wave, respectively, and k is the wave number calculated by the small amplitude wave theory. a_k and b_k in Eq. (3.5.40) are given as follows:

$$a_k = \frac{\sqrt{1+\sqrt{1+\frac{f_2^2}{\sigma^2}}}}{2\sqrt{2}}, \quad b_k = \frac{f_2}{2\sqrt{2}\sigma\sqrt{1+\sqrt{1+\frac{f_2^2}{\sigma^2}}}} \tag{3.5.41}$$

It is possible to decrease the energy of the reflected wave by changing the wave number in the onshore region. Replacing k in Eq. (3.5.40) by k', the minimum ratio

$R_{\min}$ of the reflected wave energy to the transmitted wave energy is obtained as

$$R_{\min} = \frac{1}{4}\frac{b_k^2}{a_k^2 + b_k^2} \tag{3.5.42}$$

when

$$k' = \frac{a_k}{2(a_k^2 + b_k^2)}k \tag{3.5.43}$$

The details are shown in Appendix A. The wave celerity c' calculated by using k' in Eq. (3.5.43) is larger than that by the small amplitude wave theory.

It is known that the actual wave celerity in the surf zone is also different from the value calculated by the small amplitude wave theory. Svendsen *et al.* (1978) found that the measured wave celerity in the surf zone is larger than the value $\sqrt{gh}$ obtained as the shallow water approximation of the small amplitude wave theory, and evaluated it by the celerity of a periodic bore which is given by

$$c_{\text{bore}} = \sqrt{gh}\sqrt{\frac{1}{2}\frac{d_c d_t (d_c + d_t)}{h^3}} \tag{3.5.44}$$

where d_c and d_t are the water depth at the wave crest and the wave trough, respectively. In general, $c_{\text{bore}} \geq \sqrt{gh}$. Horikawa and Isobe (1980) mentioned that the wave celerity in the surf zone can be predicted fairly well by the solitary wave theory. The wave celerity by the solitary wave theory is described as

$$c_{\text{sol}} = \sqrt{g(d_t + H)} \tag{3.5.45}$$

From the discussion above, it can be concluded that using k' in Eq. (3.5.43) instead of k is adequate in the sense that the wave celerity is getting closer to the actual wave celerity in the surf zone. In the present model, the transfer factor f_T takes discrete values and gradually change in the surf zone. In this case, the modified wave number k' should be calculated from the transfer factors at the neighboring mesh points. However, little difference was recognized on the effect

between the methods, Eq. (3.5.43) is therefore adopted to give the wave celerity in this model with replacement of f_2 in Eq. (3.5.41) by f_T for the simplicity. Since $f_T = 0$ offshoreward of the breaking point, k' equals k in the offshore region. Adopting the wave height to water depth ratio $\gamma_H = 0.78$ in the surf zone, c_{sol} can be approximated as

$$\begin{aligned} c_{\mathrm{sol}} &\simeq \sqrt{g\,(1.39h)} \\ &\simeq 1.2\sqrt{gh} \end{aligned} \tag{3.5.46}$$

The upper limit of the wave celerity is therefore made as

$$\frac{c'}{c} = \frac{k}{k'} \leq 1.2 \tag{3.5.47}$$

3.6 Dimensional Analysis of Turbulence Properties

In this section, representative values of length and velocity of turbulence, mean energy dissipation by turbulence and mean eddy viscosity will be discussed by using the dimensional analysis after Battjes (1975).

A dimensional analysis of turbulence in the surf zone concerning to horizontal dispersion in the longshore direction was done by Battjes (1975). In the first half of this part, the outline of his work will be introduced. Battjes adopted the energy cascade model to the energy dissipation process in the surf zone. It means that the turbulence consists of small-size eddies, the energy is transferred from larger size eddies to the smaller size, and then dissipates to heat.

If the wave energy dissipates through turbulence, the energy dissipation rate D_B by wave breaking per unit width and unit length could be expressed in terms of energy dissipation rate of turbulence as

$$D_B \approx \rho h^* \varepsilon \tag{3.6.1}$$

where h^* is the representative water depth and ε is vertically averaged energy dissipation rate of turbulence per unit mass. By using the representative length l and the representative velocity q for the turbulence, *i.e.* eddies, the energy of the eddies per unit mass and the representative frequency were given as q^2 and q/l, respectively. Then the energy transfer to heat through the higher frequency, that is energy dissipation rate, ε, per unit mass was determined as

$$\varepsilon \approx q^2 \cdot \frac{q}{l} = \frac{q^3}{l} \tag{3.6.2}$$

Battjes considered that the scale of the eddies was restricted by the vertical length rather than the horizontal length. Replacing l by h^*, and putting $h^* = h$, the representative velocity was obtained as

$$q \approx \left(\frac{D_B}{\rho}\right)^{1/3} \tag{3.6.3}$$

By the eddy viscosity model, the Reynolds stress in the longshore direction was expressed as

$$-\rho\overline{u'v'} = \nu_h \frac{dV}{dx} \tag{3.6.4}$$

in which ν_h is the eddy viscosity coefficient in the horizontal plane, v' and V are the turbulent component and the steady component of velocity in the longshore direction, respectively. It was considered that ν_h had a dimension of ql. Hence, ν_h could be given from Eq. (3.6.3) as

$$\nu_h \approx qh \approx h\left(\frac{D_B}{\rho}\right)^{1/3} \tag{3.6.5}$$

By using the linear wave theory on a constant slope, the energy dissipation rate was expressed as follows:

$$D_B \approx -\frac{d(E_w nc)}{dx} \approx -\frac{d}{dx}\left(\frac{1}{8}\rho g H^2 c\right) \tag{3.6.6}$$

Substituting $H = \gamma_H h$ and $c = \sqrt{gh}$, Battjes obtained

$$\begin{aligned} D_B &\approx -\frac{d}{dx}\left(\frac{1}{8}\rho g^{3/2}\gamma_H^2 h^{5/2}\right) \\ &= -\frac{5}{16}\rho g^{3/2}\gamma_H^2 h^{3/2}\frac{dh}{dx} \\ &= \frac{5}{16}\rho g^{3/2}\tan\beta\gamma_H^2 h^{3/2} \end{aligned} \tag{3.6.7}$$

where γ_H is the wave height to water depth ratio. Battjes dealt with the horizontal dispersion, but the analysis can be applied in the vertical direction. The energy of turbulence and eddy viscosity coefficient will be discussed hereafter.

The vertically averaged energy ,ϵ, of turbulence per unit mass is described from Eq. (3.6.3) as

$$\epsilon \approx q^2 \approx \left(\frac{D_B}{\rho}\right)^{2/3} \tag{3.6.8}$$

As for the eddy viscosity in the vertical plane, it can be considered that the discussion about ν_h can be applied. Hence, ν_e which is the eddy viscosity coefficient

in the vertical plane is expressed by using the energy dissipation rate D_B and the mean water depth h as

$$\nu_e \approx ql \approx h\left(\frac{D_B}{\rho}\right)^{1/3} \tag{3.6.9}$$

The Reynolds stress should be essentially determined by the flow field. However, if $\overline{u'w'}$ is proportional to ϵ, it can be described as

$$\overline{u'w'} \approx \left(\frac{D_B}{\rho}\right)^{2/3} \tag{3.6.10}$$

If the small amplitude theory holds, the energy of turbulence is expressed in terms of water depth, celerity and bottom slopes by substituting Eq. (3.6.7) into Eq. (3.6.8) as

$$\begin{aligned}\epsilon &\approx \left(\frac{5}{16}g^{3/2}\tan\beta\gamma_H^2 h^{3/2}\right)^{2/3} \\ &= \left(\frac{5}{16}\gamma_H^2\right)^{2/3} c^2\tan^{2/3}\beta\end{aligned} \tag{3.6.11}$$

The above equation means that ϵ is in proportion to the square of the celerity, and the power of two third of the bottom slope. However, one should take into account the variation of the wave height to water depth ratio γ_H.

In the same manner, ν_e is expressed from Eq. (3.6.9) as

$$\nu_e \approx \left(\frac{5}{16}\gamma_H^2\right)^{1/3} ch\tan^{1/3}\beta \tag{3.6.12}$$

The quantity is in proportion to the water depth, the celerity and the third power of the slope.

3.7 Modeling of Vertical Distribution of Undertow

The mass flux by waves which is equal to the vertically integrated value of the undertow is determined by the wave field model shown in the previous sections. The discussion in §3.6 pointed out the possibility that the vertically averaged values of the mean Reynolds stress and the mean eddy viscosity coefficient can also be obtained from D_B which is estimated by the model of the energy dissipation process.

The vertical distribution of the mean Reynolds stress and the mean eddy viscosity coefficient will be assumed as linear functions of the vertical elevation z based on the experimental results. The undertow profile will be determined from these distributions by using the eddy viscosity model. The undertow can be evaluated throughout the surf zone.

3.7.1 Modeling of Vertical Distribution of the Mean Reynolds Stress and the Mean Eddy Viscosity

Based on the experimental results shown in §2.3, the vertical distributions of the mean Reynolds stress and the mean eddy viscosity coefficient are assumed as linear functions of the vertical elevation z in each measuring line. This assumption is different from that adopted by Svendsen and Hansen (1988) or Tsuchiya *et al.* (1988). Figure 3.7.1 shows this simple model for the estimation.

First the coefficients of the linear functions for the measuring line 4 and 5 in every case of series B of the experiments described in Chapter 2 were obtained by using the regression analysis. To investigate consistently among the measuring lines and for various incident wave conditions, it should be proper to non-dimensionalize the coefficients by the water density ρ, the celerity c and the trough level d_t, which is probably proportional to the mean water depth h in the inner region, according to Eqs. (3.6.11) and (3.6.12). Equations (3.6.11) and (3.6.12) were derived with the assumption that the energy dissipation is expressed by Eq. (3.6.6), which should hold

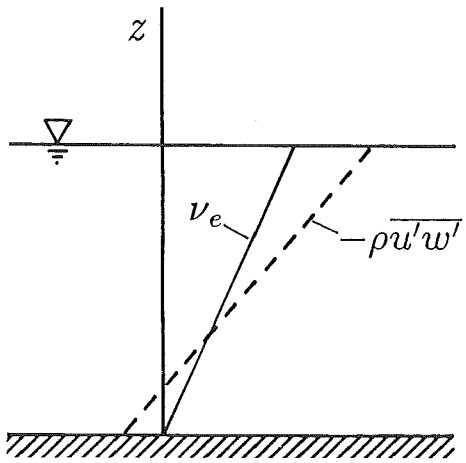

Fig. 3.7.1 Assumed distributions of mean Reynolds stress and mean eddy viscosity coefficient.

in the inner region where waves can be regarded as quasi-steady, although the energy dissipation rate will be actually evaluated by the model described in §3.5 because it can apply throughout the surf zone. Then the average of the dimensionless values of the measuring line 4 and 5 was taken for each case.

Using these parameters, the linear functions for the mean Reynolds stress $-\rho\overline{u'w'}$ and the mean eddy viscosity coefficient ν_e are expressed as

$$-\rho\overline{u'w'} = \alpha_1 \rho \frac{c^2}{d_t} z' + \beta_1 \rho c^2 \tag{3.7.1}$$

$$\nu_e = \alpha_2 c z' + \beta_2 c d_t \tag{3.7.2}$$

where α_1, β_1, α_2 and β_2 are dimensionless parameters and z' is the vertical elevation from the bottom. The wave celerity is expressed as

$$c = \sqrt{g\,(d_t + H)} \tag{3.7.3}$$

based on the solitary wave theory, where H is the local wave height. Table 3.7.1 is the list of the dimensionless parameters.

Table 3.7.1 Dimensionless parameters for the distribution of $-\rho\overline{u'w'}$ and ν_e.

case	slope	α_1	β_1	γ_1	α_2	β_2	γ_2
B–1	1/20	0.0024	–0.00058	0.0017	0.015	–0.00042	0.015
B–2	1/20	0.0027	–0.00062	0.0021	0.015	–0.0015	0.014
B–3	1/20	0.0020	–0.00026	0.0017	0.0098	0.0013	0.011
B–4	1/20	0.0022	–0.00016	0.0021	0.015	0.0015	0.016
Ave. of 1/20		0.0023	–0.00041	0.0019	0.014	0.00022	0.014
B–5	1/30	0.0018	–0.00036	0.0014	0.010	0.000066	0.010
B–6	1/30	0.0015	–0.00024	0.0013	0.017	–0.00052	0.016
B–7	1/30	0.0019	–0.00036	0.0015	0.011	–0.00043	0.010
B–8	1/30	0.0013	–0.00024	0.0011	0.0091	–0.00010	0.0081
B–9	1/30	0.0011	–0.00016	0.00094	0.0046	0.00042	0.0050
Ave. of 1/30		0.0015	–0.00027	0.0012	0.010	–0.00011	0.0099

In the table, the parameter β_2 is the dimensionless value of ν_e on the bottom ($z' = 0$) and γ_2 is the value at the trough level ($z' = d_t$). Though the magnitude of the parameters are much smaller than the values obtained from Eqs. (3.6.11) and (3.6.12), the fluctuation of the parameters are so small that they can be regarded as constants for each bottom slope. The fact that β_2 is far smaller than γ_2 is consistent with the experimental result mentioned in §2.3.4. It should therefore be possible to take $\nu_e = 0$ on the bottom. Equation (3.7.2) can be approximated as

$$\nu_e = \alpha_2 c z' \tag{3.7.4}$$

To deal with the mean Reynolds stress and the mean eddy viscosity coefficient in the surf zone which include the outer region or the wave recovery zone, it is necessary to estimate the magnitude of them by means of D_B calculated by the model described in §3.5. For this sake, it is convenient that the values are expressed in terms of dimensional parameters. Since the mean Reynolds stress can be transformed to the mean shear stress, the mean shear stress τ acting on the horizontal plane and the the mean eddy viscosity coefficient ν_e can be denoted as

$$\tau = a_\tau z' + b_\tau \tag{3.7.5}$$

$$\nu_e = a_\nu z' \tag{3.7.6}$$

where $z'\,(= z + h_0)$ is the vertical elevation measured from the bottom and a_τ, b_τ and a_ν are functions of x which can be treated as constants at a certain value of x.

By using the vertically averaged mean shear stress τ_m which is defined as

$$\tau_m = \frac{1}{d_t}\int_0^{d_t} \tau\, dz' \tag{3.7.7}$$

and the ratio of the value at the trough level to the value at the bottom

$$R_\tau \equiv \frac{\tau_{z'=d_t}}{\tau_{z'=0}} \tag{3.7.8}$$

the values a_τ and b_τ are denoted as

$$a_\tau = -\frac{2}{d_t}\frac{1-R_\tau}{1+R_\tau}\tau_m\,, \quad b_\tau = \frac{2}{1+R_\tau}\tau_m \tag{3.7.9}$$

The mean shear stress is expressed as

$$\tau = \frac{2}{1+R_\tau}\tau_m\left\{-(1-R_\tau)\frac{z'}{d_t}+1\right\} \tag{3.7.10}$$

From Eq.(3.6.10), it can be considered that the vertically averaged mean shear stress is expressed as

$$\tau_m = C_\tau \rho^{1/3} D_B^{2/3} \tag{3.7.11}$$

where C_τ is a constant. In the present study, C_τ is determined from the experimental results as

$$C_\tau = 0.02 \tag{3.7.12}$$

The value is far smaller than unity. One reason is that the representative length is given by h in §3.6 though the actual diameter of turbulent eddies should be much smaller. The ratio R_τ is determined from the values β_1 and γ_1 as

$$R_\tau = -4.0 \tag{3.7.13}$$

It should be noticed that τ becomes always zero at $z' = \frac{1}{5}d_t$ in this case. Substituting Eqs. (3.7.11), (3.7.12) and (3.7.13) into (3.7.10), τ is obtained as

$$\tau = \frac{0.04}{3}\rho^{1/3} D_B^{2/3}\left(\frac{5}{d_t}z' - 1\right) \tag{3.7.14}$$

The value d_t is calculated in the model as

$$d_t = h - a \tag{3.7.15}$$

where a is the wave amplitude calculated by the small amplitude wave theory. Although the small amplitude wave theory cannot express the wave height distribution in the surf zone accurately, it is adopted for convenience of the calculation.

The vertical distribution of the mean eddy viscosity ν_e can be obtained in the same manner. Since the value at the bottom was assumed to be zero in §2.3.4, a_ν in Eq.(3.7.6) is expressed as

$$a_\nu = 2\frac{\nu_m}{d_t} \tag{3.7.16}$$

where

$$\nu_m = \frac{1}{d_t}\int_0^{d_t} \nu_e \, dz' \tag{3.7.17}$$

From Eq.(3.6.9), ν_m can be denoted as

$$\nu_m = C_\nu h \rho^{-1/3} D_B^{1/3} \tag{3.7.18}$$

where C_ν is determined as

$$C_\nu = 0.03 \tag{3.7.19}$$

from the experimental results. Then Eq.(3.7.6) is replaced by

$$\begin{aligned} \nu_e &= 2\nu_m \frac{z'}{d_t} \\ &= 0.06\rho^{-1/3} D_B^{1/3} \frac{h}{d_t} z' \end{aligned} \tag{3.7.20}$$

3.7.2 Expression of Undertow Profile by Using the Eddy Viscosity Model

It was assumed that the eddy viscosity coefficient takes the value zero at the bottom in the previous section, but there exists the kinematic viscosity ν. Though the value ν is far smaller than ν_e in the surf zone in general, it cannot be neglected near the bottom or in the offshore region where the field is regarded as a laminar flow. Therefore, the total viscosity is defined as follows:

$$\nu_t = \nu_e + \nu \tag{3.7.21}$$

By using the eddy viscosity model, the relation between the mean shear stress τ acting on the horizontal plane and the steady current U in x-direction is expressed as

$$\tau = \rho\nu_t \frac{\partial U}{\partial z} \tag{3.7.22}$$

Substituting Eqs. (3.7.5), (3.7.6) and (3.7.21) into Eq. (3.7.22) and replacing z by z', the steady current U can be expressed in a first-order linear differential equation as

$$\frac{\partial U}{\partial z'} = \frac{a_\tau z' + b_\tau}{a_\nu z' + \nu} \tag{3.7.23}$$

The general solution of Eq. (3.7.23) is obtained as

$$\begin{aligned} U &= \int \frac{a_\tau z' + b_\tau}{a_\nu z' + \nu} dz' \\ &= \frac{a_\tau}{a_\nu} z' + \frac{a_\nu b_\tau - a_\tau \nu}{a_\nu^2} \log(a_\nu z' + \nu) + C_1 \end{aligned} \tag{3.7.24}$$

where C_1 is a integral constant. The vertically averaged value of the undertow is defined as

$$\begin{aligned} U_m &= \frac{1}{d_t} \int_0^{d_t} U \, dz' \\ &= \frac{1}{d_t} \int_{-h_0}^{\zeta_t} U \, dz \end{aligned} \tag{3.7.25}$$

From Eq. (3.3.3), it is obvious that the integrated undertow should compensate the mass flux above the trough level. Hence, U_m is calculated by using Eq. (3.3.3) as

$$U_m = -\frac{1}{d_t} M_t \tag{3.7.26}$$

Substituting Eq. (3.7.24) into Eq. (3.7.25), C_1 is determined as

$$C_1 = U_m - \frac{1}{2}\frac{a_\tau}{a_\nu} d_t - \frac{a_\nu b_\tau - a_\tau \nu}{a_\nu^3 d_t} (a_\nu d_t + \nu) \log(a_\nu d_t + \nu) - \nu \log \nu - a_\nu d_t \tag{3.7.27}$$

The value τ calculated by Eq. (3.7.14) becomes zero in the offshore region or in the wave recovery zone because D_B is zero in these regions. Then the steady current calculated by Eq. (3.7.24) becomes a uniform flow. Longuet-Higgins (1953) derived the Eulerian mass transport velocity on the assumption that the non-linear inertia terms can be neglected compared with the viscous terms as

$$U_E = \frac{a^2 \sigma k}{4 \sinh^2 kh} \left\{ 3 + kh \left(3 \frac{z^2}{h^2} + 4 \frac{z}{h} + 1 \right) \sinh 2kh \right.$$

$$+3\left(\frac{\sinh 2kh}{2kh}+\frac{3}{2}\right)\left(\frac{z^2}{h^2}-1\right)\Bigg\} \tag{3.7.28}$$

Equation (3.7.28) produces no net mass transport when using the small amplitude wave theory. In the present model, the steady current in the offshore region and the wave recovery zone is determined as

$$U_{\text{off}} = U_E + C_2 \tag{3.7.29}$$

where C_2 is the compensatory value to satisfy

$$\int_{-h_0}^{\zeta_t} U_{\text{off}}\, dz = -M_t \tag{3.7.30}$$

From Eqs. (3.7.26), (3.7.28), (3.7.29) and (3.7.30), C_2 is obtained as

$$\begin{aligned} C_2 = U_m - \frac{a^2\sigma k}{4(\zeta_t+h)\sinh^2 kh}\Bigg\{&\left(kh\sinh 2kh+\frac{\sinh 2kh}{2kh}+\frac{3}{2}\right)\frac{\zeta_t^3}{h^2} \\ &+(2kh\sinh 2kh)\frac{\zeta_t^2}{h}+\left(kh\sinh 2kh-\frac{3\sinh 2kh}{2kh}-\frac{3}{2}\right)\zeta_t \\ &-\frac{\sinh 2kh}{k}\Bigg\} \end{aligned} \tag{3.7.31}$$

Then U_{off} is expressed as

$$\begin{aligned} U_{\text{off}} =&\frac{a^2\sigma k}{4\sinh^2 kh}\Bigg[\left(3kh\sinh 2kh+\frac{3\sinh 2kh}{2kh}+\frac{9}{2}\right)\frac{z'^2}{h^2} \\ &+\left(-2kh\sinh 2kh-\frac{6\sinh 2kh}{2kh}-9\right)\frac{z'}{h} \\ &+\frac{d_t}{h}\left\{\left(1-\frac{d_t}{h}\right)kh\sinh 2kh+\left(3-\frac{d_t}{h}\right)\frac{\sinh 2kh}{2kh}+\frac{3}{2}\left(3-\frac{d_t}{h}\right)\right\}\Bigg] \\ &+U_m \end{aligned} \tag{3.7.32}$$

For the sake of smoothing the solution near the breaking point or the wave recovery point, Eq. (3.7.24) is replaced as

$$\begin{aligned} U =&\frac{a'_\tau}{a_\nu}\left(z'-\frac{d_t}{2}\right)+\frac{a_\nu b'_\tau - a'_\tau\nu}{a_\nu^2}\left(1+\log\frac{a_\nu z'+\nu}{a_\nu d_t+\nu}-\frac{\nu}{a_\nu d_t}\log\frac{a_\nu d_t+\nu}{\nu}\right) \\ &+U_m \end{aligned} \tag{3.7.33}$$

where

$$\left.\begin{aligned} a'_\tau &= a_\tau + \frac{\nu a^2 \sigma k}{2h^2 \sinh^2 kh}\left(3kh \sinh 2kh + \frac{3\sinh 2kh}{2kh} + \frac{9}{2}\right) \\ b'_\tau &= b_\tau - \frac{\nu a^2 \sigma k}{4h \sinh^2 kh}\left(2kh \sinh 2kh + \frac{6\sinh 2kh}{2kh} + 9\right) \end{aligned}\right\} \tag{3.7.34}$$

The values of the second terms in Eq. (3.7.34) are far smaller than those of the first terms in the inner region of the surf zone. In the offshore region where $D_B = 0$, Eq. (3.7.33) reduces to

$$U = \frac{a'_\tau}{2\nu} z'^2 + \frac{b'_\tau}{\nu} z' - \frac{a'_\tau}{6\nu} d_t^2 - \frac{b'_\tau}{2\nu} d_t + U_m \tag{3.7.35}$$

which is exactly same as Eq. (3.7.32) [see Appendix B]. In case of $D_B \ll 1$, the undertow profile is calculated by Eq. (3.7.35) to prevent the calculation from diverging.

3.8 Computational Results

By using the present model, at first the potential and kinetic energies of the wave motion and the energy of the organized large vortexes are obtained. The wave setup is also calculated. From the energy variations, the vertically averaged value of undertow is estimated. Finally, the profiles of the undertow are obtained with estimation of the mean Reynolds stress and the mean eddy viscosity coefficient from the energy dissipation rate.

In this section, the calculated values will be compared with the measured values which were obtained by the laboratory experiments described in §2.2. The energy variations will also be discussed with the experimental results obtained by Nagayama (1983).

3.8.1 Variations of Energies

The variation of the calculated values of the potential energy of wave motion E_p, the energy of the organized large vortexes E_v and the total energy of wave E_t for case B–1 which was described in §2.2 are shown in Fig. 3.8.1. The measured potential energy of waves is shown together in the figure. The measured and calculated breaking points, plunging points and transition points are also indicated.

For the calculation by the present model, only beach topography, period and height (or amplitude) of the incident waves are necessary as inputs. The spacing between the mesh points and the time step of the calculation were respectively 2 cm and 0.005 s for all the cases . The calculation was started from the points 100 cm offshoreward of the foot of the slopes, which was $x = -900$ cm in case B–1. The convergence of solution was assumed when the absolute errors between the values obtained from two successive cycles of the calculation at every point were less than 2% of the amplitude of the incident waves throughout the field for both the wave

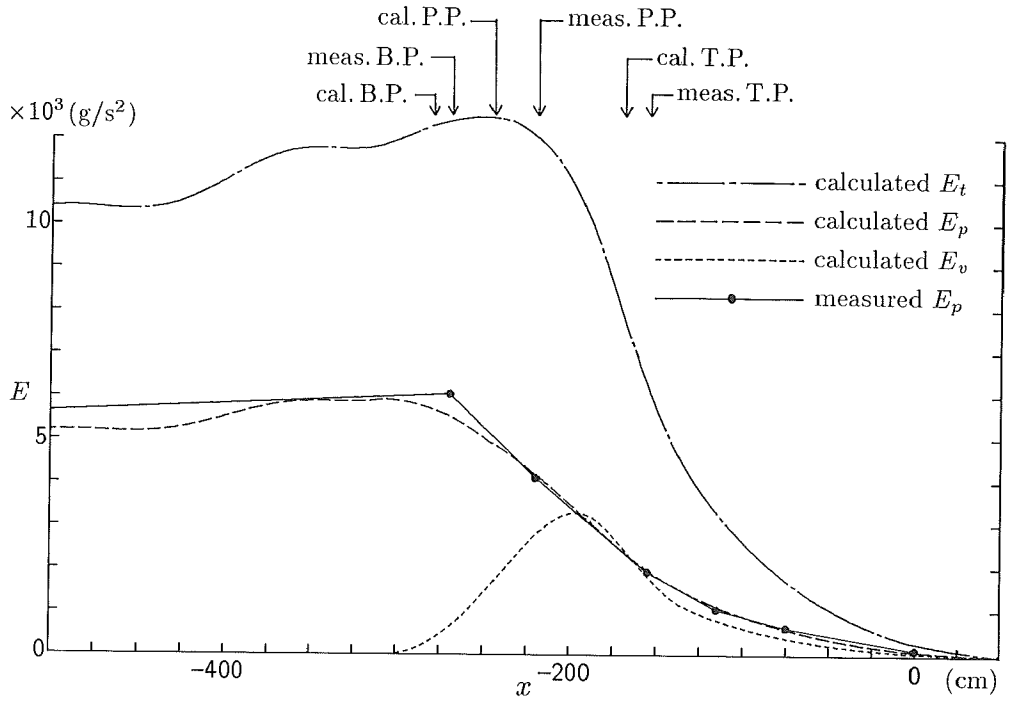

Fig. 3.8.1 Calculated and measured energy variations (case B–1).

amplitudes and the setup calculation. Other needed factors and coefficients were already given in the previous sections.

In the figure, the calculated and measured potential energy E_p are in good agreement in the surf zone; however the calculated E_p is slightly smaller than the measured value at $x = -500$ cm. The numerical reflection can be seen in the offshore region. The breaking point is estimated slightly offshoreward in spite of the smaller value of the evaluated potential energy in the offshore region. The estimated plunging point is much offshore, but the transition point is well estimated if the difference of the breaking points is taken into account. The calculated E_p begins to attenuate from the estimated breaking point in the figure, although Watanabe and Maruyama (1986) mentioned that the calculated energy still increased at the breaking point when setting $\alpha_T = 0$ at the breaking point. The reasons should be that α_T increases from the crest breaking point in this case and that the ratio between the potential energy and the kinetic energy is modified after breaking.

On the other hand, the total energy E_t does not change so much around the breaking point and rapidly decreases from the measured plunging point to the transition point. It is caused by the existence of the organized large vortexes. The magnitude of the energy of the organized large vortexes E_v is comparable to that of the potential energy E_p. The energy of the vortexes increases from the crest breaking point and takes its maximum value which is almost the same as the value of E_p near the calculated transition point.

The calculated energy transfer rate T_B from the wave energy to the energy of the vortexes and the energy dissipation rate D_B are shown in Fig. 3.8.2. The hatched area corresponds to the rate of change of the vortex energy. The qualitative agreement with the vertically averaged energy of turbulence ${u'_m}^2$ and ${w'_m}^2$ shown in Figs. 2.3.15 and 2.3.16 is good except near the plunging point where the

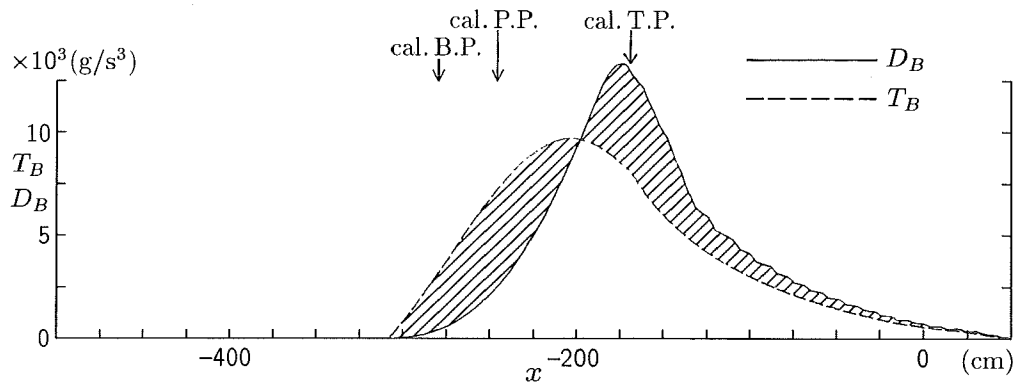

Fig. 3.8.2 Rates of energy transfer and dissipation (case B–1).

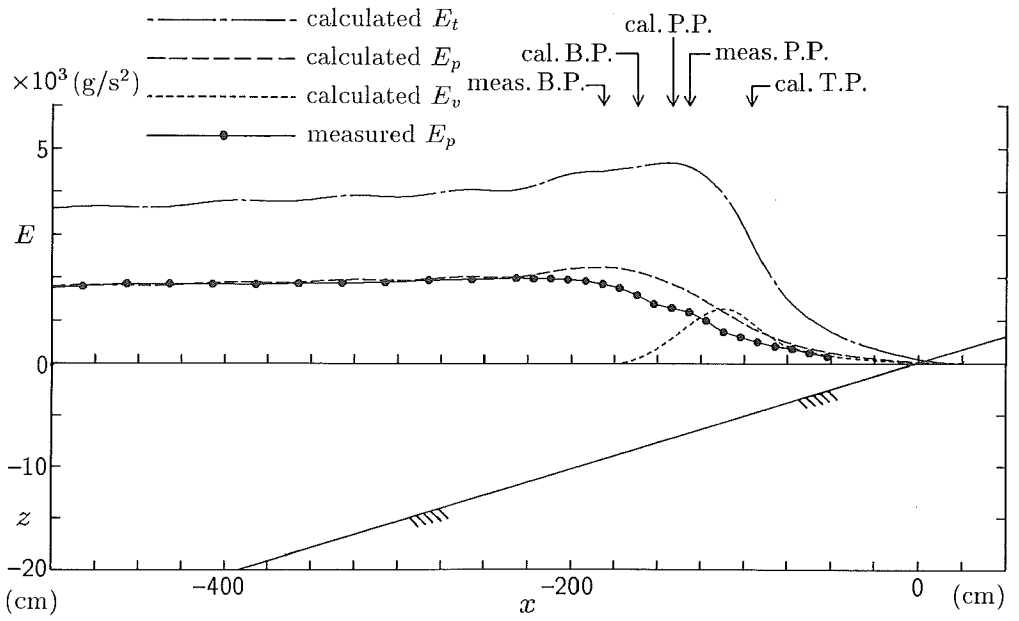

Fig. 3.8.3 Potential energies calculated by the present model and measured by Nagayama (1983) on a uniform slope (case 1).

calculated value of the energy dissipation is much larger than the measured value of the turbulence energy. But in general, it can be said that the difference of the spatial distributions between the attenuation of the wave energy and the energy dissipation is well expressed by the present model.

Figure 3.8.3 gives the comparison with the variation of the potential energy measured by Nagayama (1983) on a 1/20 constant slope (case 1). The incident wave condition is listed in Table 3.8.1. The potential energy is under-estimated in the surf zone. Since the potential energy rapidly deceases after breaking, it can be considered that the prediction of the breaking point influences much to the variations of the calculated energies in the surf zone. The calculated potential energy increases gradually up to the wave breaking point, although the measured value keeps almost same value. It should be because the small amplitude theory by which the wave energy is over-estimated in shallow water is adopted in this model [Dibajnia *et al.* (1988)].

Table 3.8.1 Conditions of experiments performed by Nagayama (1983).

case	beach type	T (s)	h_i (cm)	H_i (cm)	H_0/L_0	x_b (cm)	x_p (cm)
1	uniform	1.19	27.1	5.44	0.027	–182	–132
3	step	1.19	28.4	5.07	0.025	–358	–306
5	step	0.96	28.4	7.19	0.055	–387	–308
6	bar	0.94	28.4	6.48	0.051	–357	–331
7	bar	0.95	28.4	5.85	0.045	–357	–314

The comparisons between the calculated and measured potential energies are shown in Figs. 3.8.4 and 3.8.5 for cases 3 and 5 of the experiments by Nagayama on a step-type beach with the variations of the transfer factor f_T. The transfer factors increase from the crest breaking points according to the coefficient α_T, then

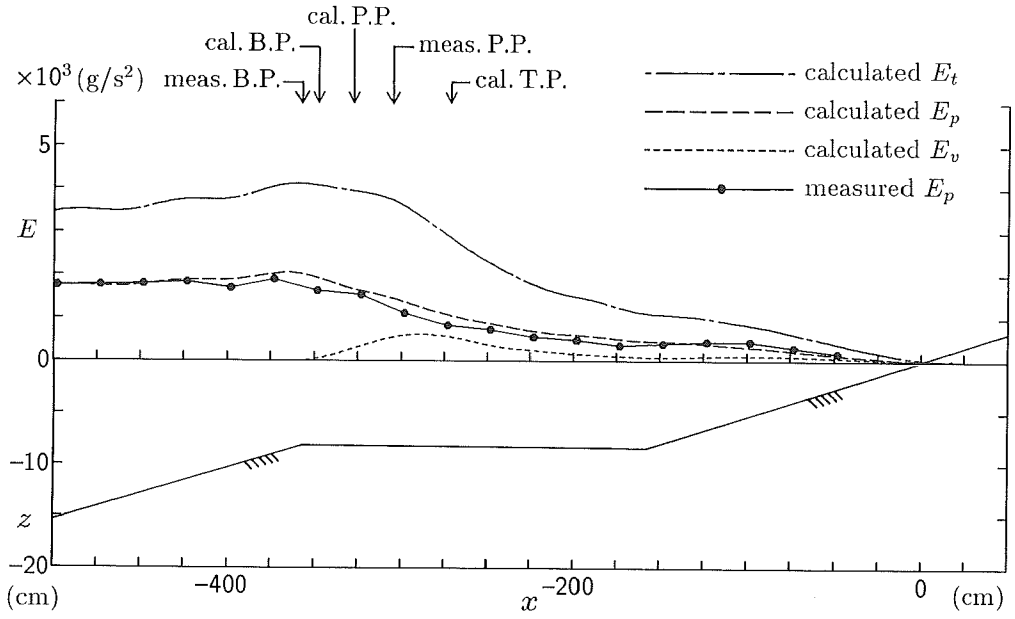

Fig. 3.8.4 Potential energies calculated by the present model and measured by Nagayama (1983) on a step-type beach (case 3).

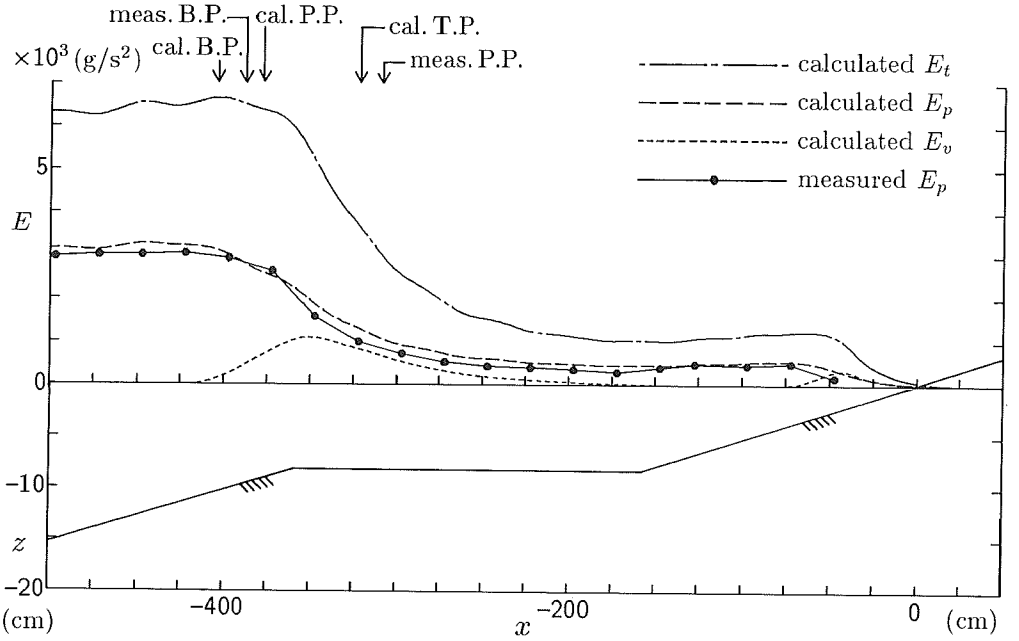

Fig. 3.8.5 Potential energies calculated by the present model and measured by Nagayama (1983) on a step-type beach (case 5).

decrease from the transition points on the flat bed. As the transfer factor becomes zero on the flat bed in case 5, waves recover at that point in calculation. On the other hand, they do not recover by calculation for case 3, although the variation of the measured potential energy suggests the wave recovery around $x = -150$ cm. However, in general, it can be said that the calculated values predict the actual energy variations well in both cases. The energy variations for case B–11 are shown in Fig. 3.8.6. The relative magnitude of the vortex energy is larger than other cases because of the steeper bottom slope offshoreward of the flat bed. The agreement is good.

Figures 3.8.7 and 3.8.8 give the comparisons of the calculated and measured potential energies for cases 6 and 7 of Nagayama's experiments on a bar-type beach. The agreement is good. However, the estimation of the second breaking points is not accurate in both cases. It is probably due to the fact that waves which have once recovered tend to break easily for the second time. The reflection at the first breaking points is too large to be neglected.

3.8.2 Vertically Averaged Undertow

Figure 3.8.9 shows the comparison of the variations of the calculated and measured values U_m of the steady current averaged vertically below the trough level for case B–1. The contributions to the calculated value of U_m from the mass flux by wave motion $U_w \left(\equiv -\frac{M_w}{d_t} \right)$ and the organized large vortexes $U_v \left(\equiv -\frac{M_v}{d_t} \right)$ are also given in the figure. The measured value is smaller than the calculated value in the outer region but is larger in the inner region. Since the measured value is almost the same as the value U_w offshoreward of the plunging point, it is considered that the actual magnitude of the contribution by the organized large vortexes is much smaller than the calculated value.

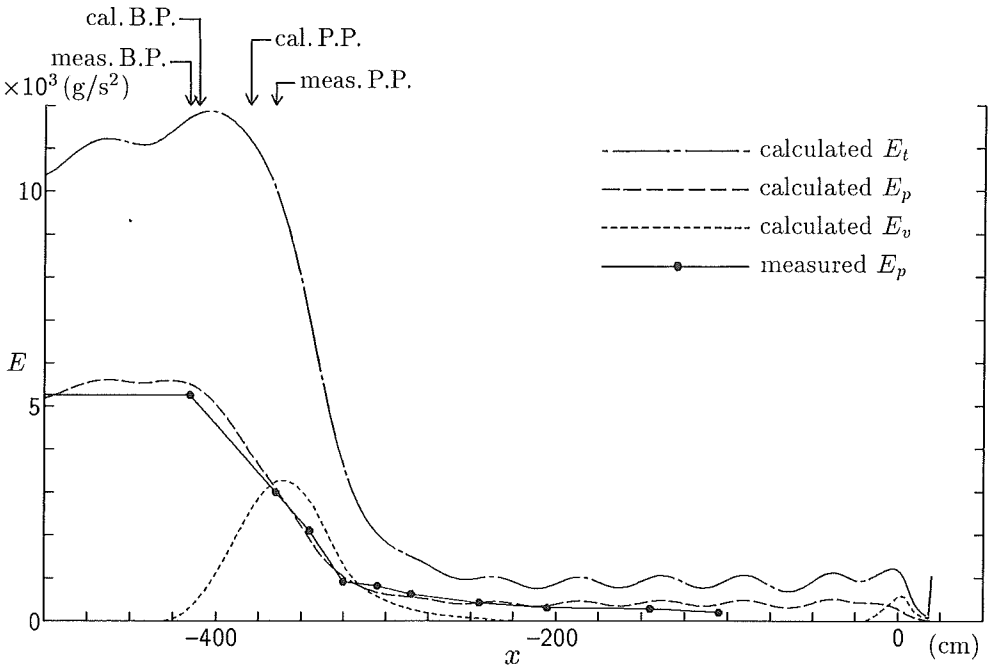

Fig. 3.8.6 Calculated and measured energy variations (case B–11).

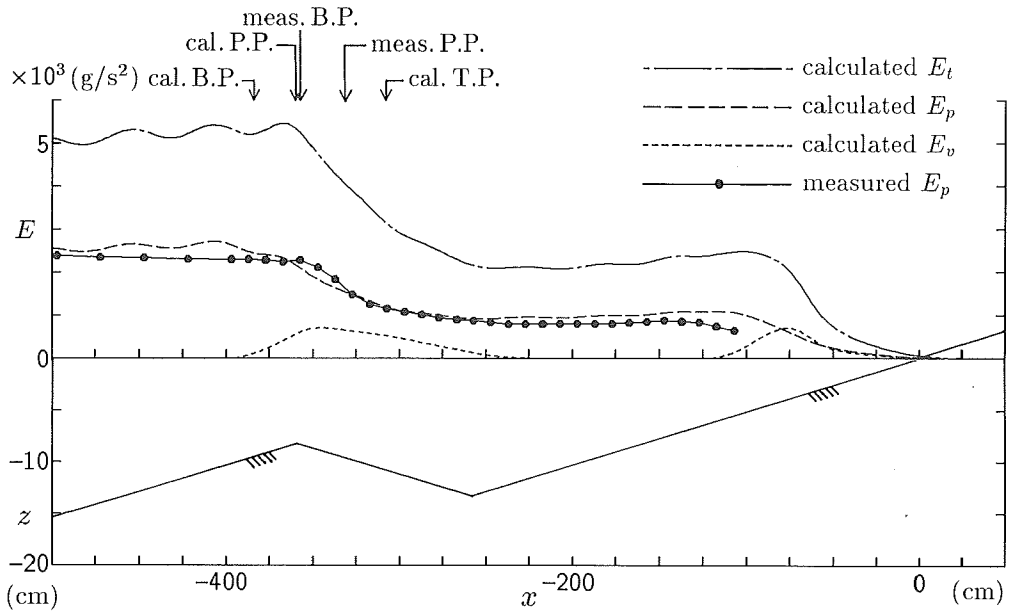

Fig. 3.8.7 Potential energies calculated by the present model and measured by Nagayama (1983) on a bar-type beach (case 6).

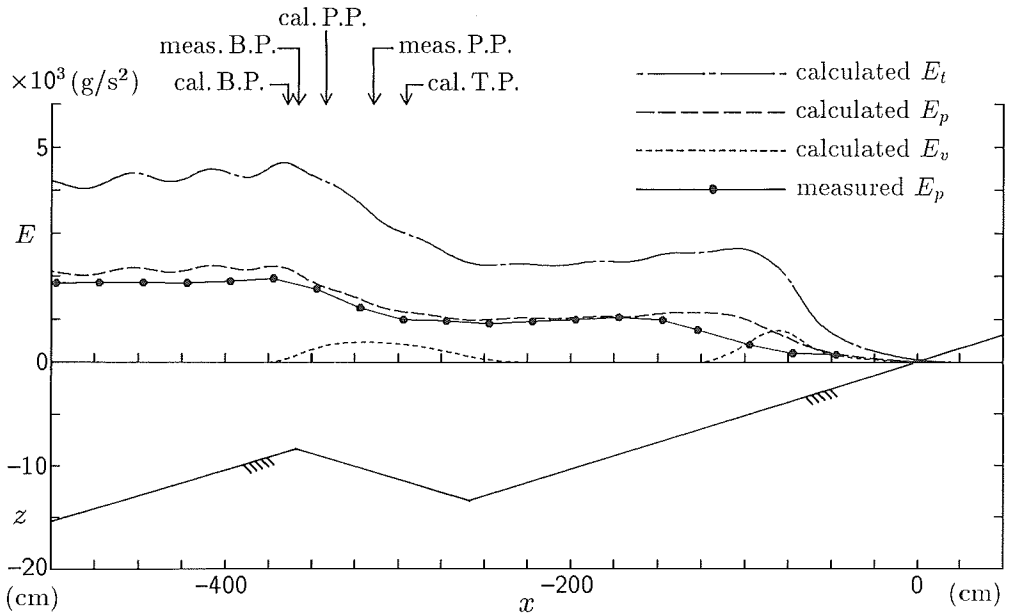

Fig. 3.8.8 Potential energies calculated by the present model and measured by Nagayama (1983) on a bar-type beach (case 7).

The calculated value of the energy dissipation around the plunging points is much larger than the measured value of the turbulence energy as already mentioned. It means that the actual energy dissipation may be smaller than the value evaluated by this model. Since the calculated potential energy agrees with the measured value as shown in Fig. 3.8.1, little energy dissipation means that the energy of vortexes must be much larger. But in the present model, the large value of the vortex energy at the plunging point makes the mass flux by the vortexes large there, which is contrary to the results shown in Fig. 3.8.9. It is probable that the structure of the organized large vortexes in the outer region is different from that in the inner region. The magnitude of the vortex energy depends on the dissipation length of vortex energy l_d which is given by Eq. (3.5.29). The influence by the difference of the structure of the organized large vortex is partly considered in Eq. (3.5.29) in this model.

The comparisons between the calculated value and measured value of U_m for cases B–4 and B–8 are shown in Figs. 3.8.10 and 3.8.11. The vertically averaged undertow is well predicted in case B–4 in the outer region, however it is rather over-estimated in case B–8. The reason for such a difference is not clear, but at least, it can be said that the prediction of the breaking point affects the evaluation of U_m especially in the outer region.

In the inner region, the calculated value is larger than the measured value in case B–4. In case B–8, the measured value fluctuates in the inner region. It cannot be concluded whether the fluctuation of the measured value is caused by the three-dimensionality of the steady current in the inner region or the error of the measurement.

3.8.3 Profiles of Undertow

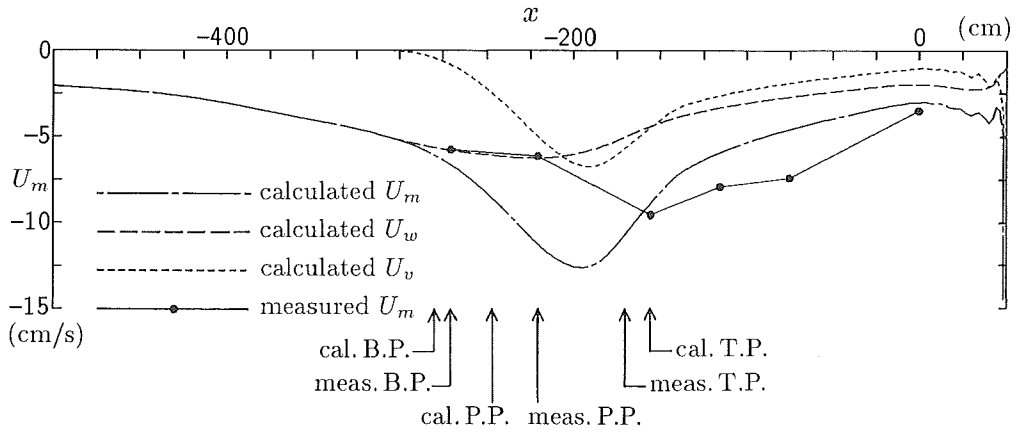

Fig. 3.8.9 Variations of calculated and measured U_m (case B–1).

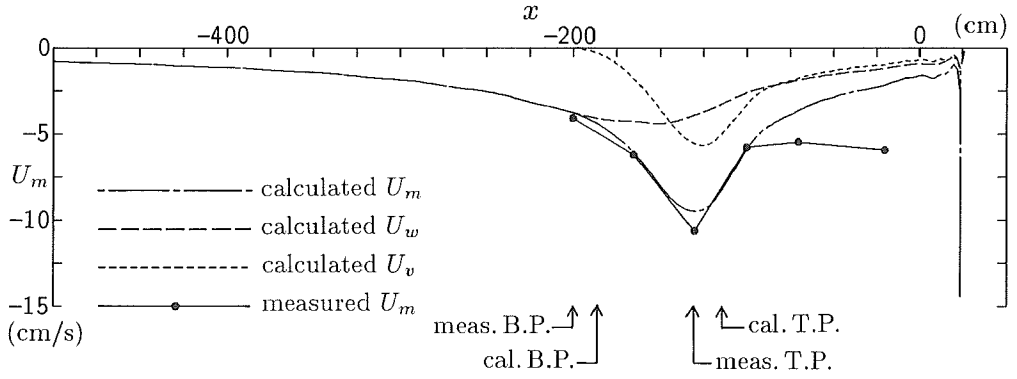

Fig. 3.8.10 Variations of calculated and measured U_m (case B–4).

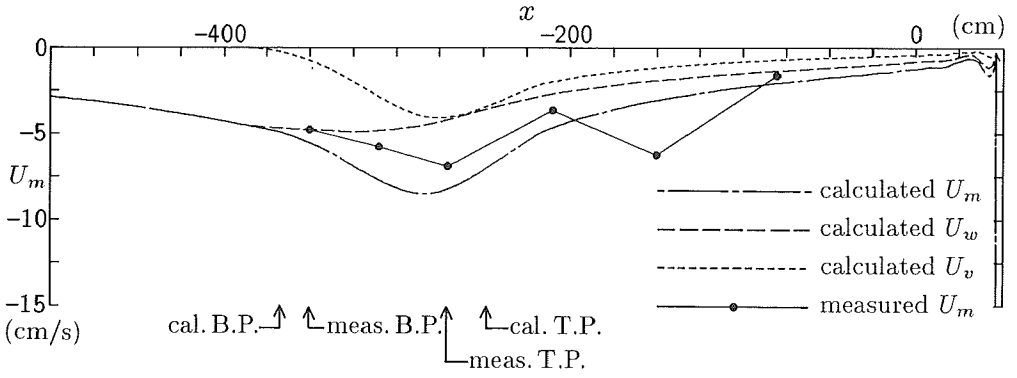

Fig. 3.8.11 Variations of calculated and measured U_m (case B–8).

The comparison of the calculated and measured distribution of the steady current in the cross-shore direction U for case B–1 is shown in Fig. 3.8.12 with the bottom profile. The variation of the mean water level which will be discussed in the next part of this section is given together. From the figure, it can be said that the profiles in the inner region are well evaluated. The calculated profiles in the outer region which decrease with the vertical elevation z' are different from the measured profiles which increase with z'. In the present model, the mean shear stress τ is almost zero at $z' = \frac{1}{5}d_t$ in the surf zone as mentioned in §3.7.1, $\frac{\partial U}{\partial z'}$ becomes also zero at that point. However, the profiles are greatly depend on the energy dissipation rate D_B. If D_B is very small as it is at the breaking point, the profile becomes almost vertical as shown around the predicted breaking point in Fig. 3.8.12. In that case, the agreement of the calculated and measured profiles is fairy good. On the other hand, as the calculated energy dissipation is larger than the measured turbulent energy near the plunging points as already mentioned in the previous part, the calculated profiles become much different from the measured value. If the evaluated energy dissipation becomes in better agreement, the profiles will also approach to the measured value near the plunging point. Since D_B changes rapidly in the outer region as shown in Fig. 3.8.2, the prediction of the breaking points has a great importance for the accurate estimation of D_B, *i.e.*, the profiles of the steady current in the outer region. The comparisons for cases B–4 and B–8 are shown in Figs. 3.8.13 and 3.8.14. The tendency is the same, but the agreement in the outer region is rather good for case B–4.

Figure 3.8.15 gives the undertow profiles for case B–11. The calculated profile does not fit to the measured profile at the plunging point, either in this case. On the offshore part of the flat bed, the form of the calculated profiles is good, although the magnitude is smaller than the measured values. The onshore side on the flat bed is a wave recovery zone. The energy transfer factor f_T becomes zero at $x = -240$

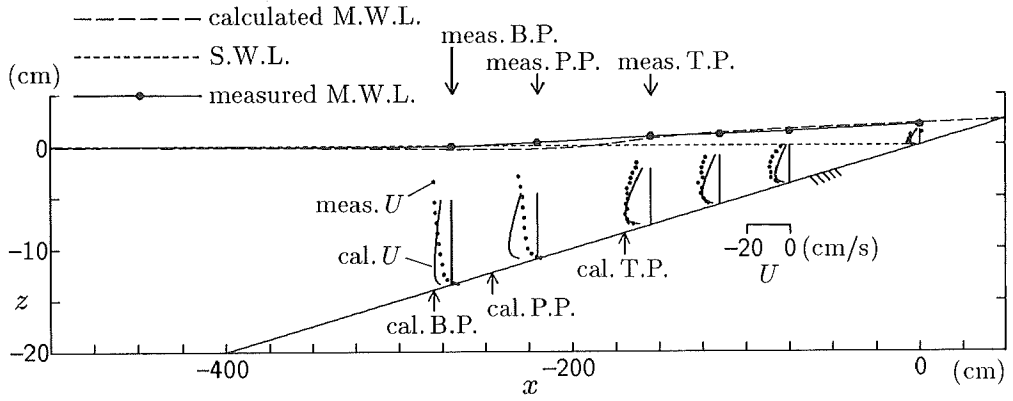

Fig. 3.8.12 Steady current distribution and the variation of mean water level (case B–1).

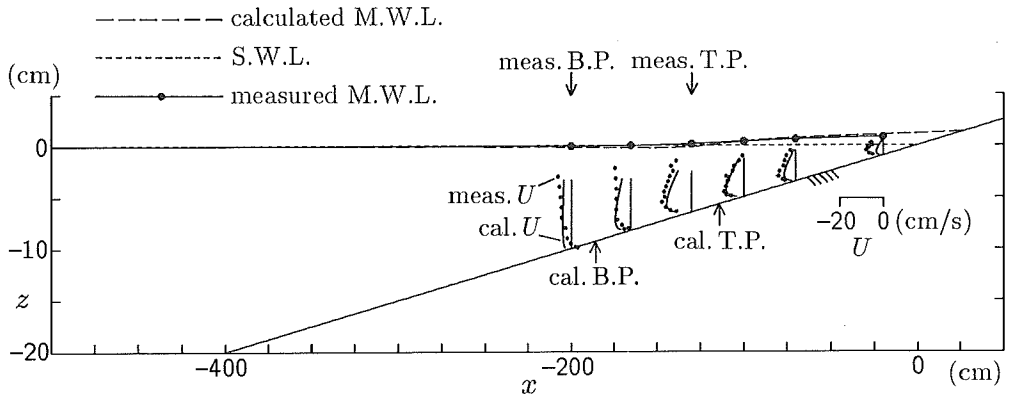

Fig. 3.8.13 Steady current distribution and the variation of mean water level (case B–4).

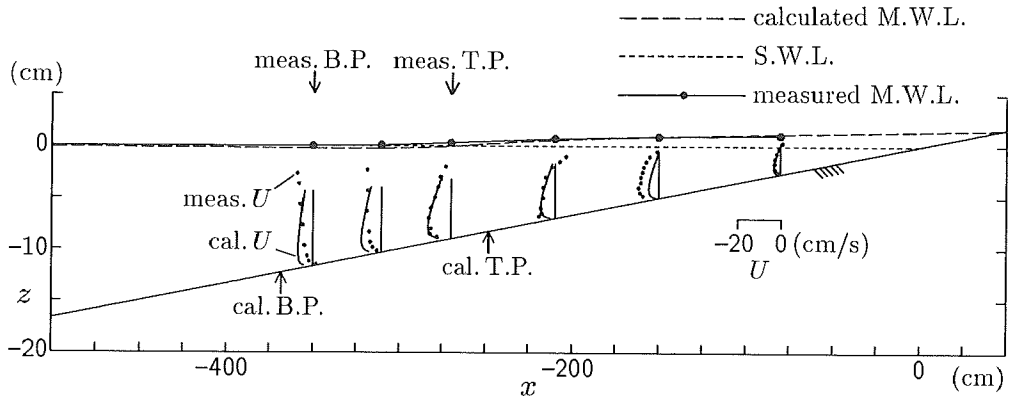

Fig. 3.8.14 Steady current distribution and the variation of mean water level (case B–8).

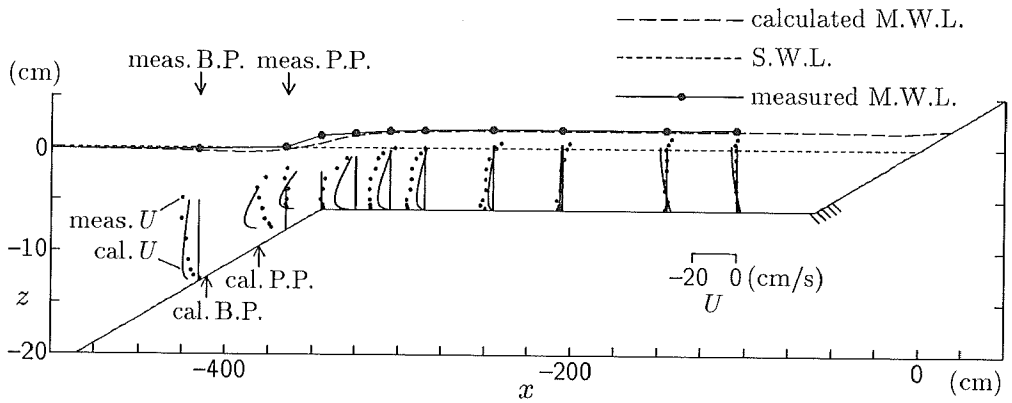

Fig. 3.8.15 Steady current distribution and the variation of mean water level (case B–11).

cm, but D_B has some value there and it becomes zero around $x = -200$ cm where the waves are regarded to recover by the calculation. The observed recovery point was $x = -115$ cm. The measured profiles are almost vertical and the magnitude is small at the measuring lines at $x = -145$ and $x = -105$ cm where the calculated profiles are the same as those by Longuet-Higgins (1953) because D_B is zero there. The figure shows that the computational result expresses the distribution of the steady current under recovering waves on the onshore side of the flat bed well. Hence, it can be concluded that the present model can deal with the steady current distributions not only for uniform but also for composite beach topographies.

3.8.4 Wave Setup and Setdown

The variations of the mean water level, that is the wave setup or setdown, are shown in Figs. 3.8.12 – 3.8.15. The agreement between the calculated and measured setup is good in all cases. The wave setdown is slightly over-estimated at the breaking points, because the radiation stress is over-estimated there by the small amplitude theory. Since the total wave energy E_t by the calculation does not change so much till the plunging point, the wave setup in the outer region is under-estimated. In other words, the wave setup lag behind the deformation of the waves. It is evident in case B–11, but the setup on the flat bed is well predicted by the present model.

CHAPTER 4

Conclusions

The present study has investigated the characteristic motion of water under breaking waves and the turbulence structure in the surf zone through detailed and precise laboratory experiments. A model for estimating the cross-shore vertical distribution of the undertow has been presented with a model of the energy transfer process in the surf zone. The main conclusions obtained in the this study are summarized as follows:

(1) The organized vortex motion caused by wave breaking is an important fluid motion which transmits the wave energy to the turbulence energy. The velocity field in the surf zone can therefore be divided into four components which are the steady current, wave motion, organized vortex motion and turbulence.

(2) The bottom boundary layer in the inner region of the surf zone does not develop well due to agitation of the turbulence from the upper layer. In such a quasi-steady breaking region, the magnitude of the steady current velocity near the bottom is large in the offshoreward direction.

(3) The mean Reynolds stress and the mean eddy viscosity coefficient in the inner region can be regarded as linear functions of the vertical elevation. The offshore directed mean shear stress on the bottom is so large that it cannot be neglected. The vertically averaged values of these two quantities can be expressed in terms of the energy dissipation rate.

(4) The transition point which is the boundary between the outer region and the inner region should be defined as the offshore end of the quasi-steady breaking region. The distance from the breaking point to the transition point can be expressed in terms of the water depth at the breaking point and the bottom

slope. The distance to the plunging point does not depend on the bottom slope.

(5) From the distribution of the energy of wave motion which can be calculated by using the time-dependent mild slope equation, the distribution of the vortex energy and the variation of the energy dissipation rate in the surf zone can be evaluated by a model. In the model, the organized large vortexes are taken into account as transmitters of energy from wave motion to turbulence in the energy transfer process. The model is able to explain the spatial difference between the wave attenuation and the production of the turbulence energy.

(6) The mass transport by breaking waves can be evaluated as the sum of two components. One component is the contribution from the wave motion which can be estimated by modifying the linear long wave theory. The other component is that by the organized large vortexes which can be estimated from the vortex energy with an assumption of the internal velocity distribution of the vortex.

(7) The momentum flux by the organized vortexes should also be taken into account. The little change of the mean water level around the wave plunging points can be rationally explained by considering the momentum flux by the vortexes.

(8) The cross-shore vertically two-dimensional distribution of the undertow which is calculated by the present model only from the incident wave conditions agree well with the measured values in the surf zone including the wave recovery zone.

The present study has introduced a new concept of energy transfer in the surf zone considering the organized vortex motion due to wave breaking. Although this idea is based on the experimental results obtained in the former half of this study, it is based on some assumptions as well. Investigations of the energy transfer process

from micro-scopic views are therefore necessary for a much more accurate estimation of the energy distribution and the impregnable description of the turbulent velocity field in the surf zone. For that sake, detailed measurements of the velocity field in the upper layer and the bottom layer are required. Though the present study dealt only with the on-offshore cross-sectional distribution of the undertow, it can be applied to the prediction of the three-dimensional distribution of the nearshore current.

REFERENCES

Bagnold, R.A. 1940: Beach formation by waves; some model experiments in a wave tank, *J. Inst. Civil Eng.*, Vol.15, pp.27–52.

Basco, D.R. 1985: A qualitative description of wave breaking, *J. Waterway Port Coastal Ocean Eng.*, Vol.111, No.2, pp.171–188.

Basco, D.R. and T. Yamashita 1986: Toward a simple model of the wave breaking transition region in surf zone, *Proc. 20th Int. Conf. Coastal Eng.*, pp.955–970.

Battjes, J.A. 1975: A note on modeling of turbulence in the surf zone, *Symp. Model. Techniques, ASCE, San Francisco*, pp.1050–1061.

Berkhoff, J.C.W. 1972: Computation of combined refraction-diffraction, *Proc. 13th Int. Conf. Coastal Eng.*, pp.471–490.

Dean, R.G. 1965: Stream function representation of nonlinear ocean wave, *J. Geophys. Res.*, Vol.70, No.18, pp.4561–4572.

Dibajnia, M., M. Isobe and A. Watanabe 1988: A comparison between finite amplitude and small amplitude waves in shoaling process, *Proc. 43rd Ann. Conf., JSCE*, No.2, pp.580–581.

Duncan, J.H. 1981: An experimental investigation of breaking waves produced by a towed hydrofoil, *Proc. Roy. Soc. London*, Ser.A, Vol.377, pp.331–348.

Goda, Y. 1970: A synthesis of breaker indices, *Proc. JSCE*, No.180, pp.39–49 (in Japanese).

Hansen, J.Buhr 1989: Waves in the surf zone analysis of experimental data, *Coastal Eng.* (in press).

Hansen, J.Buhr and I.A. Svendsen 1984: A theoretical and experimental study of undertow, *Proc. 19th Int. Conf. Coastal Eng.*, pp.2246–2262.

Hattori, M. and T. Aono 1985: Experimental study on turbulence structures under spilling breakers, *The Ocean Surface: Proc. Symp. Wave Breaking Turbulent Mixing Radio Probing*, pp.419–424.

Horikawa K., M. Isobe 1980: Dynamic character in the near shore area, *Proc. 17th Int. Conf. Coastal Eng.*, pp.480–498.

Isobe, M. 1987: Parabolic equation model for transformation of irregular waves due to refraction, diffraction and breaking, *Coastal Eng. Japan*, Vol.30, No.1, pp.33–47.

Isobe, M., N. Fukuda and K. Horikawa 1979: Two dimensional experiment on velocity field in the surf zone, *Proc. 26th Japanese Conf. Coastal Eng.*, pp.41–45 (in Japanese).

Iwagaki, Y., Y. Tsuchiya 1966: Laminar damping of oscillatory waves due to bottom friction, *Proc. 10th Int. Conf. Coastal Eng.*, pp.149–174.

Izumiya, T. and K. Horikawa 1984: Wave energy equation applicable in and outside the surf zone, *Coastal Eng. Japan*, Vol.27, pp.119–137.

Longuet-Higgins, M.S. 1953: Mass transport in water waves, *Phil. Trans. Roy. Soc. London*, Ser.A, Vol.245, pp.535–581.

Maruyama, M. and T. Shimizu 1986: Simulation model for wave deformation considering interaction of wave and beach, *Proc. 33rd Japanese Conf. Coastal Eng.*, pp.109–113 (in Japanese).

Miller, R.L. 1976: Role of vortices in surf zone prediction: sedimentation and wave forces, *Beach and Nearshore Sedimentation, Soc. Econ. Paleontol. Mineralog.*, Spec. Publ., No.24, pp.92–114.

Mizuguchi, M. 1980: An heuristic model of wave height distribution in surf zone, *Proc. 17th Int. Conf. Coastal Eng.*, pp.278–289.

Mizuguchi, M. 1986: Experimental study on kinematics and dynamics of wave breaking, *Proc. 20th Int. Conf. Coastal Eng.*, pp.589–603.

Nadaoka, K. 1986: A fundamental study on shoaling and velocity field structure of water waves in the nearshore zone, *Tech. Rep. 36*, Dept. Civil Eng., Tokyo Inst. Technol., Japan.

Nadaoka, K., M. Hino and Y. Koyano 1989: Structure of turbulent flow field under breaking waves in the surf zone, *J. Fluid Mech.* (in press).

Nadaoka, K. and F. Hirose 1986: A modeling of water particle dispersion under breaking waves in the surf zone, *Proc. 33rd Japanese Conf. Coastal Eng.*, pp.26–30 (in Japanese).

Nagayama, S. 1983: Study on the change of wave height and energy in the surf zone, *Bachelor Thesis*, Dept. Civil Eng., Yokohama National Univ., Japan (in Japanese).

Nishimura, H., K. Maruyama, and H. Hiraguchi 1983: Wave field analysis by finite difference method, *Proc. 30th Japanese Conf. Coastal Eng.*, pp.123–127 (in Japanese).

Okayasu, A., T. Shibayama and K. Horikawa 1988: Vertical variation of undertow in the surf zone, *Proc. 21st Int. Conf. Coastal Eng.*, (in press).

Okayasu, A., T. Shibayama and N. Mimura 1986: Velocity field under plunging waves, *Proc. 20th Int. Conf. Coastal Eng.*, pp.660–674.

Peregrine, D.H. 1983: Breaking waves on beaches, *Ann. Rev. Fluid Mech.*, 15: pp.149–178.

Peregrine, D.H. and I.A., Svendsen 1978: Spilling breakers, bores and hydraulic jumps, *Proc. 16th Int. Conf. Coastal Eng.*, pp.540–550.

Sakai, T., I. Sandanbata and M. Uchida 1984: Reynolds stress in surf zone, *Proc. 19th Int. Conf. Coastal Eng.*, pp.42–53.

Sawaragi, T. and K. Iwata 1974: Turbulent effect on wave deformation after breaking, *Costal Eng. Japan*, Vol.17, pp.39–49.

Seyama, A. and A. Kimura 1988: The measured properties of irregular wave breaking and wave height change after breaking on the slope, *Proc. 21st Int. Conf. Coastal Eng.*, pp.419–432.

Stive, M.J.F. and H.G. Wind 1986: Cross-shore mean flow in the surf zone, *Coastal Eng.*, Vol.10, pp.325–340.

Svendsen, I.A. 1984a: Wave attenuation and set-up on a beach, *Proc. 19th Int. Conf. Coastal Eng.*, pp.54–69.

Svendsen, I.A. 1984b: Wave heights and set-up in a surf zone, *Coastal Eng.*, Vol.8, pp.303–329.

Svendsen, I.A. 1984c: Mass flux and undertow in a surf zone, *Coastal Eng.*, Vol.8, pp.347–365.

Svendsen, I.A. 1987: Analysis of surf zone turbulence, *J. Geophys. Res.*, Vol.92, C5, pp.5115–5124.

Svendsen, I.A. and J.Buhr Hansen 1986: The interaction of waves and currents over a longshore bar, *Proc. 20th Int. Conf. Coastal Eng.*, pp.1580–1594.

Svendsen, I.A. and J.Buhr Hansen 1988: Cross-shore currents in surf zone modeling, *Coastal Eng.*, Vol.12, pp.23–42.

Svendsen, I.A. and R.S. Lorenz 1989: Velocities in combined undertow and longshore currents, *Coastal Eng.*, Vol.13, pp.55–79.

Svendsen, I.A., P.A. Madsen and J.Buhr Hansen 1978: Wave characteristics in the surf zone, *Proc. 16th Int. Conf. Coastal Eng.*, pp.520–539.

Svendsen, I.A., H.A. Schäffer and J.Buhr Hansen 1987: The interaction between the undertow and the boundary layer flow on a beach, *J. Geophys. Res.*, Vol.92, C11, pp.11845–11856.

Tsuchiya, Y., T. Yamashita and M. Uemoto 1988: A model of undertow in the surf zone, *Coastal Eng. in Japan*, Vol.30, No.2, pp.63–73.

Watanabe, A. and M. Dibajnia 1989: A numerical model of wave deformation in surf zone, *Proc. 21st Int. Conf. Coastal Eng.* (in press).

Watanabe, A., T. Hara and K. Horikawa 1984: Study on breaking condition for compound wave trains, *Coastal Eng. Japan*, Vol.27, pp.71–82.

Watanabe, A. and Y. Maruyama 1986: Numerical modeling of nearshore wave field under combined refraction, diffraction and breaking, *Coastal Eng. Japan*, Vol.29, pp.19–39.

Yamashita, T., J.R. Tallent and Y. Tsuchiya 1988: Surf zone eddy creation and propagation, *Proc. 35th Japanese Conf. Coastal Eng.*, pp.54–58 (in Japanese).

APPENDIX A

The governing equations of the time-dependent mild slope equation applied to this model are given by

$$\frac{\partial Q}{\partial t} + c^2 \frac{\partial \zeta}{\partial x} + f_A Q = 0 \tag{3.5.25}$$

$$\frac{\partial \zeta}{\partial t} + \frac{1}{n} \frac{\partial (nQ)}{\partial x} = 0 \tag{3.5.26}$$

In the derivation of the time-dependent mild slope equation, the following equations have been assumed:

$$\left.\begin{aligned} \zeta &= \hat{\zeta} e^{-i\sigma t} \\ Q &= \hat{Q} e^{-i\sigma t} \end{aligned}\right\} \tag{A.1}$$

where $\hat{\zeta}$ and $\hat{Q}$ are the complex amplitudes of the surface elevation and the flow rate, respectively. Substituting Eq. (A.1), Eqs. (3.5.25) and (3.5.26) can be replaced by

$$(f_A - i\sigma)\,\hat{Q} + c^2 \frac{\partial \hat{\zeta}}{\partial x} = 0 \tag{A.2}$$

$$-i\sigma \hat{\zeta} + \frac{1}{n} \frac{\partial (n\hat{Q})}{\partial x} = 0 \tag{A.3}$$

Eliminating $\hat{Q}$ from Eqs. (A.2) and (A.3), a single equation which includes the second derivative of $\hat{\zeta}$ is obtained as

$$i\sigma \hat{\zeta} + \frac{c^2}{(f_A - i\sigma)} \frac{\partial^2 \hat{\zeta}}{\partial x^2} + \frac{1}{n} \frac{\partial}{\partial x} \left(\frac{nc^2}{(f_A - i\sigma)} \right) \frac{\partial \hat{\zeta}}{\partial x} = 0 \tag{A.4}$$

If the water depth h and the energy transfer factor f_A are constant whole the region, n and c become also constants. Then the third term of Eq. (A.4) vanishes.

$$i\sigma \hat{\zeta} + \frac{c^2}{(f_A - i\sigma)} \frac{\partial^2 \hat{\zeta}}{\partial x^2} = 0 \tag{A.5}$$

Replacing c by σ/k, Eq. (A.5) is expressed as

$$k^2 \left(1 + \frac{i f_A}{\sigma}\right) \hat{\zeta} + \frac{\partial^2 \hat{\zeta}}{\partial x^2} = 0 \tag{A.6}$$

Assuming the form of the solution as

$$\hat{\zeta} = \xi e^{\kappa x} \tag{A.8}$$

where ξ is a complex amplitude and κ is a complex quantity which expresses the energy decay and the phase, Eq.(A.6) can be described as

$$k^2 \left(1 + \frac{i f_A}{\sigma}\right) \xi e^{\kappa x} + \xi \kappa^2 e^{\kappa x} = 0 \tag{A.7}$$

The solution is obtained as

$$\hat{\zeta} = \xi e^{-\frac{k f_A}{\sqrt{2}\sigma\sqrt{1+\sqrt{1+\frac{f_A^2}{\sigma^2}}}} x} e^{ik\frac{\sqrt{1+\sqrt{1+\frac{f_A^2}{\sigma^2}}}}{\sqrt{2}} x} \tag{A.8}$$

Now a wave field which has two regions bounded at $x = 0$ as shown in Fig. A.1 is supposed. Here it can be treated as $f_A = f_T$, because f_{b+w} given by Eq.(3.5.20) is far smaller than f_T in the surf zone and it changes little whole the field. The transfer factor f_T is zero in Region I at the left hand side of the field and takes some value f_2 in Region II at the right hand side. Though the water depth is constant in both regions, the wave number k_1 in Region I and k_2 in Region II are different according to the value of f_T as inferred from Eq.(A.8). If the wave comes from the left hand side, the complex amplitude function of the surface elevation in Region I $\hat{\zeta}_1$ consists of the incident wave component $\hat{\zeta}_i$ and the reflected wave component $\hat{\zeta}_r$ which is expressed as

$$\left.\begin{aligned} \hat{\zeta}_1 &= \hat{\zeta}_i + \hat{\zeta}_r \\ \hat{\zeta}_i = \xi_i e^{ik_1 x}&, \quad \hat{\zeta}_r = \xi_r e^{-ik_1 x} \end{aligned}\right\} \tag{A.9}$$

which has no decaying factor because of $f_T = 0$. On the other hand, $\hat{\zeta}_2$ in Region II contains the decaying factor r_2 and is denoted as

$$\hat{\zeta}_2 = \xi_2 e^{(r_2 + ik_2)x} \tag{A.10}$$

ξ_i, ξ_r and ξ_2 are complex amplitudes which are determined as

$$\xi_i = p_i + iq_i\,, \quad \xi_r = p_r + iq_r\,, \quad \xi_2 = p_2 + iq_2 \tag{A.11}$$

where p_i, q_i, p_r, q_r, p_2 and q_2 are real numbers. The boundary conditions of the surface elevation and the velocity at $x = 0$ are expressed as

$$\hat{\zeta_1} = \hat{\zeta_2} \tag{A.12}$$

$$\frac{\partial \hat{\zeta_1}}{\partial x} = \frac{\partial \hat{\zeta_2}}{\partial x} \tag{A.13}$$

Substituting Eqs. (A.10) and (A.11) into Eqs. (A.12) and (A.13)

$$\left.\begin{aligned} p_i + p_r &= p_2 \\ q_i + q_r &= q_2 \end{aligned}\right\} \tag{A.14}$$

and

$$\left.\begin{aligned} k_1\,(p_2 - 2p_r) &= k_2 p_2 + r_2 q_2 \\ -k_1\,(q_2 - 2q_r) &= r_2 p_2 - k_2 q_2 \end{aligned}\right\} \tag{A.15}$$

can be obtained. From Eqs. (A.14) and (A.15), p_r and q_r is expressed as follows:

$$\left.\begin{aligned} p_r &= \frac{1}{2}\left(p_2 - \frac{r_2 p_2 - k_2 q_2}{k_1}\right) \\ q_r &= \frac{1}{2}\left(q_2 + \frac{k_2 p_2 - r_2 q_2}{k_1}\right) \end{aligned}\right\} \tag{A.16}$$

Considering Eq. (A.8), the wave number and the decaying factor in Region II are denoted as

$$\left.\begin{aligned} k_2 &= \;\; 2a_k k_1 \\ r_2 &= -2b_k k_1 \end{aligned}\right\} \tag{A.17}$$

where

$$a_k = \frac{\sqrt{1 + \sqrt{1 + \frac{f_2^2}{\sigma^2}}}}{2\sqrt{2}}\,, \quad b_k = \frac{f_2}{2\sqrt{2}\sigma\sqrt{1 + \sqrt{1 + \frac{f_2^2}{\sigma^2}}}} \tag{A.18}$$

Then the values p_r and q_r are obtained as

$$\left.\begin{aligned} p_r &= \left(\frac{1}{2} - a_k\right) p_2 + b_k q_2 \\ q_r &= -b_k p_2 + \left(\frac{1}{2} - a_k\right) q_2 \end{aligned}\right\} \tag{A.19}$$

Substituting Eq. (A.19) with Eq. (A.11), the complex amplitude function of water surface elevation of the reflected wave can be denoted as

$$\begin{aligned}\hat{\zeta}_r &= (p_r + iq_r)\, e^{-ik_1 x} \\ &= \left[\left\{\left(\frac{1}{2} - a_k\right) p_2 + b_k q_2\right\} + i\left\{-b_k p_2 + \left(\frac{1}{2} - a_k\right) q_2\right\}\right] e^{-ik_1 x}\end{aligned} \tag{A.20}$$

It can be concluded that the reflected wave component expressed by $\hat{\zeta}_r$ in Eq. (A.20) is generated by the sudden change of the energy transfer factor. It is possible to restrain the energy of the reflected wave by apparently changing the wave number in Region II.

If using k' which does not satisfy the dispersion relation in stead of k_1 in Region II, Eq. (A.17) is replaced by

$$\left.\begin{aligned} k_2 &= 2a_k k' \\ r_2 &= -2b_k k' \end{aligned}\right\} \tag{A.21}$$

p_r and q_r are also obtained as

$$\left.\begin{aligned} p_r &= (\frac{1}{2} - \frac{k'}{k_1} a_k)\, p_2 + \frac{k'}{k_1} b_k q_2 \\ q_r &= -\frac{k'}{k_1} b_k p_2 + (\frac{1}{2} - \frac{k'}{k_1} a_k)\, q_2 \end{aligned}\right\} \tag{A.22}$$

Then the energy of the reflected wave E_R can be expressed in terms of the energy of the transmitted wave E_T as

$$E_R = \left\{\left(\frac{1}{2} - \frac{k'}{k_1} a_k\right)^2 + \left(\frac{k'}{k_1} b_k\right)^2\right\} E_T \tag{A.23}$$

where

$$E_R = \frac{1}{2}\rho g\,(p_r^2 + q_r^2), \quad E_T = \frac{1}{2}\rho g\,(p_2^2 + q_2^2) \tag{A.24}$$

The ratio of the reflected wave energy to the transmitted wave energy is calculated by

$$R_E \equiv \frac{E_R}{E_T}$$

$$= \left(\frac{1}{2} - \frac{k'}{k_1}\, a_k\right)^2 + \left(\frac{k'}{k_1}\, b_k\right)^2$$

$$= \left\{\frac{a_k^2 + b_k^2}{k_1^2}\right\} k'^2 - \frac{a_k}{k_1}\, k' + \frac{1}{4} \qquad \text{(A.25)}$$

Finally, the minimum value of R_E is given by

$$R_E = \frac{1}{4}\frac{b_k^2}{a_k^2 + b_k^2} \qquad \text{(A.26)}$$

when

$$k' = \frac{a_k}{2\,(a_k^2 + b_k^2)}\, k_1 \qquad \text{(A.27)}$$

APPENDIX B

The expansion of $\log(1+x)$ to a power series around $x=0$ is denoted as

$$\begin{aligned}\log(1+x) &= \sum_{n=1}^{\infty}(-1)^{n-1}\frac{x^n}{n} \\ &= x - \frac{x^2}{2} + \frac{x^3}{3} - \frac{x^4}{4} + - \cdots \end{aligned} \tag{B.1}$$

Hence $\log(a_\nu z' + \nu)$ and $\log(a_\nu d_t + \nu)$ can be expressed as

$$\begin{aligned}&\log(a_\nu z' + \nu) \\ &\quad = \log\nu + \log\left(1 + \frac{z'}{\nu}a_\nu\right) \\ &\quad = \log\nu + \frac{z'}{\nu}a_\nu - \frac{1}{2}\left(\frac{z'}{\nu}a_\nu\right)^2 + \frac{1}{3}\left(\frac{z'}{\nu}a_\nu\right)^3 - \frac{1}{4}\left(\frac{z'}{\nu}a_\nu\right)^4 + - \cdots \end{aligned} \tag{B.2}$$

$$\begin{aligned}&\log(a_\nu d_t + \nu) \\ &\quad = \log\nu + \log\left(1 + \frac{d_t}{\nu}a_\nu\right) \\ &\quad = \log\nu + \frac{d_t}{\nu}a_\nu - \frac{1}{2}\left(\frac{d_t}{\nu}a_\nu\right)^2 + \frac{1}{3}\left(\frac{d_t}{\nu}a_\nu\right)^3 - \frac{1}{4}\left(\frac{d_t}{\nu}a_\nu\right)^4 + - \cdots \end{aligned} \tag{B.3}$$

Substituting Eqs. (B.2) and (B.3), U in Eq. (3.7.33) is transformed as

$$\begin{aligned}U &= \frac{a'_\tau}{a_\nu}\left(z' - \frac{d_t}{2}\right) + \frac{a_\nu b'_\tau - a'_\tau\nu}{a_\nu^2}\left(1 + \log\frac{a_\nu z' + \nu}{a_\nu d_t + \nu} - \frac{\nu}{a_\nu d_t}\log\frac{a_\nu d_t + \nu}{\nu}\right) + U_m \\ &= \frac{a'_\tau}{a_\nu}\left(z' - \frac{d_t}{2}\right) + \frac{a_\nu b'_\tau - a'_\tau\nu}{a_\nu^2}\left[\, 1 + \left\{\log\nu + \frac{a_\nu}{\nu}z' - \frac{1}{2}\left(\frac{a_\nu}{\nu}z'\right)^2 + \cdots\right\}\right. \\ &\quad - \left\{\log\nu + \frac{a_\nu}{\nu}d_t - \frac{1}{2}\left(\frac{a_\nu}{\nu}d_t\right)^2 + \cdots\right\} \\ &\quad \left. - \frac{\nu}{a_\nu d_t}\left(\left\{\log\nu + \frac{a_\nu}{\nu}d_t - \frac{1}{2}\left(\frac{a_\nu}{\nu}d_t\right)^2 + \frac{1}{3}\left(\frac{a_\nu}{\nu}d_t\right)^3 - \cdots\right\} - \log\nu\right)\,\right] + U_m \\ &= \frac{a'_\tau}{a_\nu}\left(z' - \frac{d_t}{2}\right) + \frac{a_\nu b'_\tau - a'_\tau\nu}{a_\nu^2}\left[\, \frac{a_\nu}{\nu}z' - \frac{1}{2}\left(\frac{a_\nu}{\nu}z'\right)^2 + \cdots\right. \\ &\quad \left. - \frac{a_\nu}{\nu}d_t + \frac{1}{2}\left(\frac{a_\nu}{\nu}d_t\right)^2 - \cdots + \frac{1}{2}\frac{a_\nu}{\nu}d_t - \frac{1}{3}\left(\frac{a_\nu}{\nu}d_t\right)^2 + \cdots\,\right] + U_m \end{aligned} \tag{B.4}$$

The steady current U in the limit when a_ν approaches to zero (namely D_B approaches to zero) is given as

$$
\begin{aligned}
\lim_{a_\nu \to 0} U &= \lim_{a_\nu \to 0} \left[\frac{a'_\tau}{a_\nu} \left(z' - \frac{d_t}{2} \right) \right. \\
&\quad \left. + \frac{a_\nu b'_\tau - a'_\tau \nu}{a_\nu^2} \left\{ \frac{a_\nu}{\nu} z' - \frac{1}{2} \left(\frac{a_\nu}{\nu} z' \right)^2 - \frac{1}{2} \frac{a_\nu}{\nu} d_t + \frac{1}{6} \left(\frac{a_\nu}{\nu} d_t \right)^2 + \cdots \right\} + U_m \right] \\
&= \lim_{a_\nu \to 0} \left[\frac{a'_\tau}{\nu} \left(\frac{z'}{2} - \frac{d_t^2}{6} \right) + \frac{b'_\tau}{\nu} \left(z' - \frac{d_t}{2} \right) + a_\nu \frac{b'_\tau}{\nu^2} \left(-\frac{z'^2}{2} + \frac{d_t^2}{6} \right) + U_m \right] \\
&= \frac{a'_\tau}{2\nu} z'^2 + \frac{b'_\tau}{\nu} z' - \frac{a'_\tau}{6\nu} d_t^2 - \frac{b'_\tau}{2\nu} d_t + U_m \\
&= \frac{1}{2\nu} \frac{\nu a^2 \sigma k}{2h^2 \sinh^2 kh} \left(3kh \sinh 2kh + \frac{3 \sinh 2kh}{2kh} + \frac{9}{2} \right) z'^2 \\
&\quad - \frac{1}{\nu} \frac{\nu a^2 \sigma k}{4h \sinh^2 kh} \left(2kh \sinh 2kh + \frac{6 \sinh 2kh}{2kh} + 9 \right) z' \\
&\quad - \frac{1}{6\nu} \frac{\nu a^2 \sigma k}{2h^2 \sinh^2 kh} \left(3kh \sinh 2kh + \frac{3 \sinh 2kh}{2kh} + \frac{9}{2} \right) d_t^2 \\
&\quad + \frac{1}{2\nu} \frac{\nu a^2 \sigma k}{4h \sinh^2 kh} \left(2kh \sinh 2kh + \frac{6 \sinh 2kh}{2kh} + 9 \right) d_t \\
&\quad + U_m \\
&= \frac{a^2 \sigma k}{4 \sinh^2 kh} \left\{ \left(3kh \sinh 2kh + \frac{3 \sinh 2kh}{2kh} + \frac{9}{2} \right) \frac{z'^2}{h^2} \right. \\
&\quad - \left(2kh \sinh 2kh + \frac{6 \sinh 2kh}{2kh} + 9 \right) \frac{z'}{h} \\
&\quad - \left(kh \sinh 2kh + \frac{\sinh 2kh}{2kh} + \frac{3}{2} \right) \frac{d_t^2}{h^2} \\
&\quad \left. + \left(kh \sinh 2kh + \frac{3 \sinh 2kh}{2kh} + \frac{9}{2} \right) \frac{d_t}{h} \right\} \\
&\quad + U_m \\
&= U_{\text{off}}
\end{aligned}
\tag{B.5}
$$